(2)

CONTRACTOR REPORT

CR 2210-89-1
NOVEMBER 1989

AN EXPERIMENTAL INVESTIGATION OF THE FLOW FIELD AROUND YAWED STRANDED CABLES

Stephen M. Batill
Robert C. Nelson
Jose V. Nebres
Dept. of Aerospace and Mechanical Engineering
University of Notre Dame
Notre Dame, Indiana 46556

CONTRACT NUMBER N00014-83K-0239

Prepared for
Naval Coastal Systems Center
Code 2210
Panama City, FL 32407

REPORT DOCUMENTATION PAGE

1a REPORT SECURITY CLASSIFICATION: Unclassified	1b RESTRICTIVE MARKINGS
2a SECURITY CLASSIFICATION AUTHORITY	3 DISTRIBUTION/AVAILABILITY OF REPORT: Approved for public release; distribution is unlimited
2b DECLASSIFICATION/DOWNGRADING SCHEDULE	
4 PERFORMING ORGANIZATION REPORT NUMBER(S)	5 MONITORING ORGANIZATION REPORT NUMBER(S): CR 2210-89-1
6a NAME OF PERFORMING ORGANIZATION: University of Notre Dame; 6b OFFICE SYMBOL (If applicable)	7a NAME OF MONITORING ORGANIZATION: NAVCOASTSYSCEN
6c ADDRESS (City, State, and ZIP Code): Department of Aerospace and Mechanical Engineering, Norte Dame, IN 46556	7b ADDRESS (City, State, and ZIP Code): Hydromechanics Branch, Code 2210, Panama City, FL 32407-5000
8a NAME OF FUNDING/SPONSORING ORGANIZATION: Chief of Naval Research; 8b OFFICE SYMBOL (If applicable): ONT Code 235	9 PROCUREMENT INSTRUMENT IDENTIFICATION NUMBER: N00014-83K-0239
8c ADDRESS (City, State, and ZIP Code): Office of Naval Technology, 800 North Quinch Street, Arlington, VA 22217-5000	10 SOURCE OF FUNDING NUMBERS: PROGRAM ELEMENT NO: PE 62315; PROJECT NO: RN15w33; TASK NO; WORK UNIT ACCESSION NO

11 TITLE (Include Security Classification): An Experimental Investigation of the Flow Field Around Yawed, Stranded Cables

12 PERSONAL AUTHOR(S): S. M. Batill, R. C. Nelson, J. V. Nebres

13a TYPE OF REPORT	13b TIME COVERED	14 DATE OF REPORT (Year, Month, Day)	15 PAGE COUNT
Contractor	FROM 7/87 TO 11/88	November 1989	161

16 SUPPLEMENTARY NOTATION

17 COSATI CODES			18 SUBJECT TERMS (Continue on reverse if necessary and identify by block number)
FIELD	GROUP	SUB-GROUP	Hydrodynamic Forces; Flow Visualization; Stranded Cables; Cables; Vortex Shedding; Wire Ropes; Towed Cables

19 ABSTRACT (Continue on reverse if necessary and identify by block number)

An experimental study was conducted to investigate the flow field about stranded cables. The objective was to gain insight into the flow mechanisms associated with the generation of fluid forces on cables. Five rigid cable models and a circular cylinder were tested in a wind tunnel. The models represented full-scale cable geometries and were yawed at four different cable angles (90, 60, 40, and 20 degrees) for Reynolds numbers in a range from 5,800 to 13,800 based on cable diameter and freestream velocity. Smoke flow visualization and hot wire anemometry were used to collect qualitative and quantitative data, consisting of pictures of the vortex wake, vortex shedding angles and wake widths, shedding frequency and spanwise coherence of the vortex wake. Results show that the cable geometry influences the flow field about the cable.

20 DISTRIBUTION/AVAILABILITY OF ABSTRACT	21 ABSTRACT SECURITY CLASSIFICATION	
☒ UNCLASSIFIED/UNLIMITED ☐ SAME AS RPT ☐ DTIC USERS	UNCLASSIFIED	
22a NAME OF RESPONSIBLE INDIVIDUAL: K. P. Watson	22b TELEPHONE (Include Area Code): (904) 234-4643	22c OFFICE SYMBOL: Code 2210

FOREWORD

The experimental study described in this report was conducted during the period from July 1987 to August 1988 under contract N00014-83-K-0239. The research program was entitled "Flow Field Measurements on Stranded Cables" and was conducted by the Department of Aerospace and Mechanical Engineering at the University of Notre Dame, Notre Dame, Indiana for the Naval Coastal Systems Center, Panama City, Florida. The Principal Investigators for the contract were Drs. Robert C. Nelson and Stephen M. Batill. Mr. Jose V. Nebres is a Graduate Research Assistant in the Department of Aerospace and Mechanical Engineering. The Project Engineer for the contract was Mr. Kennard Watson. The authors wish to acknowledge the contributions of the Project Engineer during the program. They would also like to acknowledge the support of the Department of Aerospace and Mechanical Engineering by providing the graduate student support and research facilities necessary for the successful completion of this project.

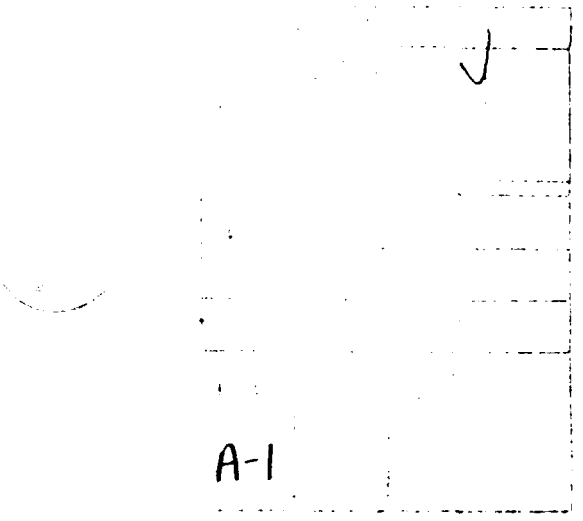

TABLE OF CONTENTS

LIST OF TABLES

LIST OF FIGURES

NOMENCLATURE

A	Frontal area = cable length x cable diameter
A_i	Loading function coefficient
B_i	Loading function coefficient
c_f	Mean force coefficient
D	Cable diameter
f	Trigonometric loading function
F	Aerodynamic force component
f_v	Vortex shedding frequency
q	Dynamic pressure = ρV^2
s	Measurement distance
S	Strouhal number
S_N	Strouhal number based on normal velocity
V	Fluid velocity
x	Measurement distance
α	Wake shedding angle
β	Cable angle
Δ	Indicates incremental value
ρ	Fluid density

SUMMARY

This report describes the results of an experimental investigation of the flow about stranded cables or wire ropes. The purpose of the study was to improve the understanding of the flow field near the cable and to develop insight into the mechanisms associated with the generation of fluid forces on the cables. Five rigid cable models and a cylinder were tested in a wind tunnel. The models represented full scale cable geometries and were yawed to four different cable angles (90°, 60°, 40° and 20°) and tested at Reynolds numbers in a range from 5,800 to 13,800 based on the mean cable diameter. Photographs from the smoke-wire and the kerosene smoke flow visualization techniques were used to qualitatively evaluate the flow fields associated with each cable geometry. These photographs were also used to determine shedding angles and the spanwise characteristics of the flows. The cross-correlation function and the spectrum were obtained from hot-wire anemometer measurements. The hot wire was also used to measure the shedding angle of the vortex filaments and the vortex shedding frequency respectively. The flow visualization data indicated significant difference in the basic flow structure for different cable geometries. The shedding frequencies for the stranded cables were in general lower than for the smooth circular cylinder. The 3x19 and 4x7 cables were found to exhibit a complex dependence on cable angle.

1. INTRODUCTION

1.1 Statement of the Problem

Large hydrodynamic forces on cables or wire ropes are observed in towed marine and airborne systems, mooring of offshore structures, and transmission lines subjected to strong winds. Cables, used in anchoring and mooring off-shore structures and barges, are subject to underwater currents and thus significant hydrodynamic forces. High voltage transmission lines subjected to strong, hurricane force winds, experience the same Reynolds number flow and therefore experience the same types of steady and unsteady fluid forces.

Stranded cables in a moving fluid can basically be characterized by the presence of mean or "steady" drag and lift forces, and transverse and in-line vibrations due to unsteady forces. The drag force on these bluff bodies is due to both viscous and pressure forces. The more intriguing and complex lift force is primarily due to the stranding geometry of the cable. The unsteady nature of the fluid forces and the ensuing vibrations are due to the periodic nature of the wake of the cable.

In a towed marine system consisting of a cable and a towed body , Horton, Ferrer, Watson and Charvoz[1987] indicated that the tow wire creates a catenary in a near vertical plane aft of the tow point. However, for certain cable geometries, the cable produces steady lift, resulting in a side force causing the cable and the towed body to kite to the lift side of the tow point. Thus the hydrodynamic lift may influence the successful operation of a towed marine system. In the case of a mechanical minesweeping system, the sweep wire creates a catenary in a near horizontal plane. However, due to the hydrodynamic lift developed by the wire ropes and the weight of the ropes, the sweep wire develops a three dimensional configuration. The cable lift produces a vertical force which causes the wire to bow up or down depending on the direction of the steady lift force. In order to achieve the goal of precise placement of towed cables, information about cable hydrodynamics is required.

Based on a survey by Griffin [1982], vortex excited oscillations of marine cables, commonly termed strumming, can result in mechanical fatigue, increased steady and unsteady hydrodynamic forces, and amplified acoustic noise. These sometimes lead to structural damage and possibly failure. Flow-excited oscillations are often a critical factor in the design of underwater cable arrays, mooring systems and offshore platforms. Since these complex structures

usually have bluff cylindrical shapes, they are conducive to vortex shedding when they are placed in a flow. Problems associated with the shedding of vortices often have been neglected in the past in relation to the design of offshore platforms and cable structures, largely because reliable experimental data and design methods have not been available. An understanding of the basic nature of the fluid and structure interactions which produces both the steady hydrodynamic forces and the vortex excited oscillations are an important consideration in the reliable design of many practical systems.

1.2 Background

A cable or wire rope is constructed by wrapping or braiding wires together according to some pattern. The basic arrangement of a cable or wire rope can be designated by two numbers. The first number refers to the number of strands and the second number refers to the number of wires per strand. An example considered in this paper is a 3x19 cable which has three primary strands with 19 wires in each strand. The strands of a cable are twisted or laid in a direction about the cable axis. The direction of the twist is referred to as the "lay". A cable is called "right" lay if, as viewed along the cable axis, the strands pass from left to right as they move away from the viewer. A "left" lay cable has the opposite orientation of the strands. Another characteristic is the direction of the lay of the wires within each strand. A cable with the wires laid opposite that of the lay of the strands is termed "regular" lay while that with the wires laid in the same direction as the strands is called "lang" lay. There are numerous other variations in wire arrangement which can be made to modify the cable geometry. For certain applications wires within individual strands can be twisted together to add an irregular character to the cable surface. This type of cable is referred to as "serrated" and a cable of this type was considered during this study.

A cable yawed in a flow experiences drag due to the viscous resistance and nonuniform surface pressures, and lift primarily due to the nonuniform surface pressures. The cable stranding is the primary cause of the nonuniform surface pressures associated with the lift generation. The description of the fluid forces acting on a cable is similar to traditional airfoil notation with some modifications as indicated below. Horton, et. al. [1987] proposed that cable drag can be resolved into the normal and tangential components with respect to the axis of the cable. The normal and tangential drag, and lift forces can be

expressed in terms of a mean nondimensional force coefficient and a loading function which is used to include the dependence on cable orientation. The cable orientation can be expressed in terms of the cable angle, β, which is the angle between the longitudinal axis of the cable and the free stream flow velocity or a cable yaw angle which is the complement of the cable angle. The force component can be written as:

$$F = q\ A\ c_F\ f(\beta)$$

where

F = normal drag, tangential drag, or lift force

$q = \rho V^2/2$, dynamic pressure, where ρ is fluid density and V is fluid velocity

A = frontal area = cable diameter x cable length

c_F = experimentally determined mean force coefficient

$f(\beta)$ = trigonometric loading function

β = cable angle.

The form of the loading function can be determined from experimental measurements. The following form,

$$f(\beta) = A_o + A_1 \cos\beta + B_1 \sin\beta + A_2 \cos 2\beta + B_2 \sin 2\beta$$

where A_o, A_1, B_1, A_2, B_2 are loading function coefficients was used by Horton, et.al.[1987] and shown to be reasonably accurate for a range of cable angles. The normal drag, tangential drag, and lift forces each has different mean force coefficients and loading function coefficients. The dependence of the loading coefficients on the cable geometry must be determined empirically.

Horton, et. al. [1987] conducted tow tank tests where the lift and normal drag forces were measured for a range of different cable angles. The tangential drag was not determined due to the difficulty of isolating the tangential drag force from the tensile loading on the model. The data obtained were used to calculate the mean force coefficients, and the coefficients of the loading functions. The normal drag and lift forces were quantified as a function of cable angle for the five different test cables. It was the complex and somewhat unexpected behavior of the tow tank results that prompted the study described in this test report.

Steady lift development has been quantified for only a few cables. The flow patterns leading to the production of steady lift on either strumming or rigid cables have not been qualitatively or quantitatively measured nor has the mechanism for steady lift production been determined. One possible explanation for the steady lift reflects the concept that the cable acts like an airfoil. When a cable is yawed to the flow, the upper and lower surfaces of the cable profile as viewed in the flow plane are not symmetric and thus there is an effective camber associated with the cross section. This may cause a low pressure region to arise over the convex side of the cable. The lift mechanism is therefore due to the profile geometry of the cable. Since the profile geometry varies widely with cable angle one would therefore expect a complex dependence of the lift force on cable angle. A second possible explanation proposes that the complex, yawed cable cross section is such that boundary layer separation occurs earlier on one side of the cable than on the other. The assertion is that lift is produced by asymmetric separation of the turbulent boundary layer. The steady lift is produced by surface pressure differences caused by the difference in separation points from the top and bottom of the cable and the unsteady lift component is a result of the movement of the separation points. Simpson [1979] proposed similar explanations regarding the production of mean steady lift by stranded cables but these have not been substantiated. Horton, et. al. [1987] found that based on their measurements the lift force developed on a right lay cable over the angle range of $0 < \beta < 90^{o}$, where the β is the cable angle, is equivalent to that developed by a left lay cable except that the direction of the lift vector is reversed. This implies that regardless of the mechanism creating the lift, the steady state lift force is influenced by the cable stranding.

Much of the vortex shedding phenomenon which cause the transverse and in-line vibrations for a cable have been studied using the unyawed circular cylinder. In a two-dimensional flow around a cylinder, at certain Reynolds numbers, energy is not dissipated directly in an irregular wake, but is first transformed into very regular individual vortices. These vortices do not mix with the outer flow and are dissipated by the internal friction only after a long time. Some of the streamlines move in a wavy path between the vortices, while other streamlines are closed around the vortex centers. The phenomenon was first studied experimentally by Benard [1908], it was however von Karman [1911] who gave an explanation to it.

Schaeffer and Eskinazi [1958] investigated the behavior of vortices at the range 50 < Re < 125. They observed that the vortex street may be divided into three distinct areas, namely: the 'formation', 'stable', and 'unstable' regions. The formation region is the region immediately behind the body in which the vortex develops . The stable region is the region of the fully developed stable vortex street in which the vortices display a periodic laminar regularity. The unstable region is farther downstream and exhibits irregular behavior and the eventual transition to turbulence. Above a Reynolds number of approximately 125, a completely stable vortex is not apparent.

Votaw and Griffin [1971] forced cables and a circular cylinder into transverse vibration and measured the length of the formation region. The models were perpendicular to flow, i.e. cable angle of 90°, at a Re=240 and 500. They based the length of the vortex formation region on the location of the maximum velocity fluctuation at the centerline of the wake. They observed a reduced formation region and an increased amplitude of velocity fluctuation at the centerline as a consequence of the forced vibration.

Chiu and Lienhard [1967] developed an analytical solution to the flow around yawed cylinders and concluded that the vortex centers move in a straight line as they convect downstream. A particle thus moves in a corkscrew motion about the path of a vortex center. Ramberg [1979] conducted a series of hot-wire measurements and a flow visualization study of yawed cylinders and has shown that the vortex filaments make a angle with the cable axis, that is they are not aligned with the cable axis. He has also shown that at certain special end conditions, another mode of vortex shedding exists.

Vortex shedding process creates fluctuating asymmetric pressure distributions about a cable. One complete vortex shedding cycle consists of two vortices of opposite sign shed, one after the other, from opposite sides of the cable. During this cycle, the cable is forced to vibrate, or strum, due to the alternating pressure distribution. One shedding cycle causes the cable to respond with one vibrational cycle transverse to the wake and two vibrational cycles in line with the wake. This is because one vibrational cycle in the vertical plane is caused by two vortices, while one vibrational cycle in the horizontal plane is caused by each shed vortex.

From accelerometer readings, Horton, et. al. [1987] measured the vibrational or unsteady lift and drag forces. A comparison of the mean unsteady to steady normal drag forces for the cable models reveal the unsteady to steady

drag force ratio of 1:20. Thus the measured unsteady drag forces are a small percentage of the mean steady drag forces. Comparison between the unsteady and steady force ratio for the cable models show that the unsteady lift forces are significantly greater than the steady lift forces. The ratio of the unsteady to steady lift forces are of the order 5:1. This ratio is one hundred times greater than that observed for normal drag.

The non-dimensional frequency used to describe the periodic nature of the vortex wake is the Strouhal number,

$$S = f_V D / V$$

where

f_V = vortex shedding frequency in Hz

D = cable diameter

V = fluid velocity

The shedding frequency is based on the period associated with the shedding of a vortex pair with vorticity of opposite sense.

Lienhard [1967] compiled results of investigations on the behavior of Strouhal number with Reynolds number and the results are shown in Figure 1. The Strouhal number for a relatively wide range in Reynolds numbers, i.e. $300 < Re < 3x10^5$ is in the range from 0.18 to 0.22. The results presented in this report are in this Reynolds number range. For the yawed cylinder, Ramberg [1978] reported that under certain special conditions the Strouhal number would be the same as that of the unyawed cylinder if the tangential velocity component of the flow has no effect on the shedding frequency. Thus for the yawed cable, a modified form of the Strouhal number based on the component of the free stream velocity normal to the longitudinal axis of the cable can be defined.

$$S_N = f_V D / (V \sin \beta).$$

The assumption that the shedding characteristics are dependent upon the normal component of the free stream velocity is referred to as the Independence Principle. For yawed cylinders or cables free to vibrate Dale et. al. [1968] found that the vortex shedding frequency increases in steps corresponding to natural frequencies of the cylinder or cable. This phenomenon called "lock-on" occurs because the cylinder or cable tends to vibrate at or near one of its

natural frequencies. Ramberg [1978] asserts that in infinitely rigid cylinders that don't lock-on, the Independence Principle is not valid.

Horton, et. al.[1987] used a test apparatus with a cable that was free to vibrate. The vortex shedding frequency was observed to decrease as the cable angle was reduced in agreement with the Independence Principle. There was also a dependence upon cable geometry. The Strouhal number varied from a low S=0.18 for the smooth 1x19 cable to a high value of S=0.22 for the 4x7 cable. Yet the effect did not seem so significant since the average Strouhal numbers are within 10 per cent of S=0.20 which is the circular cylinder value.

Votaw and Griffin [1971] measured the Strouhal numbers of unyawed cables and observed slightly elevated values for cables with three and four strands as compared to values of cables with five and six strands. The differences were not so significant however since they were still within the range $0.18 < S < 0.22$.

Horton, et. al. [1987] observed the amplitudes measured from the midspan to be highest for the 4x7 cable in the tow tank tests of the flexible cables. The 4x7 cable was the roughest cable of the four tested. The highest vibration amplitudes were observed at the smallest cable angle. This was apparently due to the excitation of lower mode frequencies as the shedding frequency is reduced at the smaller angles. These tests indicated that the lift generation was dependent on both cable geometry and Reynolds number and that the Independence Principle could not be used to successfully scale the lift coefficient data. This indicates the need for additional testing to help determine the mechanisms associated with the steady lift generation.

1.3 Scope of Current Work

The work described in this Test Report was conducted in order to evaluate the flow field characteristics of five stranded cables and circular cylinder of similar diameter. Both quantitative hot wire flow field measurements and qualitative flow visualization studies were performed in order to increase the understanding of this complex three dimensional flow. These tests were designed to complement the recent experimental work of Horton, et. al. [1987] and help to explain some of the results achieved in those earlier tests.

The models used were the 1x19, 7x7, 3x19, 4x7 serrated, 6x25 lang lay cables, and a circular cylinder of similar diameter. Wind tunnel models of the cables were developed to create reasonably rigid and straight replicas of the

actual cable geometries. The models were rigidly fixed in a wind tunnel test section and were yawed to four different cable angles, namely 90°, 60°, 40°, and 20°. The wind tunnel tests were performed at two flow velocities corresponding to Reynolds number 5,800 and 13,800 based on the cable diameter. The flow conditions were selected based on the range of practical applications.

The vortex shedding frequency for each of the above test cases were measured using a single wire hot-wire probe placed in the wake of the model. The cable shedding frequencies were compared with that of the cylinder. The influence of cable stranding on the vortex shedding was investigated by rotating the cable about its axis while the hot wire probe remained fixed. The result of an incremental rotation is similar to that associated with translating the hot wire along the span of the cable. The 3x19 cable was selected for this test due to its more prominent standing. The spanwise structure of the wake was also evaluated by measuring the cross-correlation function between the hot-wire signals from the two probes at various positions in the wake. The 4x7 serrated and the 6x25 lang lay cables were used for the cross correlation wake measurements. The cross correlation data were used to calculate the shedding angles of the vortex filaments.

Qualitative comparison of flow fields around all of the cables and the cylinder were accomplished through flow visualization. Still pictures were taken using the smoke wire technique for the low Reynolds number case of 5,800; and the kerosene smoke technique for the high Reynolds number case of 13,800. The smoke wire technique was used for the low Re case due to the greater detail it provides. Because the smoke wire technique does not work as well for the high Re case, the kerosene smoke technique was used. Plan, axial and side view photographs were taken, and quantitative results were developed from the visualization records.

The aim of this research is to provide additional information on the complex physics associated with this unsteady, three dimensional flow around stranded cables. Horton, et. al. [1987] notes that very little data is available for the various characteristics of stranded cables. This is because researchers in the aerospace and the hydrodynamic communities have traditionally focused their attention on smooth cylinders. This report furnishes some additional information and should provide a basis for further numerical and experimental work on fluid flow around stranded cables.

2. STRANDED CABLE MODELS

2.1 Basic Geometric Description

The series of experiments described in this report were conducted using a number of stranded cable configurations. A stranded cable or wire rope is actually a complex three dimensional slender body. The baseline model used for comparison purposes was a circular cylinder. The five cable models were developed using the same cables tested by Horton et.al. [1987] and included the 1x19, 7x7, 3x19, 4x7 (serrated) and a 6x25 (lang lay) . The length of the cable models varied depending upon the cable angle since the geometry of the wind tunnel test section was fixed. In order to develop an understanding of the streamwise cross sectional geometry associated with a yawed, stranded cable the following study was performed.

2.1.1 Cross Section Profiles of Yawed Cables

Figure 2 presents two views of a stranded cable, yawed to a moving fluid. The top view shows a cable yawed to the flow and "sliced" at an angle equal to the cable angle. The side view shows a schematic of the resulting effective cross section which is presented to the oncoming flow. The cross-section varies widely for each type of cable, cable angle, and position along the cable longitudinal axis at which the "slice" is made. The effective cross section could also be varied by fixing the plane of the "slice" and rotating the cable about its longitudinal axis. Different angles of rotation simulate the different spanwise locations along the cable.

A simple computer program was developed in order to visualize the effective cross sections for stranded cables at different cable angles and different angles of rotation. The "outer" strands of the cable were modeled as circular cylinders and their relative positions defined for an unyawed cable. Using the description of a double helix presented by Stein and Bert [1962], the locus of points representing the intersection of the perimeter of the individual circular strands with a plane inclined at the cable angle were determined and plotted. The resulting plots only approximate the cable cross section since they do not provide the detail associated with the wire distribution in each strand. Figure 3 illustrates the resulting cable geometries for a cable with six external strands at four different cable angles and various longitudinal positions. The six strand cable shown in Figure 3 approximates the cross-sections of the 7x7 and

the 6x25 cables. These two cables both have six outer strands althougn they have different number of wires per strand. The inner strands were not plotted since they do not affect the perimeter of the cross section. Figure 4 shows representative examples of cable cross-sections with three, four and twelve outer strands.

It can be seen from the cross-section geometries that the cross sections for the yawed cables are asymmetric. For the cables plotted in Figure 3, which are right lay cables, and for the particular flow orientations shown, the top surface appears to be less "rough" in comparison with the bottom surface. For a left lay cable, the geometries will be the same except that they will be upside down. Due to the asymmetry in the cross section, an asymmetric pressure distribution can be developed and a net lift force can be generated.

The mechanism by which the lift is generated is still not well understood. Considering the possible mechanisms briefly outlined in the previous section, the cross section shapes shown in Figure 3 appear to support the supposition that an effective camber is developed and that the upper surface (for the orientations shown) may develop a lower pressure and thus a net lift force is developed as shown in Figure 5.

2.2 Wind Tunnel Models

One of the initial goals of the effort was to establish a procedure for wind tunnel model fabrication . A number of alternative methods for developing the wind tunnel models were considered ranging from using actual metal cables, those used by Horton et.al. [1987], to fabricating wire ropes using lightweight, flexible materials such as plastic tubing. After weighing the relative merits and suitability of each it was decided to develop the wind tunnel models by casting solid plastic models from specially fabricated molds. The models were assembled from epoxy castings which were either center drilled or cast with center holes and mounted on a steel shaft to provide strength and stiffness.

The sample cable specimens provided by NCSC were used as the masters to develop the molds for each model. A segment , approximately 1 foot long, was cut from the original cable and placed and centered in a mold former. There was approximately a 1 inch gap between the cable and the former wall. The former/cable assembly was filled with RTV compound and placed in a vacuum chamber which was used to eliminate the air bubbles from the RTV. The former/cable assembly was then mounted in a hydraulic press which had

been modified to stretch and straighten the cable (some preliminary straightening of the models was done by hand in order to eliminate most of the curvature which normally occurs in the this type of stranded cable). After the RTV was cured, the assembly was removed from the press and the former opened and the cable and its RTV "sleeve" removed. The "sleeve" was slit and the cable removed. The RTV "sleeve" was replaced in the former and served as the master mold for the casting of the cable model model segments.

Segments of the cable models were then cast from epoxy by filling the mold, again placing it in the vacuum chamber to eliminate any bubbles from the epoxy and allowing the epoxy to cure. A small plastic tube was placed and centered in the mold in order to produce a hollow casting. Figure 6 is a schematic of the casting assembly. Segments of the cable models were then cast by filling the space between the mold and the tube with epoxy. The mold/casting assembly was again placed in the vacuum chamber. This eliminated any bubbles from the epoxy prior to allowing the epoxy to cure. After the epoxy was cured, the plastic tube was pulled out, and the hollow epoxy casting taken out of the RTV "sleeve".

The hollow segments with slightly oversized center holes which facilitated proper alignment were mounted alternately with half inch segments which fit snugly in the steel shaft. These half inch segments were fabricated from an epoxy casting similar to the hollow segments however the plastic tube was not placed in the center in order to produce a solid casting. The solid casting was then cut into half inch pieces and center drilled to a diameter that fit snugly on the steel shaft. The hollow and half inch segments were then positioned and glued to the steel shaft in such a way that the cable stranding remained continuous. The fidelity of the casting was excellent and the resulting models satisfied all of the requirements for the tests considered in this study. It should be noted that there is one difference between the cast models and the actual cables. The cast models are "solid" so that no fluid can pass through the wires which make up the cable. For an actual cable, depending upon the tension in the cable and the wire pattern, it might be possible for some cable geometries to be somewhat porous. The models tested in this study would not represent this type of cable.

Models for each of the cables and the circular cylinder were fabricated. Table 1 is a summary of the models used for this test program. The nominal and actual diameters were taken from Horton et.al.[1987] and since the models

tested were cast directly from their original steel cables these values were used to describe the cable size. The model lengths defined in Table 1 were determined by the two foot square cross section of the wind tunnel.

The stiffness of the resulting wind tunnel models was then a function of the internal support rod and the epoxy shell. An effective stiffness for each model was determined by simply supporting each model near the end in a horizontal plane and measuring the vertical deflection of the midpoint. The midpoint deflection was due to the uniform weight distribution and was used to estimate an effective EI for the cable models. EI is the product of the modulus of elasticity of the material and the second area moment of inertia of the cable cross section. Table 1 includes the weight per length and the midpoint deflections for each model for a cable length of 5.85 ft.. This length corresponds to the longest cable model tested. These values of EI were then used to estimate the first bending natural frequency for a uniform, simply supported beam and these estimates are also included in Table 1. As will be shown later in the report, these frequencies are well below the observed shedding frequencies for the tests conducted in this study. Static deformation of the models was only considered significant for the 20° cable angle case and was corrected as discussed in the following sections.

This approach for fabricating the wind tunnel models has proven quite efficient and in the future may allow for some special features for these models. If the hollow center shaft is used then the models can be fit with surface pressure taps and surface pressure distributions developed. This method could also allow for the instrumentation of the models with miniature surface pressure transducers which could be used to make dynamic or unsteady surface pressure measurements. The models may also allow for the introduction of smoke tracers such as titanium tetrachloride, see Visser,Nelson and Ng [1988], at the surface of the model. Though these modifications were not employed in the current models, the potential for modifying these models or fabricating additional models using the same methods does exist.

3. EXPERIMENTAL FACILITIES AND INSTRUMENTATION

The series of experiments described in this test report were conducted at the University of Notre Dame Aerospace Laboratory. The wind tunnels used for the testing are specifically designed for smoke flow visualization and have been used extensively for basic flow physics studies. Separate test sections were used for the quantitative hot wire tests and the qualitative flow visualization studies. For both tests, the full scale cable models described in the previous section were used. The hot wire anemometry results were analyzed on-line using a digital dynamic signal analyzer. A majority of the flow visualization photographs were taken using a 35 mm camera and some results were analyzed using a digitizer and a photographic enlarger.

3.1 Wind Tunnels

The wind tunnel used in the experiments was a low turbulence, subsonic wind tunnel located at the University of Notre Dame Aerospace Laboratory. The tunnel is an indraft, open circuit type which exhausts to the atmosphere as illustrated in Figure 7. The inlet of the tunnel consists of a 24:1 area contraction with 12 anti-turbulence screens located just upstream of the inlet. This provides a near uniform freestream velocity profile in the test section with a turbulence intensity of less than 0.1%. A test section of 2 ft by 2 ft cross section fits into the tunnel. A special extended test section was used for these tests due to the length of the cable model at the 20° cable angle. Downstream of the test section is a flow restrictor consisting of a square box filled with straw tubes held in place by screens at either end. The large pressure drop across the flow restrictor reduces the effect of outside disturbances on the flow in the test section. The flow is then expanded through a diffuser. The diffuser has a 4.2° angle of divergence and is 13.78 ft long. The tunnel is powered by an eight-bladed 3.94 ft diameter fan directly coupled to an 18.6 kW AC induction motor located at the end of the diffuser section. The flow velocity is monitored through a digital differential manometer which displays the velocity measured by the pitot tube placed in the flow.

3.2 Model Support Systems

The two basic tests described in this report required the development of two wind tunnel test sections. One section was used for the flow visualization tests and included the capabilities for smoke sheet generation , windows for strobe and laser lighting and windows for still and high speed photography. The other was used for the hot wire measurements in the wake of the stranded cable. Figures 8 and 9 are schematics for these two test sections. The cables were mounted from either the front wall or the floor of the test section depending upon the requirements of the particular test. The preferred orientation placed the model in an inclined configuration since any model curvature due to model weight would be confined to a vertical plane although this configuration could not be used for all the tests. For the cases where the horizontal configuration was used, a mid span support in the form of a thin wire was used to eliminate the curvature of the model for the $\beta = 20°$ orientation.

The visualization section is shown in Figure 8. The views of the test section in this figure are from the front of the test section, with a viewpoint slightly below the floor downstream of the end of the test section. For the inclined configuration the models were supported from a pivot on the bottom of the section and were set to the required orientation relative to the free stream and then passed out of the top of the test section at an appropriately positioned port. For the horizontal configuration the models were supported by a special fitting which was the same diameter as the model and was glued to the front glass wall of the test section. This allowed for an unobstructed view down the axis of the model. This test section was also equipped with a smoke wire and smoke wire coating device upstream of the model and in the same vertical plane as the model. Figure 10 illustrates a schematic of the smoke wire assembly and wire coating apparatus. The smoke wire was used for both the planview and side view visualization studies so it was used with the model in both the inclined and horizontal configurations. For the planview studies the models were illuminated through the bottom of the test section and photographed through the front window of the test section. For the sideview and axial view studies, the model was placed in the horizontal configuration and again illuminated through the bottom of the test section. In both cases the strobe lamps were located outside the bottom wall facing up. Aluminum sheets placed on the bottom wall inside the test section were used to create a 3/4 inch slit to

illuminate the smoke sheet. This isolated the lighting on the smoke sheet and minimized reflections from the back wall of the tunnel.

The hot wire section is shown in Figure 9. The model was supported in a yoke on the front wall of the section and was allowed to pivot to the required orientation relative to the free stream and then pass out of the test section on the rear wall through an appropriately positioned port. The entire top wall of the tunnel is free to traverse with the hot wire. The wire was free to move laterally, longitudinally and vertically in the wind tunnel so that complete wake surveys could be developed. The traversing system used a Digital Equipment Corporation PDP 11/23 computer to control movement of the probe in the streamwise, spanwise and vertical directions. The test section was originally used by Payne[1985] and more information about the test section can be found in this reference. The system was found to have an overall positional accuracy of approximately ±1 mm. A second fixed hot wire was supported from the bottom of the test section and remained stationary relative to the cable during the tests.

3.3 Flow Visualization

One of the primary goals of this test program was to use flow visualization to describe the flow field near the yawed, stranded cables. This required the development of lighting and photographic methods suitable for this complex, three dimensional flow field. During the initial phases of the effort the following viewing methods and visualization methods were used.

1. Smoke wire tracer, planform view
2. Smoke wire tracer, axial view
3. Smoke wire tracer, side view
4. Kerosene smoke tracer, axial view
5. Kerosene smoke tracer, side view

These tests were conducted using flood , laser sheet and stroboscopic lighting. Data were collected with both 35mm camera records and video tape recording. These tests served as a basis for the flow visualization tests conducted as part of this research program.

3.3.1 Smoke Generation

Two flow visualization techniques were used, namely, the smoke-wire technique, see Batill and Mueller [1981] and the kerosene smoke technique, see Mueller [1981]. The primary benefit of the smoke wire technique is that it

produces very fine streaklines that provides excellent detail in the flow field. This however requires a synchronized camera and strobe system because the smoke only lasts a few seconds. The smoke-wire technique is limited to velocities less than 25 ft/sec. The kerosene smoke technique provides a continuous and more dense smoke at the higher speeds. It does not however afford the detail that the smoke wire technique provides.

The smoke-wire technique requires the introduction of a fine stainless steel wire into the flow upstream of the region which is to be marked with the smoke tracer. For this application a 0.003 inch diameter wire was positioned vertically upstream of the model as illustrated in Figure 10. The wire was coated with mineral oil and is heated by passing a controlled electric current through the wire for a prescribed time interval. The wire was pre-tensioned to approximately 11 oz. to compensate for the thermal expansion when the wire is heated. Due to surface tension, the oil "beads" on the wire and when heated fine filaments of smoke are emitted from each bead and form a sheet of smoke in a flow. The ends of the thin wire are attached to brackets that move laterally so that the desired location of the smoke sheet can be achieved. This is illustrated in the side view of Figure 10.

Event timing for use of the smoke wire is critical and a specially designed timing and control system was used for these experiments, see Batill and Mueller [1980]. A controllable DC current can be passed through the thin wire for a variable length of time. Simultaneously, a signal can be sent to the camera with a variable delay to trigger a photograph. The delay is important because after current application, it takes a fraction of a second for a good quality smoke sheet to appear. The camera then is activated and simultaneously triggers a flash from the strobes.

The oiling mechanism in Figure 10 consists of a cotton "swab" which is moistened with oil and slides up and down the smoke-wire so that a thin uniform coating of oil can be deposited on the wire. The cotton "swab" is attached to a support that goes through the top wall of the test section and is pulled up or down by a cord that is attached to a pulley. The oiler can be lowered down and pulled up by the experimenter from below and outside the test section. After an oiling, the oiler support is removed from the test section through the top wall opening. The opening is closed by a spring loaded door so as not to affect the flow in the test section.

The kerosene smoke method was specifically developed for use in the Notre Dame Aerospace Laboratory. The short high contraction ratio inlet on the wind tunnel is designed in order to provide a means whereby smoke generated outside of the wind tunnel can be rapidly introduced into the test section with a minimum amount of diffusion. The method uses the smoke generator and rake shown in Figure 11. Smoke filaments are injected by this equipment at the entrance to the inlet of the wind tunnel just upstream of the anti-turbulence screens. The smoke generator consists of 4 kerosene reservoirs which drip kerosene onto electrical strip heaters. The 750 watt heating elements cause the kerosene to evaporate and produce a dense white smoke. The smoke is then cooled and filtered and distributed using the smoke rake. The number and position of the smoke filaments is controlled by positioning the smoke rake. This method of flow visualization is best suited for speeds in excess of approximately 15 ft/sec and was used for the high speed testing, approximately 45 ft/sec, during the test described in this report.

As briefly mentioned earlier, a third method for smoke generation was also considered. This involved using the titanium tetrachloride $TiCl_4$ smoke vapor method described by Visser, et.al. [1988]. A thin stainless steel tube was mounted to the downstream side of one of the cable models and the $TiCl_4$ vapor was introduced into the wake of the cable. This method showed good promise and might be considered for future visualization studies. No photographs were taken using this technique.

3.3.2 Lighting and Photography

Three possible lighting techniques were evaluated as part of this test program: flood, laser sheet and stroboscopic. Flood lighting was adequate although there were certain limitations. The high intensities required in order to achieve adequate illumination of the smoke tracers, for either smoke generation technique, creates a considerable heating problem. Since much of the interior of the wind tunnel is black to improve photographic contrast, the continuous high intensity flood lighting can result in significant temperature increases and there have been cases where the walls of the test section have begun to "smoke". Controlling the position of the flood lighting was also difficult and reflected light from the glass front wall or the "black" back wall would degrade the contrast of the flow visualization records.

Laser sheet lighting similar to the technique described by Nelson [1983] was also evaluated. Both vertical and horizontal light sheets were developed but the width of the light sheet and the orientation of the smoke relative to the model did not provide adequate illumination of the near model flow field. Though this technique is well suited for certain applications, it was not used for the detailed flow visualization studies in this report.

The stroboscopic lighting technique proved to be the most suitable for this application. Four GenRad Strobolume Model 1540 strobe set in a single flash mode were used to provide lighting for the flow visualization photographs. The models were illuminated through the bottom of the test section and photographed through the front window of the test section. For the sideview and axial view studies, the model was placed in the horizontal configuration and again illuminated through the bottom of the test section. In both cases the strobe lamps were located outside the bottom wall facing up. Aluminum sheets placed on the bottom wall inside the test section, created a sheet of light to illuminate the vertical plane containing the smoke. This isolated the lighting on the smoke sheet and minimized reflections from the back wall of the tunnel.

Both the side view and axial view photographs were taken using the smoke-wire and kerosene smoke tracers and the models were placed in the horizontal configuration as illustrated in Figure 8. The smoke was introduced upstream of the model using both methods in a vertical plane at or near the centerline of the wind tunnel. The smoke then convected as a vertical sheet down the tunnel and impinged on the model. The side view photographs were taken by focusing on this vertical sheet of smoke as it interacted with the model. The focal plane of the camera was the vertical smoke sheet. The axial view photographs were taken by aligning the camera along the longitudinal axis of the cable. For the axial views the smoke sheet would pass through the focal plane of the camera and thus would only be in focus in the region immediately adjacent to the model. This created some distortion of the viewing field.

Plan views of the model were taken using the smoke-wire technique since it provided a nearly uniform sheet of smoke. The model was supported in the inclined configuration and illuminated with the strobes from below. The smoke sheet was in a vertical plane as it convected down the tunnel and the camera was aligned normal to this vertical sheet and focused on the sheet.

The camera used for all the still photography was a 35 mm Nikon FM2 with a motor drive and mounted on a tripod. The lens used was a standard 50

mm f/1.4 lens. Two types of film were used during this study. Kodak TMAX 400 and a more recent product TMAX P3200 were used. The faster film, TMAX P3200, was preferred since it allowed for a higher f stop and thus a greater depth of field for most of the application.

Video records were obtained for the smoke wire and kerosene tracers and indicated potential for future work. The video proved unsuitable for the smoke-wire tracers since the event was so rapid (approximately 1 sec) and the proper electronics necessary to synchronize the strobes, video and the smoke-wire were not developed. High speed motion picture records were also taken using a Milliken DBM-5 camera at a frame rate of 64 frames per second and the kerosene smoke tracers. The camera was coordinated with the strobe flash and Eastman 7224 4-X Negative film was used. Higher frame rates were tried (128 fps) but the strobe flash intensities are significantly reduced at the higher flash rate and they provided inadequate illumination.

3.3.3 Quantitative Evaluation of Visualization Results

Attempts were made to extract quantitative as well as qualitative information from the flow visualization records. Plan view photographs were used to attempt to identify the orientation of the wake relative to the cable model. Side view photographs were used to identify the growth of the wake as it convects downstream and the spacing of the vortices in the wake.

The 35mm negatives were projected on an Itek Wayne-George Division T36/36-10 X-Y Coordinate Digital Converter. This consisted of a table where a pointer can be positioned at a desired point in the projected image. The Itek Wayne-George Division data readout system monitors the location of the pointer and displays the X and Y coordinates of the desired point. The data readout system was connected to a MINC 11 Digital Equipment Corporation computer. When a desired point on the projected image has been selected, the user triggers the Wayne-George system to send the X-Y readings of the point to the MINC 11 computer. Data points from the photographs are then stored and/or reduced by the MINC 11 computer.

The side view photographs were made with readily identifiable reference marks placed in the viewing field. The reference marks were used to align the photographs and indicate the position at which the smoke sheet impinged on the model. A photographic enlarger of Model 470 Federal Mfg. & Eng'g. Corp. was used to project the images on the digitizing table. The enlarger's capability

of adjusting the image size was used to compare an image from flow visualization photographs with a reference scale.

3.4 Hot Wire Measurements

Two DANTEC hot wire probes of Type 55P11 were used for the fixed and traversing probes. The two probes were operated by a TSI Inc. Intelligent Flow Analyzer 100 anemometry system. The anemometry system was calibrated with the aid of an auxiliary Nicolet 4094 digital oscilloscope. The two signals from the IFA 100 were then processed by a Scientific-Atlanta SD 380 signal analyzer. The spectrum, auto-correlation and cross-correlation outputs were displayed and plotted with a Hewlett-Packard 7470A plotter. The data acquisition system is illustrated in Figure 12.

The hot wire set-up was used to collect the spectrum and cross-correlation data. Two hot wire probes were used: one which is fixed and another one which traverses with 3 degrees of freedom. The signals are acquired using an integrated hot wire anemometry system and sent to a digital signal analyzer where the spectrum and cross-correlation data were generated.

3.4.1 Hot-Wire Data Acquisition

The hot wire anemometry system was calibrated with an overheat ratio of 1.8. A square wave test was done on the IFA for optimum frequency response and an overshoot of less than 13% was maintained. Data collected from the system was processed by the SD 380 and presented in the form of plots of the spectrum and the cross-correlation functions. For the spectrum measurements, the frequency ranges used were 400 Hz and 1000 Hz. The corresponding frequency resolutions were 1 Hz and 2.5 Hz respectively, and the sampling rates were 1,024 and 2,564 points per sec respectively. For the cross correlation measurements, the frequency ranges used were 2 kHz and 4kHz and the corresponding sampling rates were 5,128 and 10,309 points per sec respectively.

Two vortex series of measurements were performed. The first series of tests were spectrum measurements and involved all six models with the probe at three different locations. This was done at the low speed of 18.7 fps only. In the second series of tests both spectrum and cross-correlation measurements were made but it involved only the cylinder, 4x7 cable and the 6x25 cable. The

latter was done at the two speeds of 18.7 fps and 44.9 fps and at different spanwise locations.

For the first series of tests only the traversing probe was used. The probe was positioned at three locations in the vertical plane midway between the front and back walls. The three locations are shown in Figure 13. The tests were done at three positions so that comparison of the measurements could be made. The positions were also located such that the hot wire will only sense the frequency of the upper row of vortices without interference from the lower row. At each location, the test was done for each cable angle of 90°, 60°, 40° and 20°; and for each model. The spectrum for each case was obtained and the dominant frequency determined from the graphical data. Using the SD 380's averaging capability, 200 spectra were averaged to obtain the spectrum.

Using the same hot wire set-up the second set of tests were performed. For these tests the vortex shedding frequency was taken along with the time shift/cross-correlation measurements. The traversing hot wire probe was positioned at two or three spanwise locations, with the fixed probe taken as the reference. Both probes maintained a distance of 3.75 in. downstream and 1.25 in. up from the center of the cable cross-section. This location is equivalent to position (6,2) *in Figure 13.*

The spanwise locations were determined by measuring the peak-to-peak distance in a cable and designating it as the unit span. The reference point at which the fixed probe was located was selected such that the fixed probe was downstream and above a peak. Since there were no peaks in a cylinder, a unit span of 1.52 in. was taken. The unit span for the 4x7 cable was 1.30 in. and that for the 6x25 cable was 0.65 in. The distances between the fixed and traversing probes were then designated by per cent of the unit span. The cylinder had the traversing probe at 100 % and 200% away from the fixed probe while the 4x7 and 6x25 cables had the traversing probe at 50%, 100%, and 150% away from the fixed probe. At 20° cable angle however, the small unit span of the 6x25 cable gave some difficulty in placing the traversing probe at 50% and 100% spanwise locations. In order to have data at four locations, the 200% and 250% spanwise locations were added instead. For each of the models and velocities, and for each of the spanwise locations, the spectrum and cross-correlation functions were obtained.

The fixed probe always provided the spectrum at the reference spanwise location. At the same reference location, the cross-correlation became the auto-

correlation function of the fixed probe signal. At the other spanwise locations, the traversing probe signal gave the spectrum, while the cross-correlation function was that of the traversing probe signal against the fixed probe signal. Plots of the spectrum and the cross-correlation functions were generated from the SD 380 for each case. The dominant peak in the spectrum was marked and the corresponding frequency noted as the shedding frequency. In the cross-correlation, the peak nearest zero was marked and the corresponding timeshift noted as timeshift between the traversing probe and the fixed probe signals.

4. DISCUSSION OF RESULTS

4.1 Preliminary Phase Flow Visualization

A preliminary series of flow visualization experiments were conducted in order to qualitatively evaluate the difference between each of the cable models and to provide data for use in selection of two models for more detailed quantitative study. A majority of these results were acquired using the smoke-wire tracer technique at a Reynolds number of approximately 6000 based on the cable diameter of 0.625 inches. Appendix A contains a complete set of photographs for each of the six models in both plan view and side view for a free stream velocity of 18.7 ft/sec. Some of the photographs appearing in Appendix A also appear as Figures in the report when appropriate.

Figures 14-16 illustrate two of the basic types of visualization data and represent the results achieved on the baseline cylinder configuration. Figure 14 shows both a planform view and axial view of the cylinder model for a cable angle of 90°, with the smoke-wire tracer at a speed of 18.8 ft/sec (Re = 6000). For the cable angle of 90° the side view and the axial view are the same. Figures 15 and 16 show similar results for the cylinder at cable angle of 60° and 20° respectively. In each case for the planview, the smoke wire was positioned as closely as possible to the centerline of the model. As can be seen from the photographs, all of the smoke filaments appear to pass to the "front" of the model . It is not possible to "split" the filaments with the model, but by varying the lateral position of the wire, the vertical smoke sheet can be placed as close as possible to the model such that all of the smoke filaments pass to the same side of the model. The periodic shedding of vorticity into the wake is clearly visible in each photograph. The near two-dimensional character of the flow is also visible in the plan view photographs. Since the models extend from tunnel wall to tunnel wall, the flow near the ends of the models has been influenced by the tunnel boundary layer. The location of the spanwise vortices is indicated by the regions of dense smoke in the plan view photographs. These regions are reasonably uniform across the wind tunnel. In Figure 14, which shows the complete model, there is a significant modification of this structure near the top and bottom wall. The region of disturbance appears to extend approximately 2 inches into the tunnel which implies that there are approximately 20 inches of near uniform flow along the span of the model. The four "bright " regions along

the floor of the tunnel are created by the positioning of the four strobe lights, The regions in between the bright spots are not devoid of smoke but appear dark because the lighting is nonuniform this close to the lower wall. Figures 15 and 16 also indicate some of the limitations associated with the axial views. Although good flow detail can be achieved quite near the model as the model is yawed, in particular to the 20° cable angle, there is significant distortion of the image as the sheet of smoke moves into and out of the focal plane of the camera. A majority of the results presented on the cables are therefore limited to the side view photographs where this distortion is eliminated.

Figures 17 to 19 present side views for the cylinder model at the low and high speed test points (Re = 6000 and 14,600) using the two visualization techniques for comparison for cable angles of 90°, 60° and 20°. The four white "triangles" in the photographs are used as alignment and spatial reference marks to identify the location where the flow impinges on the models. The kerosene smoke tracer is introduced upstream of the tunnel contraction section as five single filaments. The filaments are approximately 1/2 inches in diameter when they reach the model. They are positioned in a manner such that two of the filaments pass over the top of the model and two pass under and the middle filament is "split" by the model. As the model is yawed, Figures 18 and 19, the point at which the smoke sheet impinges on the model also moves downstream and the near wake region is somewhat masked by the light reflected from the model. This is one of the disadvantages of the side view but since the overall wake remains in focus for the entire photograph it was determined that this view provided the most useful information.

The flow field associated with the circular cylinder is consistent with all previous studies on this configuration. The flow about the cylinder is laminar and transition takes place in the wake. Vorticity shed from the upper and lower separation points forms into discrete vortices of opposing sense in the wake. The transition in the wake is evident in the axial view photographs of Figures 14-16 and the presence of discrete vortices is present over this wide range of yaw angles. The vortex dominated wake is evident in the side views in Figures 17-19 although the spacing appears to be modified for the yawed cylinder. For the circular cylinder there appears to be no noticeable variation in the form or structure of the wake region for this range of Reynolds number as would be expected.

4.1.1 Plan view and Side view Results, All Models, Re ≈ 6,000

As indicated, Appendix A contains the visualization results for each of the cable models. The plan view for each of the models and test conditions are presented first and are followed by the side view photographs. The plan view photographs indicate a similar flow structure for each of the models but with some noticeable differences. The 1x19 and the 7x7 cables show a similar type of transition occurring in the wake shear layer with predominantly two dimensional behavior over the center section of the model. The transition appears to move somewhat closer to the cable for the 7x7 model. Some care must be exercised in evaluating these photographs since they are all taken at different points in the "shedding cycle" and the transition regions are not fixed in space.

The 3x19 cable is very coarse and does demonstrate a somewhat different wake behavior. Close inspection of the near wake region for the 60° cable angle shows a very definite spanwise variation in the wake formation which correlates very well with the cable geometry. This correlation is not as apparent for the 40° and 20° cable angles. There are two possible explanations. First, the spanwise periodicity doesn't occur for these cable angles, or second, since it was very difficult to position the smoke-wire so that the smoke sheet impinged on the model at exactly the same point, particularly for the smaller cable angles, the periodicity is not shown in the photograph. Although an attempt was made to position the smoke-wire as accurately as possible, the smoke sheet appears to be farther away from the model near the downstream end of the model for both the 40° and 20° cases . The 3x19 cable does not display the same regular vortex formation in the plan views and it would be very difficult to identify a spanwise filament from the photographs.

The 4x7 serrated model also presents a very coarse profile to the oncoming flow. The wake structure is much less apparent for the 4x7 cable than for the other configurations. Again close inspection of the near wake region at the 60° cable angle appears to indicate a spanwise periodicity, particularly near the lower part of the cable where the smoke appears to be closer to the cable surface. In contrast to the 3x19 cable, the structure for the 4x7 cable repeats every two strands. It is difficult to draw any significant conclusions from these two observations but there is an indication that the near wake structure is influenced by the cable configuration.

The side view photographs provide additional detail on the cable wake structure. The trends in the wake characteristics are similar for the cylinder, 1x19, 7x7 and 6x25 configurations for all yaw angles. At the 90° cable angle the formation of the alternating vortex wake is apparent and the wake width decreases and vortex spacing increases as the cable angle decreases. The diffusion and mixing of the smoke streaklines does seem to be a bit more rapid for the cable designs than for the circular cylinder.

The wake structures for the 3x19 and the 4x7 configurations are somewhat different than the other configurations. The vortex structure in the wake is not as distinct. The near field wake, within three to five cable diameters appears to be thinner than the other configurations. At the 20° cable angle, these two configurations developed wakes which were narrower and again appeared to take longer to develop. One anomaly was the behavior of the 4x7 cable at the 60° cable angle. Unlike this cable at the other angles, the wake did grow quite rapidly and the vortices in the wake appear to be almost aligned, not staggered as in the other cases.

No significant streamline curvature was detected from the side view photographs which might have indicated a sense or presence of a net lift force on the stranded cables.

4.2 Detailed Cable Flow Studies

The preliminary studies discussed above were used as a basis to select two of the cable configurations for more detailed study. These cables were selected based on their current use in towed marine systems.

4.2.1 Cylinder, 4x7 and 6x25 Cable Flow Fields

Additional visualization results were acquired for the circular cylinder, 6x25 and 4x7 cable models. This primarily involved conducting a second series of tests at the higher Reynolds number. Figures 20 - 27 compare the side view photographs for the 6x25 and 4x7 cables at each cable angle and at Reynolds numbers of approximately 6000 and 14,600 , corresponding to air speeds of 18.7 and 44.9 ft/sec respectively. This speed range corresponds to an approximate speed range of 0.75 to 1.80 kts for the same cable in water. The cable performance over this Reynolds number range is similar to that discussed in the previous section. The vortex spacing is quite comparable at a given cable angle, as one would expect if the Strouhal number is constant over this

Reynolds number range. This is most apparent in the $\beta = 90°$ case. The 4x7 cable exhibits the reduced wake width and an extended formation length with a less regular wake structure at both Reynolds numbers.

An attempt was made to determine if the flow visualization would indicate a dependence upon the specific cross section at a given cable angle. This was accomplished by rotating the cable while keeping the sheet of the smoke fixed. This is the same as the variation noted in the cross section shape when the computer simulation of the cable profile was discussed earlier in the report. This study was conducted using the side view photographs at the low Reynolds number. The results indicated no appreciable variation in the flow patterns as a function of the cable rotation from these photographs. The detailed near wake structure is not readily apparent in the side view photographs and though the plan view photographs did imply some spanwise periodicity for the 4x7 cable, this structure was not apparent in the side view photographs.

4.2.2 Quantitative Evaluation of Photographic Data

Quantitative information about the wake structure and in particular about the vortex shedding characteristics was extracted from the flow visualization photographs. This was done in order to provide a means of comparison with the hot wire results as well as to provide additional information on the flow field. Three separate studies were performed using the visualization data discussed in the previous section. These studies included a measurement of the shedding angle, a determination of the wake width as a function of downstream distance and an estimate of the convective speed of the vortices in the wake.

The shedding angle is defined as the angle between an assumed straight vortex filament convecting in the wake of the cable and the velocity vector in the plan view and is shown schematically in Figure 28. Ramberg [1979] discussed the dependence of shedding angle on cable angle in his flow visualization data for yawed circular cylinders. However, the variation in shedding angles with cable angle, which is an additional indication of the three dimensional character of the wake flow, is not well understood. Plan view flow visualization photographs such as that in Figure 14 show filaments which are not straight lines. The flow is quite complex and the orientation of the vortex filaments appears to be a strong function of the upstream flow and end conditions on these finite length cables. For the purpose of this analysis, a straight line filament was assumed and the data from the photographs was

developed by fitting a line through a number of points along a given filament. This information was collected for the circular cylinder and the 6x25 cable since the wake structure was reasonably distinct for these two configurations. The first three filaments downstream of the model were identified for each cable angle. The angle associated with a straight line fit to each filament is given in Table II along with an estimate of the error associated with this measurement. A summary plot of the shedding angle vs. cable angle is also shown in Figure 29. For the 90°, 60° and 40° cable angles the shedding angle is equal to the cable angle, within the error bounds on this data. For the 20° case there is a marked difference between the shedding angle and the cable angle. The error bars shown are the standard deviation of the sample population of 12 filaments.

Another consideration was associated with the wake development and size. The wake generally consisted of the vortex formation region and a transition region. The formation region was composed of well defined turbulent vortices of increasing size. This region generally had 2 to 4 readily identifiable vortices in the side view photographs before rapid dissipation to turbulence was observed.

Again, though this data was quantitative, it is still subjective and should only provide a rough basis of comparison. Typical wake profiles are shown schematically in Figure 30. The average width of profiles like these were obtained and the results are given in Table III for the circular cylinder, 4x7 and 6x25 cables at both low and high Reynolds numbers. The 4x7 cable has generally a thinner wake width as compared to the cylinder and 6x25 cable as was discussed earlier with the simple qualitative comparison of the side view photographs. This appears to be due to the generally longer formation region of the 4x7 cable. The cylinder and the 6x25 cable have a short formation region followed by an unstable region with 2 to 4 turbulent vortices before total turbulence is observed. In the 4x7 cable wake, there is no apparent unstable region. Right after formation, the vortices dissipate very rapidly. This may be a result of the rougher cable surface on the 4x7 cable. For the smaller cable angles there were situations in which it was very difficult to identify the position of coherent vortices in the wake or cases with very irregular vortex spacings. This was more frequently observed in the 4x7 cases. Table III indicates that the spacing was not a function of Reynolds number for the cable angles of 90° and 60°, although there appeared to be some variation with Reynolds number at the

lower cable angles. This result should be considered preliminary due to the highly subjective nature of this data.

The average vortex spacing discussed in the previous paragraph was used with the shedding frequency results (discussed in the next section), to estimate the convective speed of the vortices in the wake. The results are presented in Table IV. The vortex convective velocity was calculated by multiplying the average spacing by the shedding frequency. Schaefer and Eskinazi [1958] asserts a value for the vortex center velocity to be 0.91 times the freestream velocity. This would mean 17.0 fps for the low speed and 40.9 fps for the high speed. Results in Table IV show vortex center velocities in reasonable agreement with these values.

4.3 Hot Wire Measurements : Cylinder, 4x7 and 6x25 Cable Models

All models were tested to obtain the vortex shedding characteristics at the flow velocity of 18.7 fps. Table V shows the shedding frequencies of all models for this test condition as well as the calculated Strouhal number based on both free stream velocity and normal velocity. Only the 4x7 , 6x25 and the circular cylinder were tested at the higher velocity of 44.9 ft/sec. These results are presented in the form of the frequency spectra in Appendix B. These same three models were used to study the dependence of shedding frequency on spanwise orientation along the cable and these results are summarized in Table VI for both Reynolds numbers.

4.3.1 Wake Spectrum

The hot wire data shown in Appendix B gives an indication of the character of the wake. At cable angles of 90° the peak in the frequency spectrum is very well defined, particularly at the lower speed, for the cylinder and the 6x25 cable and somewhat less so for the 4x7 cable. As the cable angles decrease, the shedding frequency decreases except in the case of the 4x7 cable which actually shows a marked increase in the shedding frequency at 60° cable angle at both Reynolds numbers .

4.3.2 Strouhal Number

The cables show a generally higher Strouhal number than the cylinder at 20°, 40°, and 60° cable angles. For the 90° case, the cables generally have lower Strouhal numbers than the cylinder. The Strouhal number is plotted

against the cable angle in Figure 31. The line drawn is the curve that was fit to the data points for the circular cylinder. The 4x7 cable has the greatest Strouhal number of all of the models for a cable angle of 20° while it has the lowest Strouhal number at 90°. Horton, et. al. [1987] obtained almost the same results for the yawed cables in their experiments with cables free to vibrate. However their values for the 90° case indicate that the cables have higher values compared to the cylinder. This difference may be attributed to the flexibility of their models or to the difference in boundary conditions.

It has been generally observed that the vortex shedding frequency as well as the Strouhal number, based on free stream velocity, decreases as the cable angle is decreased. In order to evaluate if this variation was consistent with the Independence Principle, a modified Strouhal number was computed by replacing the free stream velocity V with Vsin β. In so doing only the normal component of the velocity, which is Vsin β, is considered in computing the Strouhal number and the tangential component is neglected. The resulting modified Strouhal number, S_N, which is based on the normal component of velocity is plotted in Figure 32 . The plot shows that this modified Strouhal number does not remain constant for different cable angles. The values increase as the cable angle is decreased. Thus for the conditions set in this test, the Independence Principle fails. Therefore, the tangential component and other three dimensional effects influences the vortex shedding from yawed cables.

The above result supports the conclusion of Ramberg [1978] that the Independence Principle is not valid for rigid cylinders in general. He states that it is only valid for flows around rigid cylinders with special end conditions, and for the case of cylinders free to vibrate. Horton, et. al. [1987] used test conditions similar to that of this study, except that their cables are free to vibrate and found that the Independence Principle applies for their measurements. It is however worth pointing out that the Independence Principle may still be reasonable approximation for the cylinder model except for the 20° cable angle. These results suggests that the tangential component of the velocity may have a greater effect on the Strouhal number for the stranded cables than on the Strouhal number for the circular cylinder.

The shedding frequencies were measured for two different freestream velocities of 18.7 fps and 44.9 fps corresponding to approximately 6,000 and 14,600 Re based on actual diameter. The measurements were obtained with

the cylinder model, the 4x7 cable, and the 6x25 cable and the results are presented in Table VI. It can be observed that shedding frequencies are higher for the high velocity case. Corresponding Strouhal numbers were calculated based on freestream velocity and are presented in Table VII. From this data, the plots in Figure 33 were developed. Shown on each plot are the Strouhal number data for both the high and low velocities. There appears to be no significant dependence on Reynolds number in this range.

The vortex shedding frequencies were measured for at least three different spanwise locations for three models: the cylinder, the 4x7 cable and the 6x25 cable. The Strouhal number was calculated and the results demonstrate that it is independent of the spanwise location. The plots for the Strouhal number vs. spanwise location for the cylinder, 4x7 and 6x25 cables are shown in Figure 34. The plots exhibit no apparent variation in Strouhal number as the hot wire is traversed spanwise.

4.3.3 Spanwise Measurements - Wake Coherence

The cross-correlation information generated by the signal analyzer is presented in detail in Appendix C. The input signals were from the two probes in the wake at different spanwise locations. The plots showed a strongly correlated periodic signal indicating two very similar input signals of periodic nature. The frequency of the plotted periodic signal was calculated by measuring the average period and then taking the reciprocal. The calculated frequency agreed very well with the measured shedding frequency from the spectrum analysis.

The plots also showed a time shift especially those for the yawed cases. The presence of a time shift means that there is a temporal shift in the two periodic signals. Since the two probes were located at the same relative distance behind the cable for both yawed and unyawed cases, a time shift implies a spanwise variation in the flow field. The time shift data were taken by measuring the time difference of the nearest peak from zero. For the configuration used in this test, a positive time shift means that the traversing probe signal is lagging the fixed probe signal. A negative time shift means that the traversing probe signal leads that of the fixed probe. Table VIII shows the time shift in seconds for all the test cases.

All the data indicated a positive time shift for the yawed cases. The 90° case generally resulted in much smaller time shifts with several cases having

very small negative values. The time shifts indicated for the "zero span" spacing between the two probes are actually the auto-correlation for the fixed probe. Ideally, these time shifts must be zero since there should be no phase shift in a signal compared to itself. Again, the values are very small and they can be considered as zero. The general trend in the time shift is that it increases as the cable angle is decreased. Another general trend is that as the spanwise distance between probes is increased, the time shift increases, seemingly in a linear manner. The time shift can be interpreted as being caused by difference between the cable angle and the shedding angle . In Figure 35, Cases (a) and (b) illustrate the two possible ways the filaments could shed. In Case (a), the shedding angle is greater than the cable angle. Here the vortex filament strikes probe A first before hitting probe B. Therefore, signal B would be lagging and the resulting time shift would be positive. In Case (b), the shedding angle is smaller than the cable angle. Signal B would lead signal A, resulting in a negative time shift. Since for all yawed cases the time shifts are positive, Case (a) appears to be the way the filaments are shed.

In Figure 36, a model is yawed at a cable angle β, the vortex filament along A' B' which is convecting in the downstream direction at an angle α which is greater than β. Point A is the location of the fixed probe, and B is the location of the moveable probe; and the distance between them is Δs. As the filament reaches A, B' will be in the position shown and differ from B by a distance Δx. The distance Δx, equal to B'B, can be approximated from the time shift data. It is assumed that if a signal is taken at B', it would be in-phase with A since both are on the same vortex filament. The distance B'B is therefore equal to the delay of the signal B with respect to A, which is the time shift Δt, multiplied by the vortex convective velocity V_C. The shedding angle α, is given by:

$$\alpha = \text{Arctan} \left[\Delta s \sin \beta / (\Delta s \cos \beta - \Delta x) \right]$$

The vortex convective velocity was not measured in this experiment. Schaefer and Eskinazi [1958] determined the vortex convective velocity using both analytic and experimental methods. The vortex convective velocity ratio is the vortex velocity divided by the freestream velocity. For a Re = 62, for which the wake is laminar, they calculated the ratio to be equal to 0.91. But the Re range of the current study is of the range 10^3 to 10^4, which is in the transition region. In this region, there was no sure way of knowing whether 0.91 is still

valid. The shedding angles were then calculated for different vortex convective velocity ratios ranging from 0.6 to 1.0. The calculated shedding angles were then compared with those obtained from the visualization data. It turned out that a ratio of 0.7 best matches the shedding angles at the 20° cable angle case. The calculated shedding angles are presented in Table IX. The Table shows quite good agreement among shedding angle values for different spanwise locations and freestream velocities. The average value for each model and cable angle case is summarized in Figure 37.

Figure 37 indicates a definite variation between the shedding angles and cable angles for the 60° and 40° cable angle cases. The digitized photographs showed filaments that are almost parallel to the model for these two cases. But with the greater amount of information available from the averaged cross-correlation data, the shedding angles calculated from the cross-correlation should be more accurate. Obviously the limitation associated with the selection of the convective velocity limits the use of this approach. For the 90° case, there is agreement in both methods that the filaments are generally shed parallel to the model.

5. CONCLUSIONS AND RECOMMENDATIONS

The results of an experimental investigation of the flow about stranded cables or wire ropes have been presented. The goal of the study was to improve the understanding of the flow field near the stranded cable and to develop additional insight into the mechanisms associated with the generation of fluid forces on the cables. Five rigid cable models and a cylinder were tested in a wind tunnel. The models represented full scale cable geometries and were yawed to four different cable angles (90°, 60°, 40° and 20°) and tested at Reynolds numbers in a range from 5,800 to 13,800 based on the cable diameter. Wind tunnel models were developed by casting epoxy replicas of actual stranded cables. The models provided excellent geometric defintion of the stranded cables and adequate strength and stiffness. This method of cable model fabrication may also allow for measurement of surface pressure distributions in future tests.

Smoke flow visualization and hot wire anemometry were used to collect both qualitative and quantitative information on the flow around the cables. The smoke-wire technique provided good detail on the flow field near the cables in both plan and side views. Axial views for the yawed cables were degraded by distortion of the image and the inability to properly focus on the smoke. The smoke-wire technique was limited to free stream velocities less than 25 ft/sec and the kerosene smoke filament method was used for the higher flow velocities. The kerosene method provided good quality visualization data for flow speeds up to 50 ft/sec although only side view visualization data was collected using this technique.

Photographs from the smoke-wire and the kerosene smoke flow visualization techniques were used to qualitatively evaluate the flow fields associated with each cable geometry. The following qualitative observations were made concerning the visualization results.

1. Though no special end treatments were considered for this series of wind tunnel tests, the tunnel boundary layers did not appear to significantly alter the free stream flow which was uniform for a majority of the span of the cables. The wind tunnel boundary layers did alter the flow near the ends of the cable models and the extent to which this may have altered the overall flow characteristics has not been determined.

2. The results achieved for the circular cylinder where consistent with those presented in the literature which may indicate that the end effects were not significant.

3. The overall wake structure was similar for the cylinder, 1x19, 7x7 and 6x25 models. There was a noticeable difference in the wake structure for the 3x19 and 4x7 cable models. This was primarily noted in the side view photographs.

4. The 3x19 and 4x7 configurations indicated a periodic variation in the formation region along the span of the cable which was aligned with the cable geometry. This periodic variation was not evident farther downstream in the wake.

5. As the cables were yawed to the flow, the wake width appeared to decrease with increased yaw, i.e., decreased cable angle.

6. There was no obvious indication in the visualization photographs that the yawed cables were developing steady lift such as the presence of significant streamline curvature. The sense of the steady lift could not be determined from the visualization data.

7. The cable geometry does influence the flow field about the stranded cable and this is evident in the visualization data.

8. There was no apparent variation in wake structure over the Reynolds number range considered in these tests.

The flow visualization photographs were also used to provide quantitative information such as shedding angles and vortex spacing wake widths. Though this data was limited by the accuracy with which distinct values could be identified on the visualization photographs, it did provide useful information.

9. The vortex shedding angle was similar to the cable angle for the 90°, 60° and 40° cable angles. The was a marked difference between the cable angle and the shedding angle for the 20° cable angle case.

10. The 4x7 cable had a noticeably thinner wake than the circular cylinder or 6x25 cable and apparently a longer formation region.

The hot-wire anemometer measurements provided additional quantitative information on the cable flow fields. The on-line data acquisition and processing of the hot wire data using the SD-380 Dynamic Signal Analyzer

allowed significant amounts of data to be collected and analyzed in a reasonable period of time. The spanwise variation in the wake structure was studied using two single wire, hot wire probes. The following observations were made concerning the hot wire data.

11. The characteristic shedding frequency was very evident in the wake frequency spectrum at a location six diameters downstream and two diameter normal to the wake centerline. The spectral content of the wake signal was well defined for the 90° cable angles for all models but was broader band for the lower cable angles.

12. The dominate shedding frequency, and thus Strouhal number based on free stream velocity, decreased with decreasing cable angle, except for the 4x7 cable which showed a marked increase in shedding frequency as the cable angle was reduced from 90° to 60°.

13. The Strouhal number based on free stream velocity was greater for the yawed cables than for the yawed circular cylinder but it was less for the unyawed cables than that of the unyawed cylinder.

14. The Strouhal number based on normal velocity is not independent of cable angle for any of the models tested for the range of 20° to 90° in cable angle. This implies that the Independence Principle does not apply to these configurations in this Reynolds number range.

15. There was no significant variation in shedding characteristic over this Reynolds number range.

16. The cross correlation data did not indicate any significant spanwise variations in the wake structure at the point at which the hot wire measurements were made.

These results illustrate the complexity of the stranded cable flow field. They compliment the results achieved in earlier experimental studies for similar cable geometries.

As in most research programs, experimentation often introduces as many questions as it provides answers. The following recommendations should be considered for future studies on the flow around stranded cables.

1. The effect of end treatment on the finite length cables must be addressed. Previous efforts have indicated the significant influence associated

with the end conditions on a finite length cable but most have been conducted in a different Reynolds number range. Endplates or other methods for isolation from the wind tunnel boundary layers should be considered.

2. Because of the unique model fabrication technique developed for this test program it would be possible to construct a new set of models which could be used to obtain mean and unsteady surface pressures. Base pressure could be measured along the span of the models for various cable geometries. Circumferential pressure distributions could be measured at selected spanwise stations. The mean pressures could be integrated to estimate the steady sectional lift component as a function of the cross flow geometry.

3. The hot wire surveys conducted as part of this program were limited to a small number of points in the wake. More detailed hot wire surveys should be undertaken, particularly closer to the model in the wake formation region, in order to gain additional insight into the wake formation process. Spanwise structure may be more readily apparent from such measurements.

4. Although the smoke-wire and kerosene smoke streaklines provided excellent flow photographs for the present study, consideration should be given to using the titanium tetrachloride technique. The advantage of using the $TiCl_4$ as a tracer is that it can be introduced into the flow from the surface of the model. This technique could provide additional information on the flow field in the formation region and highlight the spanwise flow near the surface of the models.

5. Since vibration of the stranded cables is of significant practical importance, both free and forced vibrations studies of the yawed stranded cable should be considered. The flow visualization methods developed in this effort could be modified to allow for the investigation of the unsteady flow associated with the dynamic cable motions. Conditional sampling of hot wire data could also be considered for the dynamic response measurements.

6. REFERENCES

Batill, S.M., Mueller, T.J., "Visualization of Transition in the Flow over an Airfoil Using the Smoke-Wire Technique", AIAA Journal, Vol.19, No.3, March 1981

Blevins, R. D., Flow-Induced Vibration, Van Nostrand Reinhold Company, New York, 1977, Ch. 3, p. 11-54

Chiu. W. S. and Lienhard, J. H., "On Real Fluid Flow Over Circular Cylinders," Transactions of the ASME, Journal of Basic Engineering, p. 851-857, December 1967

Dale, J., Mensel, H. and McCandless, J., "Dynamic Characteristics of Underwater Cables: Flow Induced Transverse Vibrations," Naval Air Development Center-AE-6620, 1966

Every, M. J., King, R., and Griffin, O. M., "Hydrodynamic Loads on Flexible Marine Structures Due to Vortex Shedding," Paper presented at the ASME Winter Annual Meeting, Fluids Engineering Division, November 1981

Gerrard, J. H., "The Mechanics of the Formation Region of Vortices Behind Bluff Bodies," Journal of Fluid Mechanics, Vol. 25, p. 401-413, 1966

Griffin, O. M., "Flow-Induced Oscillations of OTEC Mooring and Anchoring Cables: State of the Art," Naval Research Laboratory Memorandum Report 4766, May 1982

Hanson, A. R., "Vortex Shedding From Yawed Cylinders," AIAA Journal, Vol. 4, No. 4, p.738-740, April 1966

Horton, K. J. et. al., "Measurement of the Hydrodynamic Force and Strum Characteristics of Stranded Cables," Naval Coastal Systems Center Technical Memorandum 471-87, December 1987

Horvath, T. J., Jones, G. S. and Stainback, P. C., "Coherent Shedding from a Circular Cylinder at Critical, Supercritical, and Transcritical Reynolds Numbers," Society of Automobile Engineers Technical Paper Series 861768, October 1986

Mueller, T.J., "On the Historical Development of Apparatus and Techniques for Smoke Visualization of Subsonic and Supersonic Flows," AIAA Paper No. 80-0420, 11th Aerodynamic Testing Conference, March 1980

Nelson, R.C., "The Use of Flow Visualization for Vortex Trajectory Mapping", Flow Visualization III, Proceedings of the Third International Symposium on Flow Visualization, W.J. Yang, Ed., Hemisphere Pub., 1985.

Payne, F. M., "The Structure of Leading Edge Vortex Flows Including Vortex Breakdown," Ph. D. Dissertation, University of Notre Dame, p. 38-43, May 1987

Prandtl, L. and Tietjens, O. G., Applied Hydro- and Aeromechanics, 1st ed., McGraw-Hill Book Co. Inc., p. 130-136, 1934

Ramberg, S. E., "The Influence of Yaw Angle Upon the Vortex Wakes of Stationary and Vibrating Cylinders," Naval Research Laboratory Memorandum Report 3822, August 1978

Ramberg, S. E. and Griffin, O. M., "Velocity Correlation and Vortex Spacing in the Wake of a Vibrating Cable," Transactions of the ASME, Journal of Fluids Engineering, Vol. 98, p. 10-17, March 1976

Ramberg, S. E. and Griffin, O. M., "Vortex Formation in the Wake of a Vibrating Flexible Cable," Transactions of the ASME, Journal of Fluids Engineering, Vol. 96, p. 317-322, December 1974

Roshko, A., "Experiments on the Flow Past a Circular Cylinder at Very High Reynolds Number," Journal of Fluid Mechanics, Vol. 10, p. 345-356, 1961

Schaefer, J. W. and Eskinazi, S., "An Analysis of the Vortex Street Generated in a Viscous Fluid," Journal of Fluid Mechanics, Vol. 6, p. 241-260, 1959

Schlichting, H., Boundary Layer Theory, 7th ed., p. 248-253, 1979

Simpson, A., "Fluid Dynamic Stability Aspects of Cables," Proceedings of the Mechanics of Wave-Induced Forces on Cylinders, p. 90-132, T. L. Shaw, ed., Pitman Advanced Publishing Program, London, 1979,

Smith, R. A., Woo, T. M. and Kao, T. W., "Experiments on Flow About a Yawed Circular Cylinder," Transactions of the ASME, Journal of Basic Engineering, p. 771-776, December 1972

Stein, R. A. and Bert, C. W., "Radius of Curvature of a Double Helix", Transactions of the ASME, Journal of Engineering for Industry, p. 394-395, August 1962

Van Atta, C. W., "Experiments on Vortex Shedding From Yawed Circular Cylinders," AIAA Journal, Vol. 6, No. 5, p. 931-933, May 1968

Visser, K. D., Nelson, R. C. and Ng, T. T., "Method of Cold Smoke Generation for Vortex Core Tagging", AIAA Journal of Aircraft, Vol. 25, No. 11, pp.1069-1071, November 1988.

Votaw, C. W., and Griffin, O. M., "Vortex Shedding From Smooth Cylinders and Stranded Cables," Transactions of the ASME, Journal of Basic Engineering, Vol. 93, p. 457-460, 1971

MODEL	NOMINAL DIAMETER (INCHES)	ACTUAL DIAMETER (INCHES)	WEIGHT/ LENGTH (LB/FT)	MIDPOINT DEFLEC. (INCHES)	EI (LB-FT^2)	CABLE ANGLE 90°	60°	40°	20°
MODEL LENGTH (FT)				(5.85 FT MODEL)		2.00	2.31	3.11	5.85
							FIRST BENDING MODE NATURAL FREQUENCY (HZ)		
CYLINDER	0.625	0.625	0.361	-	-	-	-	-	-
1X19 CABLE	0.625	0.632	0.311	1.3	44	26.5	19.9	11.0	3.1
7X7 CABLE	0.625	0.640	0.292	1.3	41	26.4	19.8	10.9	3.1
3X19 CABLE	0.625	0.615	0.190	3.6	10	16.2	12.1	6.7	1.9
4X7 CABLE (SERRATED)	0.797	0.700	0.295	1.1	49	28.7	21.5	11.9	3.4
6X25 CABLE (LANG LAY)	0.625	0.625	0.310	1.4	41	25.6	19.2	10.6	3.0

Table I. Physical Characteristics of Cable Models.

PHOTO NUMBER	FILAMENT NUMBER	CABLE ANGLE 20°	40°	60°	90°
CYLINDER MODEL AT 18.7FPS					
	1	34°	34°	53°	99°
1	2	36°	36°	54°	98°
	3	36°	39°	55°	95°
	1	44°	31°	64°	102°
2	2	44°	36°	65°	108°
	3	39°	27°	65°	108°
	1	32°	35°	51°	97°
3	2	39°	35°	50°	94°
	3	42°	36°	53°	97°
	1	30°	44°	-	79°
4	2	30°	44°	-	97°
	3	31°	43°	-	78°
MEAN		36.4°	36.6°	56.7°	96.0°
STD. DEV.		5.2°	5.2°	6.2°	9.3°
6X25 CABLE AT 18.7FPS					
	1	34°	43°	59°	100°
1	2	36°	39°	59°	101°
	3	32°	40°	60°	107°
	1	21°	33°	65°	102°
2	2	31°	31°	68°	99°
	3	31°	38°	69°	99°
	1	29°	42°	63°	84°
3	2	29°	43°	71°	83°
	3	31°	44°	68°	97°
	1	35°	39°	64°	94°
4	2	37°	41°	62°	86°
	3	41°	44°	64°	-
MEAN		32.2°	39.8°	64.0°	95°
STD. DEV.		5.0°	4.2°	4.0°	8.0°

Table II. Shedding Angles of Vortex Filaments from Digitized Plan View Photographs.

	CABLE ANGLE			
	20°	40°	60°	90°
CYLINDER MODEL				
18.7 FPS	2.2	3.1	3.1	3.3
44.9 FPS	2.0	3.1	3.2	3.3
4X7 SERRATED CABLE				
18.7 FPS	2.1	2.8	2.7	2.9
44.9 FPS	2.2	2.6	2.3	2.5
6X25 CABLE				
18.7 FPS	2.0	3.1	2.8	3.3
44.9 FPS	2.2	2.9	2.7	3.2

Note: All wake widths are in inches.

Table III. Wake Width Estimated from Flow Visualization Data.

	CABLE ANGLE			
	20°	40°	60°	90°
CYLINDER MODEL, V=18.7 FPS				
AVE. SPACING, IN.	5.6	4.7	2.9	3.1
AVE. SPACING STD. DEV.	1.1	0.8	0.6	0.7
SHED. FREQUENCY, HZ	46	57	72	79
VCV, FPS	21.3	22.4	17.6	20.7
VCV STD. DEV., FPS	2.0	1.5	0.9	1.2
CYLINDER MODEL, V=44.9 FPS				
AVE. SPACING, IN.	4.5	4.3	3.1	2.8
AVE. SPACING STD. DEV.	2.5	0.6	0.4	0.2
SHED. FREQUENCY, HZ	114	144	169	187
VCV, FPS	42.6	51.4	44.2	43.5
VCV STD. DEV., FPS	8.9	2.6	1.5	0.7
4X7 CABLE, V=18.7 FPS				
AVE. SPACING, IN.	5.6	4.9	3.2	3.6
AVE. SPACING STD. DEV.	0.5	1.8	0.7	0.6
SHED. FREQUENCY, HZ	45	53	67	57
VCV, FPS	20.9	21.5	17.8	17.1
VCV STD. DEV., FPS	0.9	3.2	1.0	0.9
4X7 CABLE, V=44.9 FPS				
AVE. SPACING, IN.	4.6	6.1	2.8	3.7
AVE. SPACING STD. DEV.	0.6	0.5	0.2	0.6
SHED. FREQUENCY, HZ	111	136	167	138
VCV, FPS	42.6	68.9	39.2	42.4
VCV STD. DEV., FPS	2.1	2.9	0.7	2.1
6X25 CABLE, V=18.7 FPS				
AVE. SPACING, IN.	3.7	4.8	2.9	3.0
AVE. SPACING STD. DEV.	1.1	0.7	0.3	0.2
SHED. FREQUENCY, HZ	50	62	66	73
VCV, FPS	15.3	25.0	15.8	17.9
VCV STD. DEV., FPS	1.4	1.5	0.4	0.3
6X25 CABLE, V=44.9 FPS				
AVE. SPACING, IN.	4.8	3.3	3.7	3.1
AVE. SPACING STD. DEV.	0.4	0.3	0.8	0.3
SHED. FREQUENCY, HZ	120	154	165	174
VCV, FPS	47.9	42.9	50.9	45.1
VCV STD. DEV., FPS	1.6	1.1	3.4	1.1

Table IV. Vortex Center Velocity Estimates from Flow Visualization Data.

CABLE ANGLE	CYL	1X19	7X7	3X19	4X7	6X25
			VORTEX SHEDDING FREQUENCY, HZ			
HOTWIRE PROBE AT 1.875 INCHES DOWNSTREAM AND 0.625 INCHES UP						
90°	78	79	75	70	58	76
60°	69	72	71	86	57	70
40°	54	66	67	60	53	66
20°	41	47	48	55	49	48
HOTWIRE PROBE AT 3.75 INCHES DOWNSTREAM AND 0.625 INCHES UP						
90°	78	79	75	69	56	76
60°	67	72	70	83	62	70
40°	56	64	66	61	56	66
20°	42	48	48	54	50	50
HOTWIRE PROBE AT 3.75 INCHES DOWNSTREAM AND 1.25 INCHES UP						
90°	79	79	75	69	57	76
60°	68	71	73	84	61	69
40°	56	61	70	56	58	65
20°	43	46	46	53	50	49
AVERAGE OF ABOVE THREE MEASUREMENTS						
90°	78	79	75	69	57	76
60°	68	72	71	84	60	70
40°	55	64	68	59	56	66
20°	42	47	47	54	50	49
ACTUAL CABLE DIAMETER IN INCHES						
	0.625	0.632	0.640	0.615	0.700	0.625
STROUHAL NO. BASED ON FREESTREAM VELOCITY						
90°	0.218	0.222	0.214	0.190	0.178	0.212
60°	0.189	0.202	0.203	0.231	0.187	0.194
40°	0.154	0.179	0.193	0.162	0.174	0.183
20°	0.117	0.132	0.135	0.148	0.155	0.136
STROUHAL NO. BASED ON NORMAL VELOCITY						
90°	0.218	0.222	0.214	0.190	0.178	0.212
60°	0.219	0.233	0.235	0.267	0.216	0.224
40°	0.240	0.279	0.300	0.252	0.270	0.285
20°	0.342	0.387	0.395	0.433	0.453	0.399

Table V. Vortex Shedding and Strouhal Number Data, Freestream Velocity = 18.7 FPS.

SPANWISE LOCATION % UNIT SPAN	CABLE ANGLE 20°	40°	60°	90°
CYLINDER, UNIT SPAN = 1.52 INCHES , V=18.7 FPS				
0	47	57	72	79
100	47	57	71	80
200	45	58	73	79
CYLINDER, UNIT SPAN = 1.52 INCHES , V=44.9 FPS				
0	110	143	169	189
100	125	143	169	187
200	108	145	169	186
4X7 CABLE, UNIT SPAN = 1.30 INCHES , V=18.7 FPS				
0	44	53	65	57
50	44	53	65	57
100	45	53	67	57
150	47	54	69	57
4X7 CABLE, UNIT SPAN = 1.30 INCHES , V=44.9 FPS				
0	115	136	169	137
50	110	134	165	137
100	100	139	165	140
150	120	134	167	139
6X25 CABLE, UNIT SPAN = 0.65 INCHES , V=18.7 FPS				
0	51	61	67	73
50	-	61	64	73
100	-	62	65	73
150	51	63	69	73
200	49	-	-	-
250	49	-	-	-
6X25 CABLE, UNIT SPAN = 0.65 INCHES , V=44.9 FPS				
0	125	155	165	175
50	-	155	164	173
100	-	152	166	174
150	112	152	164	172
200	113	-	-	-
250	128	-	-	-

Table VI. Spanwise Variation in Vortex Shedding Frequency (Hz).

POSITION % UNIT SPAN	CABLE ANGLE 20°	40°	60°	90°
CYLINDER, UNIT SPAN = 1.52 INCHES, V=18.7 FPS, DIA. = 0.625 INCHES				
0	0.131	0.159	0.201	0.220
100	0.131	0.159	0.198	0.223
200	0.125	0.162	0.203	0.220
CYLINDER, UNIT SPAN = 1.52INCHES, V=44.9 FPS, ACTUAL DIA. = 0.625 INCHES				
0	0.128	0.166	0.196	0.219
100	0.145	0.166	0.196	0.217
200	0.125	0.168	0.196	0.216
4X7 CABLE, UNIT SPAN = 1.30INCHES, V=18.7 FPS, DIA. = 0.700 INCHES				
0	0.137	0.165	0.203	0.178
50	0.137	0.165	0.203	0.178
100	0.140	0.165	0.209	0.178
150	0.147	0.168	0.215	0.178
4X7 CABLE, UNIT SPAN = 1.30INCHES, V=44.9 FPS, DIA. = 0.700 INCHES				
0	0.149	0.177	0.220	0.178
50	0.143	0.174	0.214	0.178
100	0.130	0.181	0.214	0.182
150	0.156	0.174	0.217	0.181
6X25 CABLE, UNIT SPAN = 0.65INCHES, V=18.7 FPS, DIA. = 0.625 INCHES				
0	0.142	0.170	0.187	0.203
50	-	0.170	0.178	0.203
100	-	0.173	0.181	0.203
150	0.142	0.175	0.192	0.203
200	0.136	-	-	-
250	0.136	-	-	-
6X25 CABLE, UNIT SPAN = 0.65INCHES, V=44.9 FPS, DIA. = 0.625 INCHES				
0	0.145	0.180	0.191	0.203
50	-	0.180	0.190	0.201
100	-	0.176	0.193	0.202
150	0.130	0.176	0.190	0.200
200	0.131	-	-	-
250	0.148	-	-	-

Table VII. Strouhal Number Based on Freestream Velocity.

SPANWISE DISTANCE % UNIT SPAN	CABLE ANGLE 20°	40°	60°	90°
CYLINDER MODEL, V=18.7 FPS, D=0.625 INCHES, UNIT SPAN=1.52 INCHES				
0	0.00000	0.00010	0.00010	0.00010
100	0.00498	0.00312	0.00049	-0.00117
200	0.00762	0.00186	0.00098	-0.00254
CYLINDER MODEL, V=44.9 FPS, D=0.625 INCHES, UNIT SPAN=1.52 INCHES				
0	0.00000	0.00000	0.00000	0.00000
100	0.00205	0.00068	0.00057	0.00039
200	0.00400	0.00146	0.00059	0.00088
4x7 SERRATED CABLE, V=18.7 FPS, D=0.700 INCHES, UNIT SPAN=1.30 INCHES				
0	0.00000	0.00010	0.00010	0.00010
50	0.00186	0.00186	0.00088	0.00010
100	0.00479	0.00361	0.00234	0.00049
150	0.00566	0.00459	0.00342	0.00049
4x7 SERRATED CABLE, V=44.9 FPS, D=0.700 INCHES, UNIT SPAN=1.30 INCHES				
0	0.00000	0.00010	0.00010	0.00010
50	0.00088	0.00068	0.00039	-0.00020
100	0.00176	0.00127	0.00078	0.00010
150	0.00292	0.00166	0.00107	0.00010
6x25 LANG LAY CABLE, V=18.7 FPS, D=0.625 INCHES, UNIT SPAN=0.65 INCHES				
0	0.00000	0.00010	0.00010	0.00010
50	-	0.00088	0.00068	0.00010
100	-	0.00166	0.00088	-0.00059
150	0.00332	0.00225	0.00186	-0.00098
200	0.00391	-	-	-
250	0.00488	-	-	-
6x25 LANG LAY CABLE, V=44.7 FPS, D=0.625 INCHES, UNIT SPAN=0.65 INCHES				
0	0.00000	0.00010	0.00010	0.00010
50	-	0.00020	0.00010	0.00010
100	-	0.00049	0.00049	0.00010
150	0.00088	0.00068	0.00049	-0.00020
200	0.00146	-	-	-
250	0.00166	-	-	-

Table VIII. Time Shift in Seconds Based on Freestream Velocity.

	SPANWISE DISTANCE % UNIT SPAN	CABLE ANGLE			
		20°	40°	60°	90°
CYLINDER MODEL					
V=18.7 FPS					
	100	38.8	55.4	62.6	96.9
	200	32.1	43.8	62.6	82.5
V=44.9 FPS					
	100	38.4	47.1	67.5	84.5
	200	37.7	47.7	63.7	83.8
	AVERAGE	36.75	48.5	64.1	86.9
4X7 SERRATED CABLE					
V=18.7 FPS					
	50	34.8	63.7	71.6	88.6
	100	43.4	62.9	75.9	86.6
	150	35.3	58.3	75.5	87.7
V=44.9 FPS					
	50	38.5	60.1	72.5	96.5
	100	38.5	58.3	72.5	88.4
	150	42.3	55.3	71.4	88.9
	AVERAGE	38.8	59.8	73.2	89.5
6X25 LANG LAY CABLE					
V=18.7 FPS					
	50	-	62.0	78.9	87.3
	100	-	60.4	71.6	98.1
	150	40.2	57.8	76.9	98.9
	200	36.2	-	-	-
	250	36.2	-	-	-
V=44.9 FPS					
	50	-	50.0	65.9	84.0
	100	-	53.1	76.0	87.0
	150	29.7	52.0	70.2	94.0
	200	33.6	-	-	-
	250	31.7	-	-	-
	AVERAGE	34.6	55.9	73.3	91.6

NOTE: DATA BASED ON ASSUMED VORTEX CONVECTION VELOCITY RATIO = 0.7

Table IX. Shedding Angles in Degrees Calculated from Cross Correlation Data.

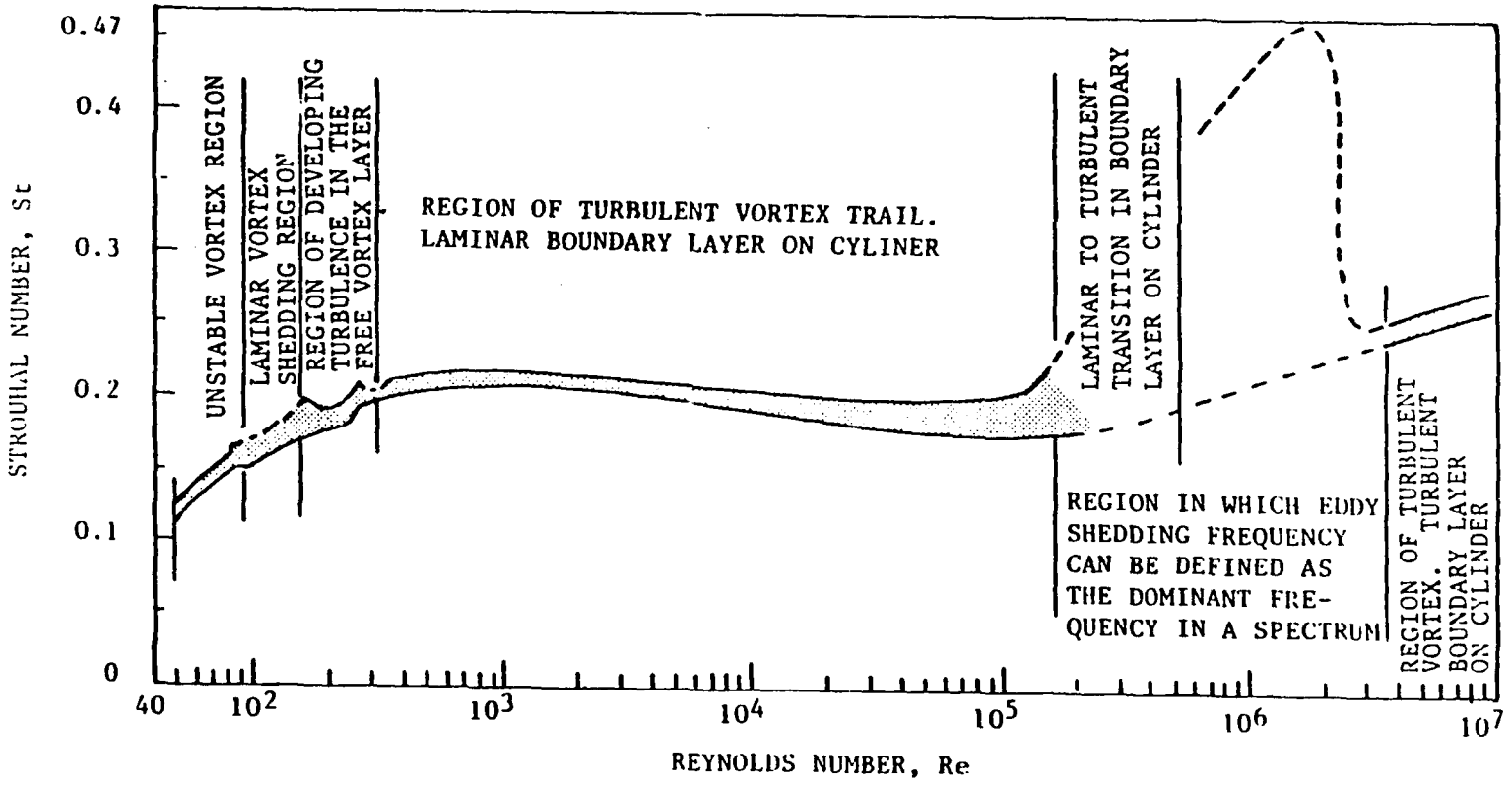

Figure 1. Strouhal - Reynolds Number Relationship for Cylinders Normal to the Flow (Adapted from Horton et al).

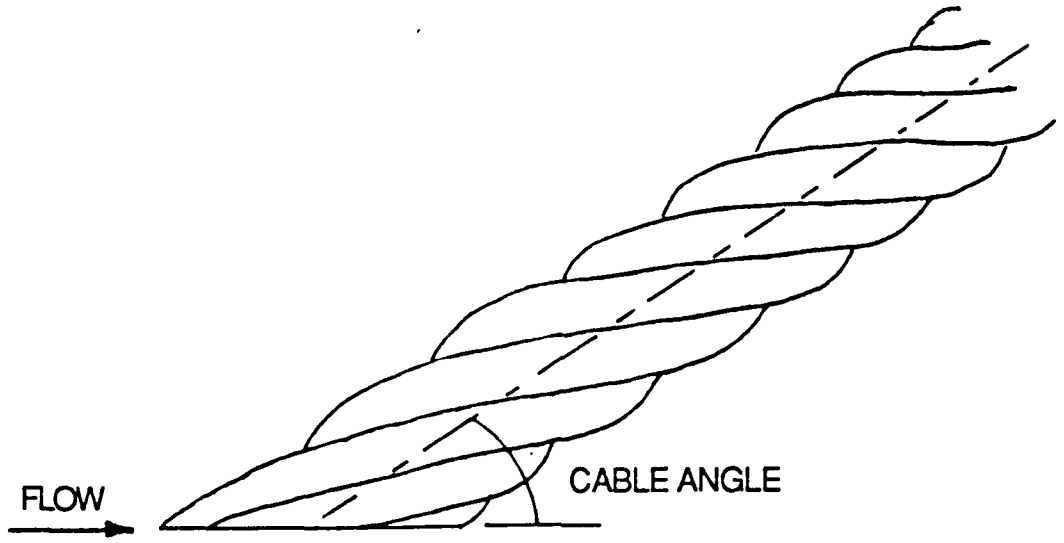

(a) TOP VIEW

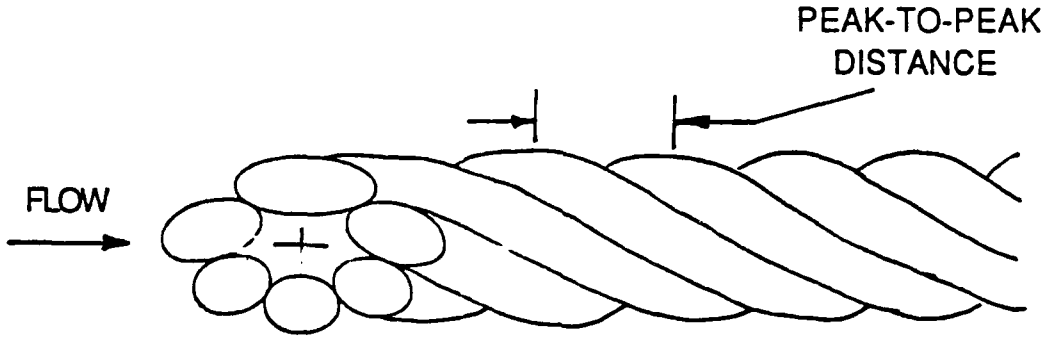

(b) SIDE VIEW

Figure 2. Orientation of the Cross - Section with Respect to the Flow and the Cable.

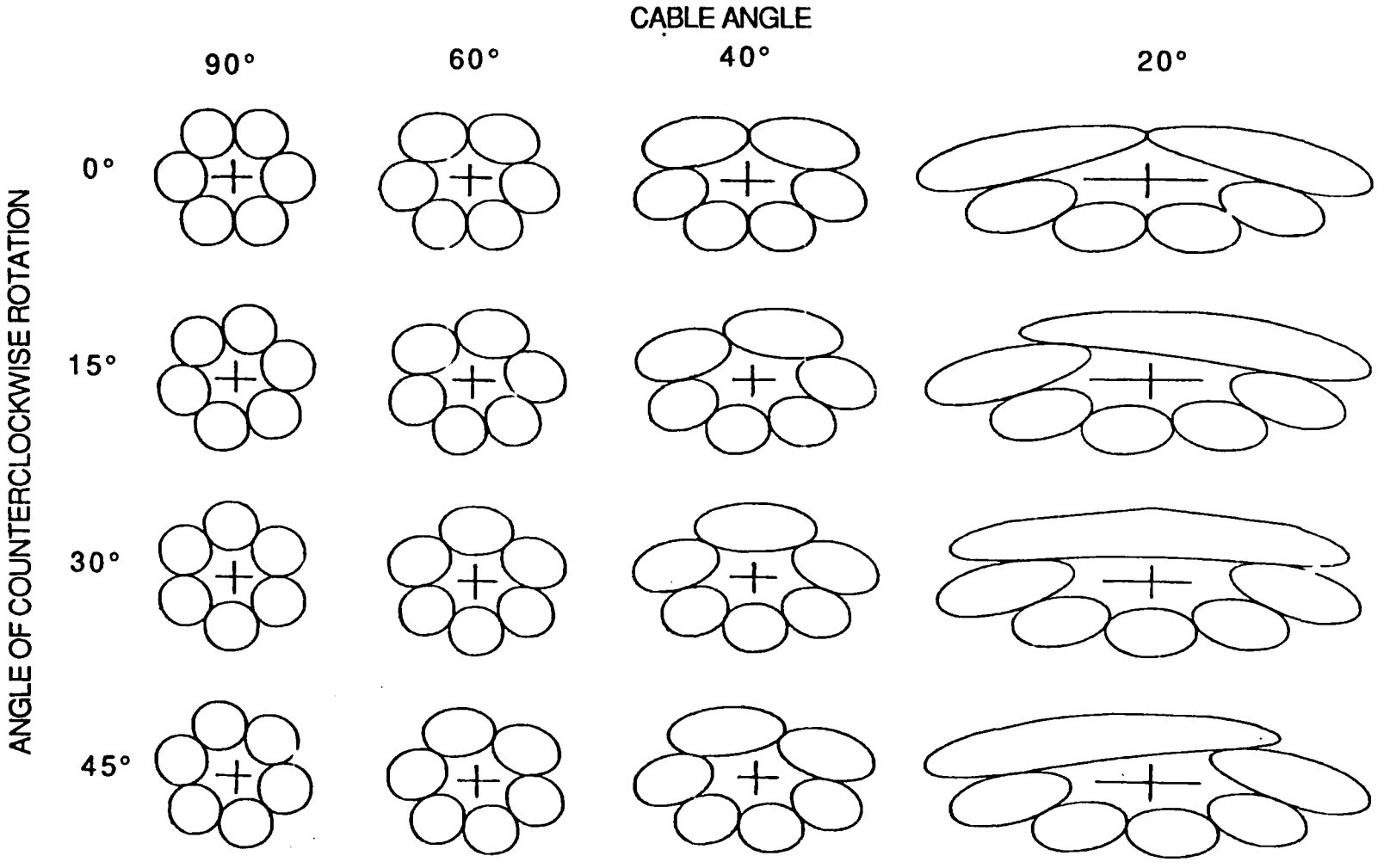

Figure 3. Six - Strand Cable Cross - Section (7x7 and 6x25 Cables, Right Lay, Expanded 1.6 Times).

(a) THREE STRANDS
(e.g. 3X19 CABLE)

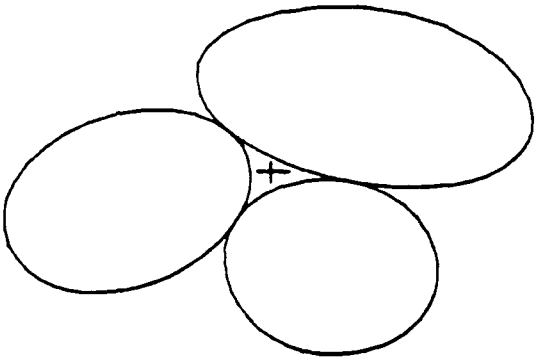

(b) FOUR STRANDS
(e.g. 4X7 CABLE)

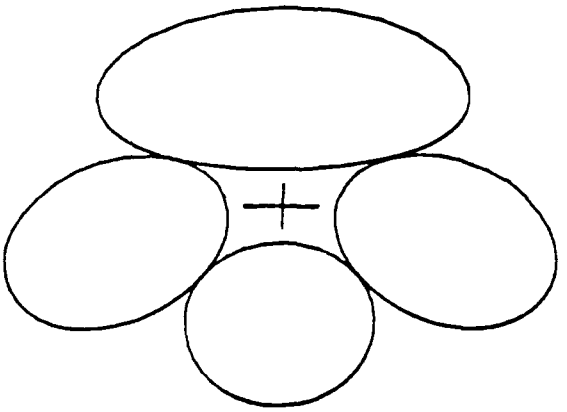

(c) TWELVE STRANDS
(e.g. 1X19 CABLE)

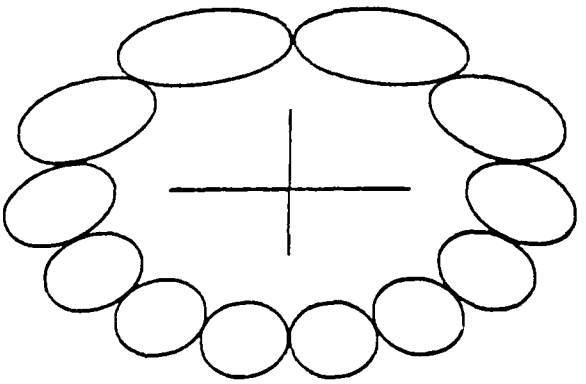

Figure 4. Cross - Sections at 40° Cable Angle, Right Lay, Expanded 3.1 Times.

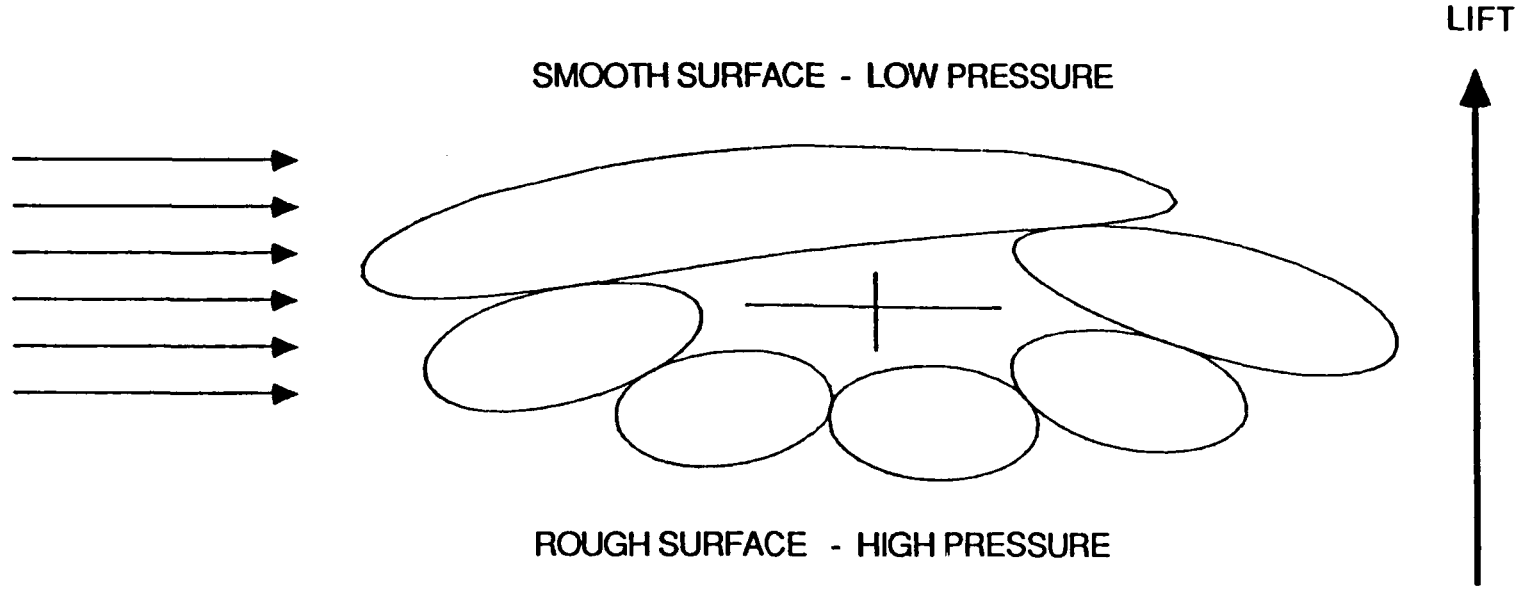

Figure 5. Lift Generation on a Six - Stand Right Lay Cable at 20° Cable Angle and 45 Rotation, Expanded 3.1 Times.

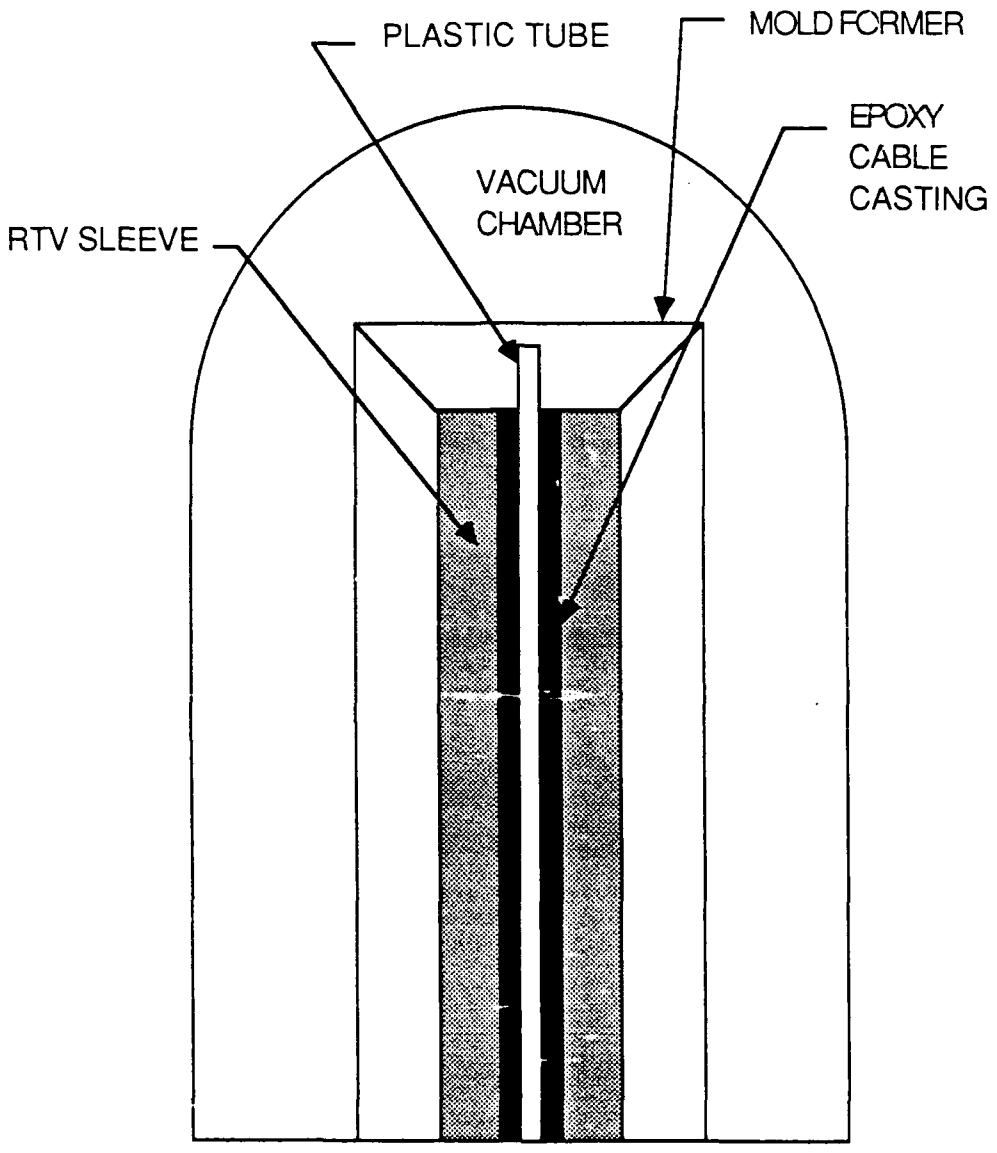

Figure 6. Schematic of Casting Assembly for Epoxy Models

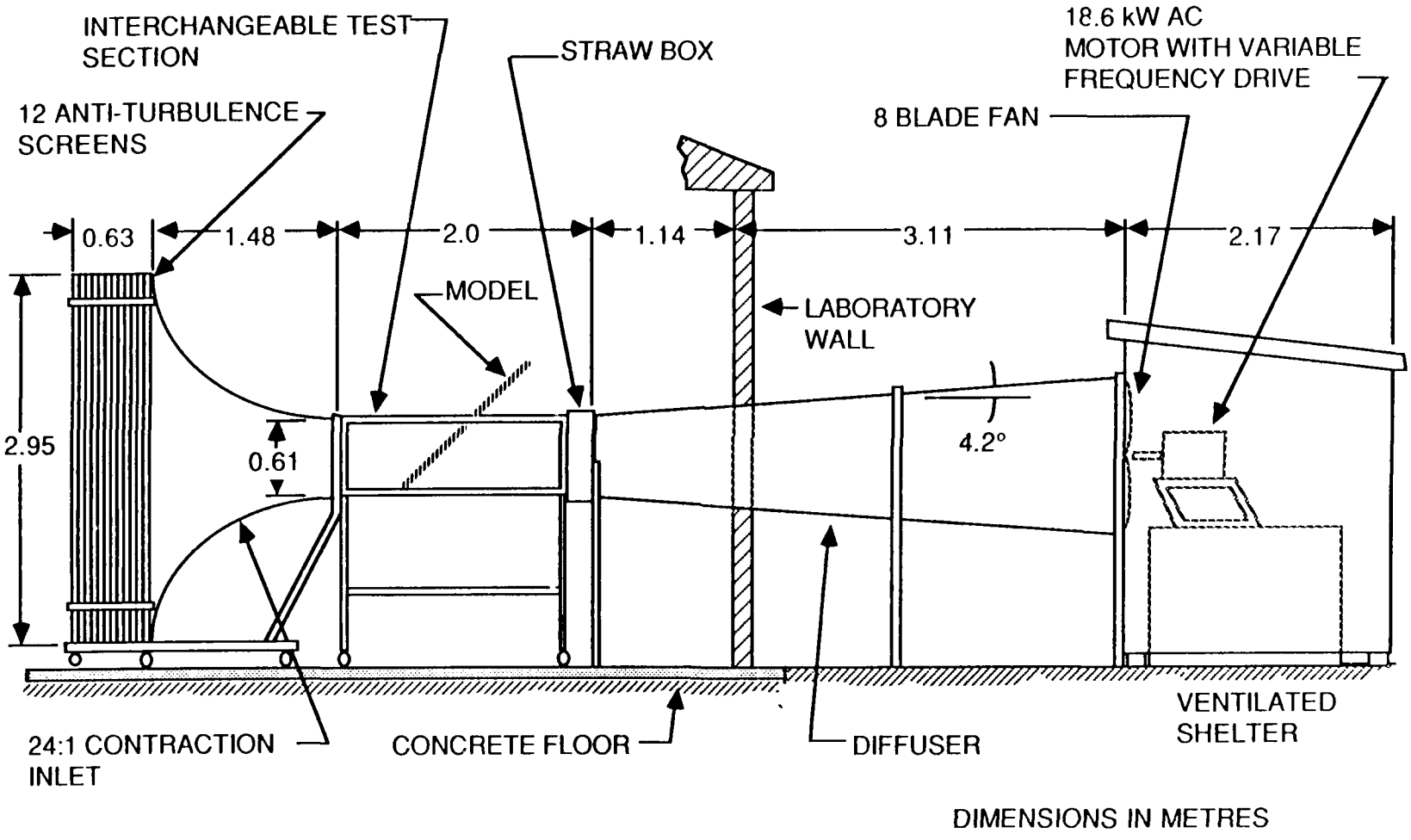

Figure 7. University of Notre Dame Wind Tunnel Facility

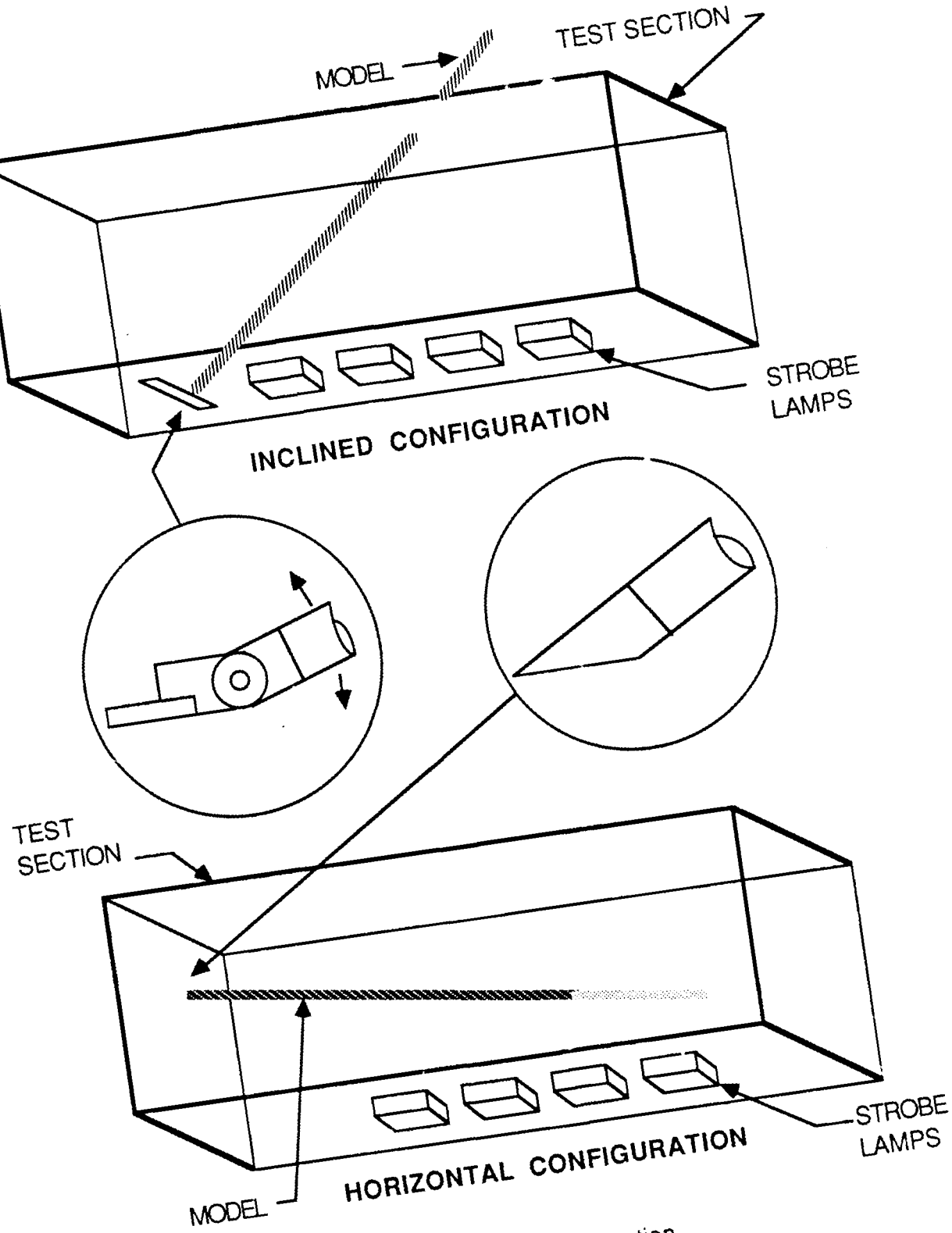

Figure 8. Cable Configurations for Flow Visualization

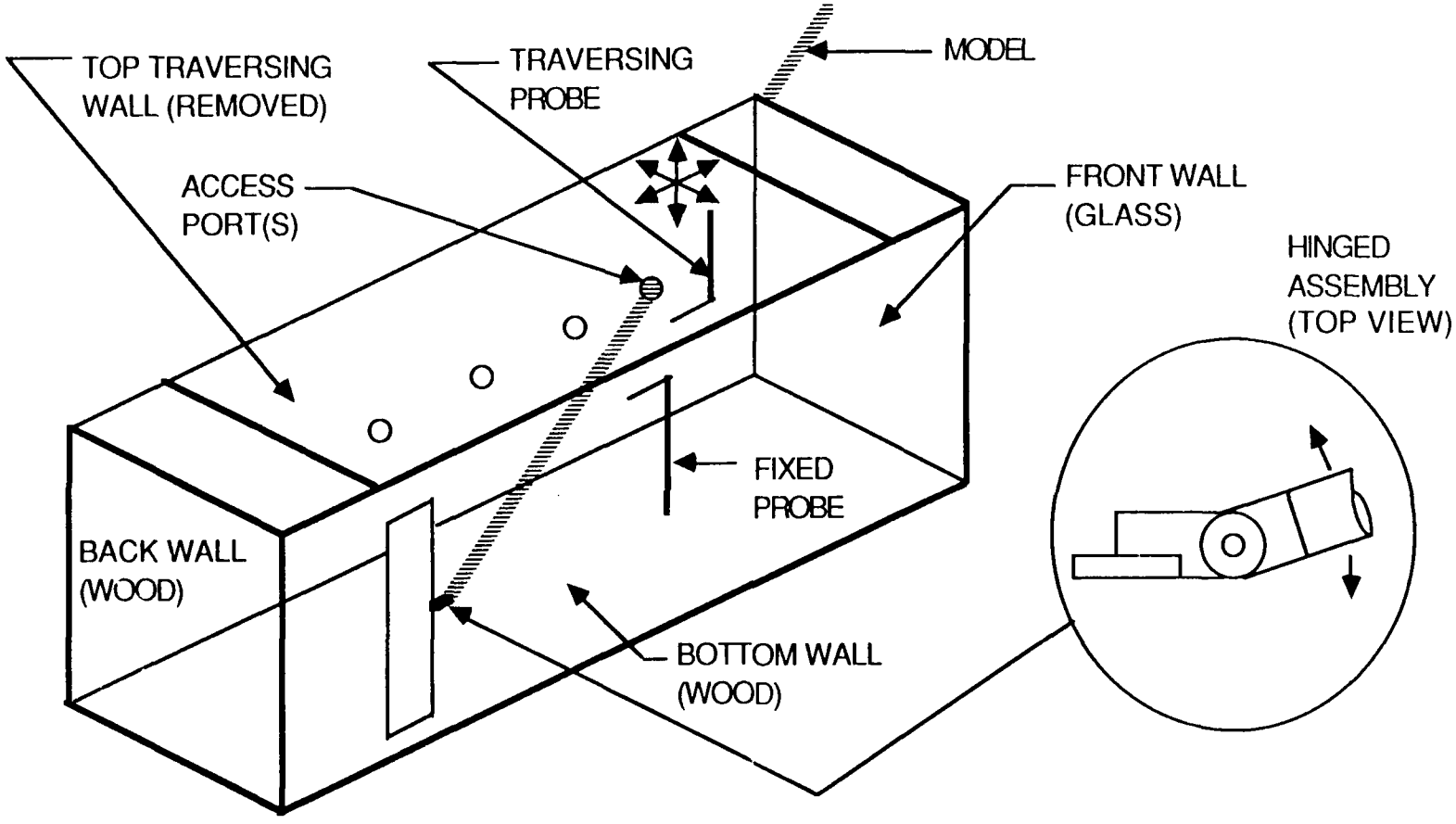

Figure 9. Hot Wire Set - Up

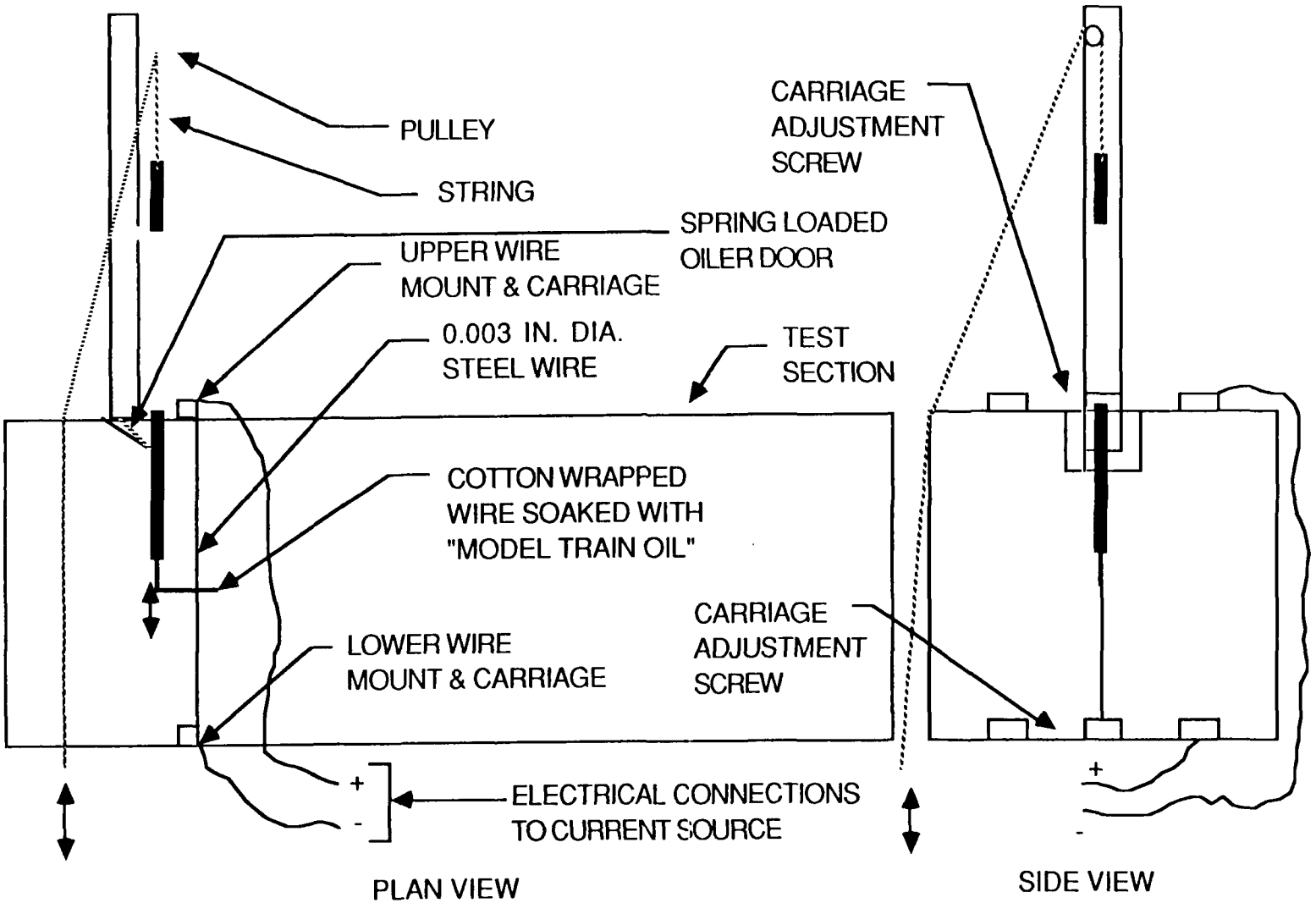

Figure 10. Smoke Wire and Oiler System

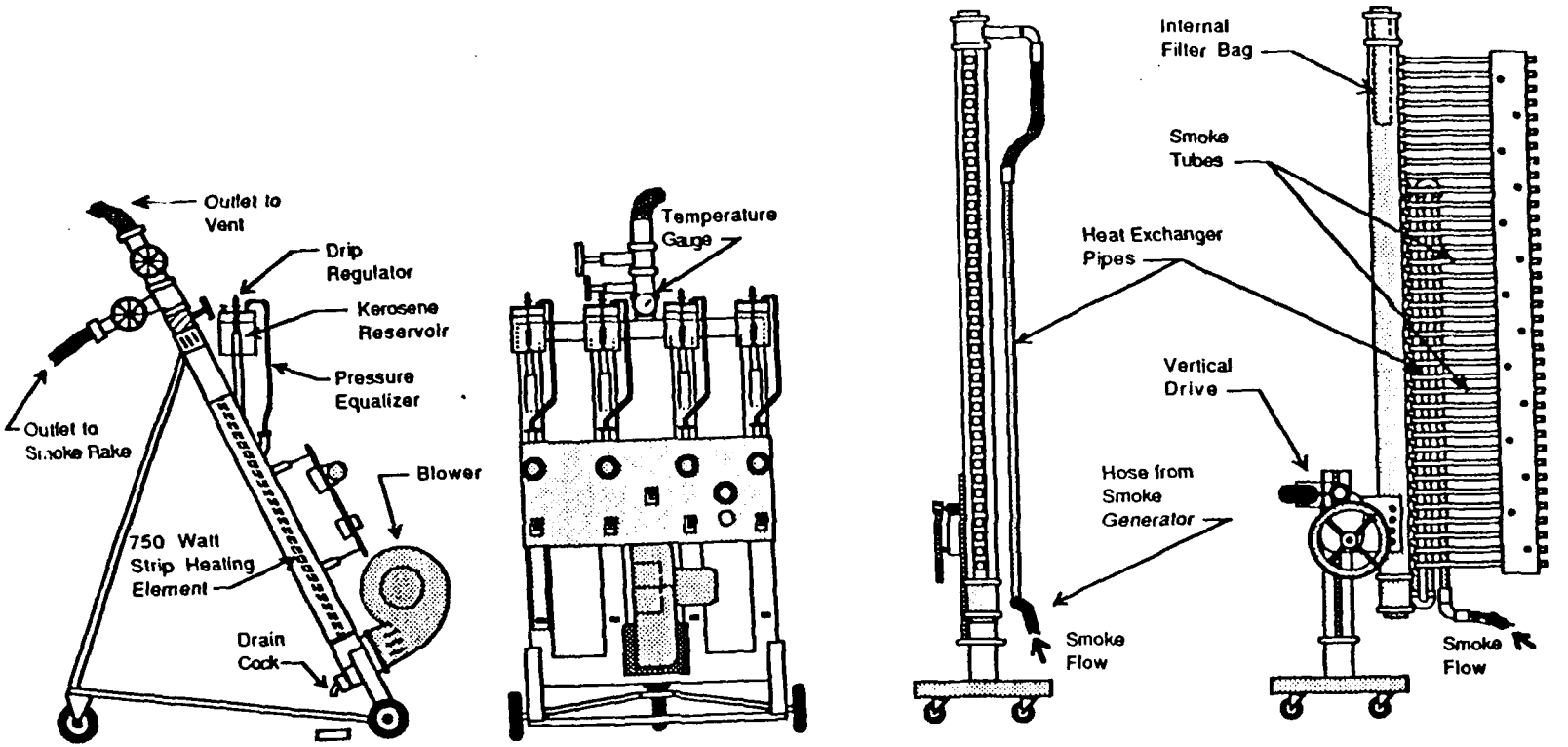

Figure 11. Smoke Generator and Rake.

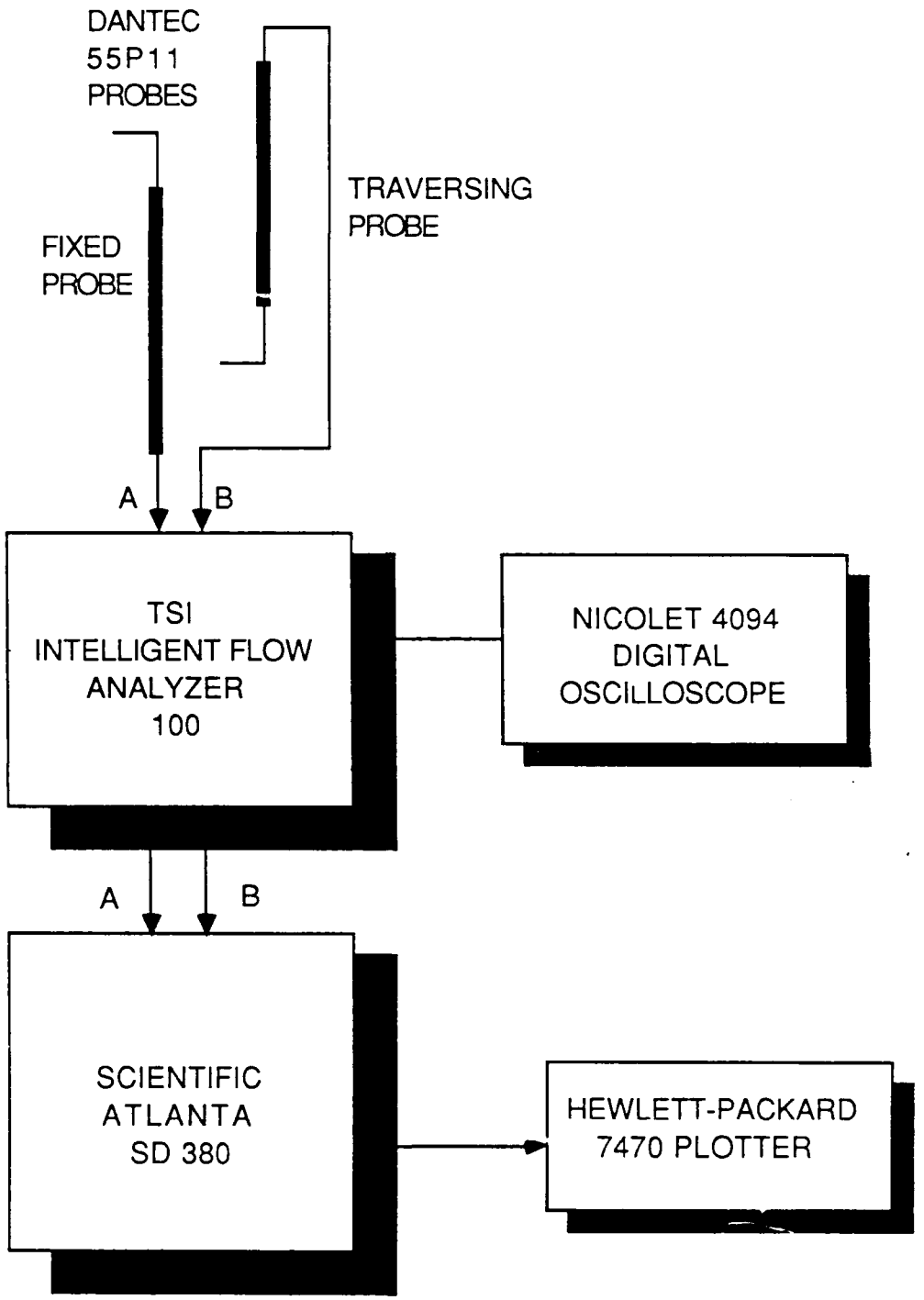

Figure 12. Hot Wire Data Acquisition System

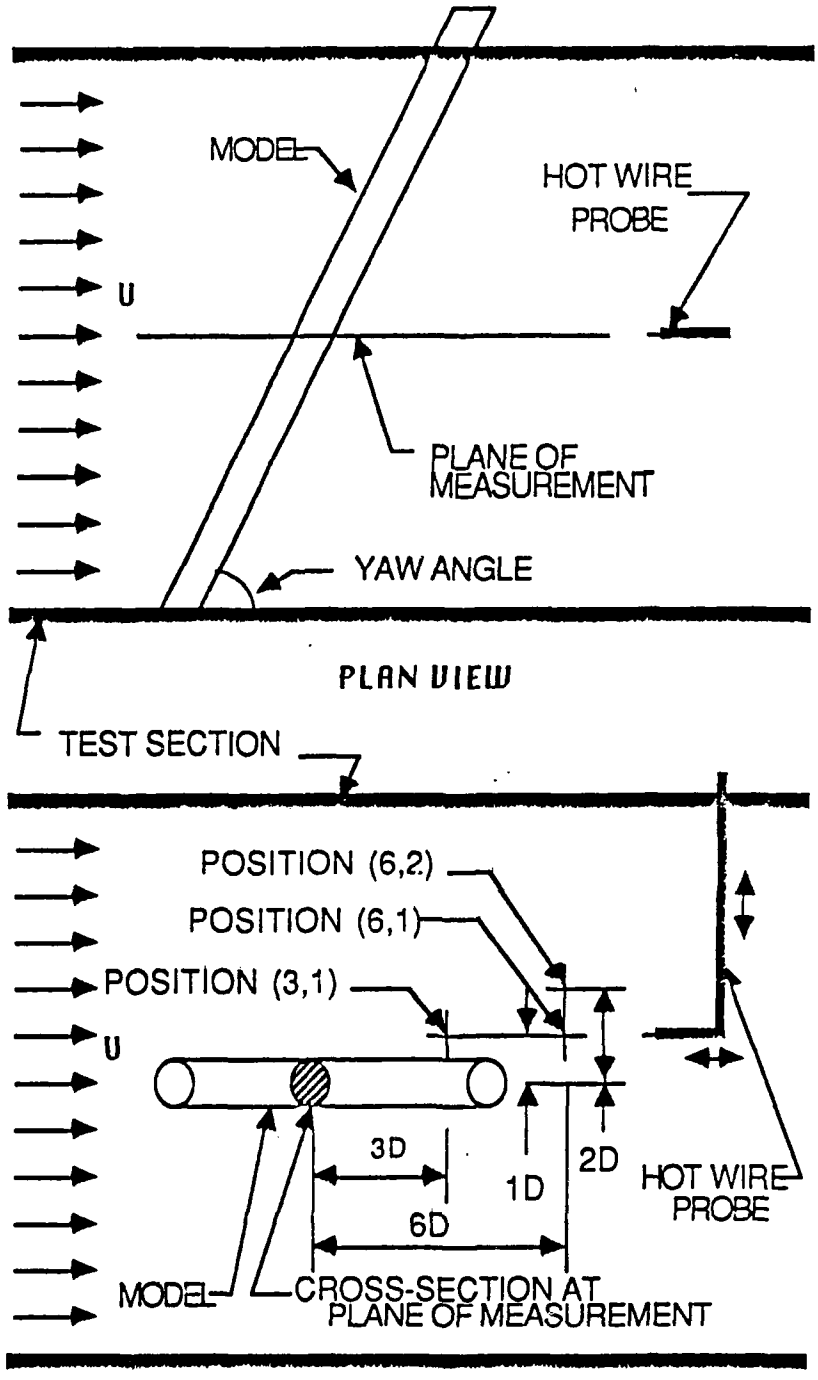

Note: All test positions are on the same horizontal plane. The unit D, is one nominal diameter equal to 5/8 in.

Figure 13. Hot Wire Measurement Points.

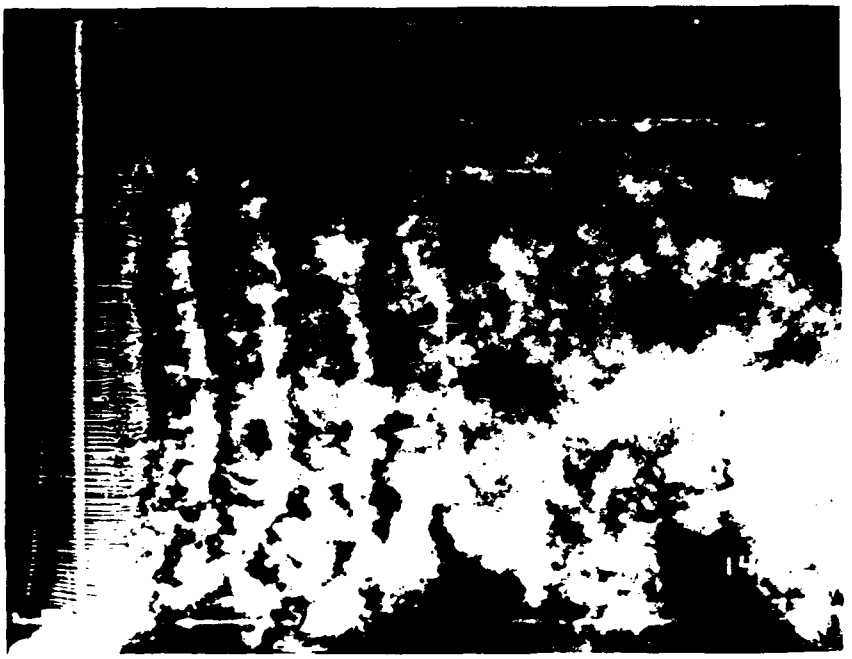

CYLINDER, 90° CABLE ANGLE, 18.7 FPS, PLAN VIEW

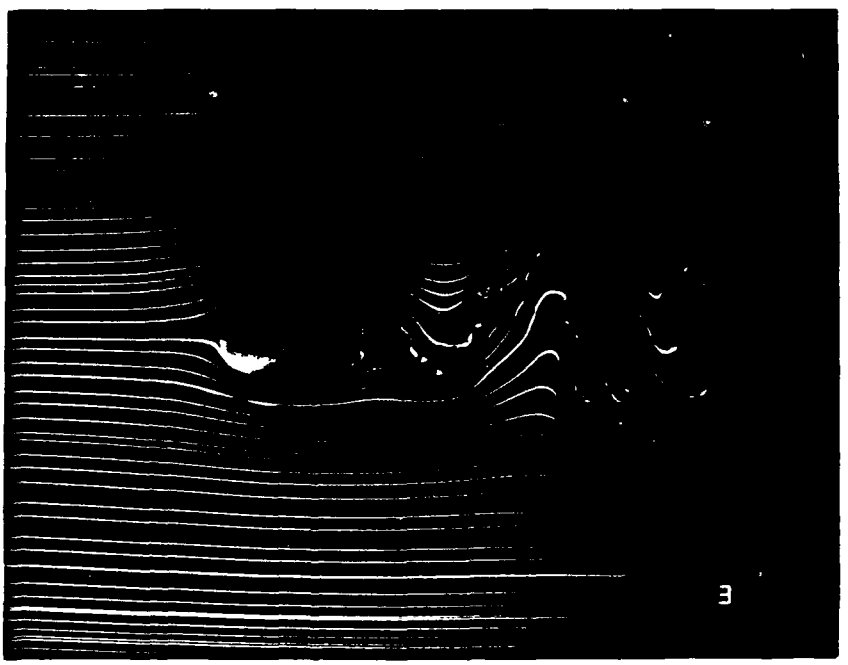

CYLINDER, 90° CABLE ANGLE, 18.7 FPS, AXIAL VIEW

Figure 14. Plan and Axial Views of the Cylinder, $\beta = 90°$

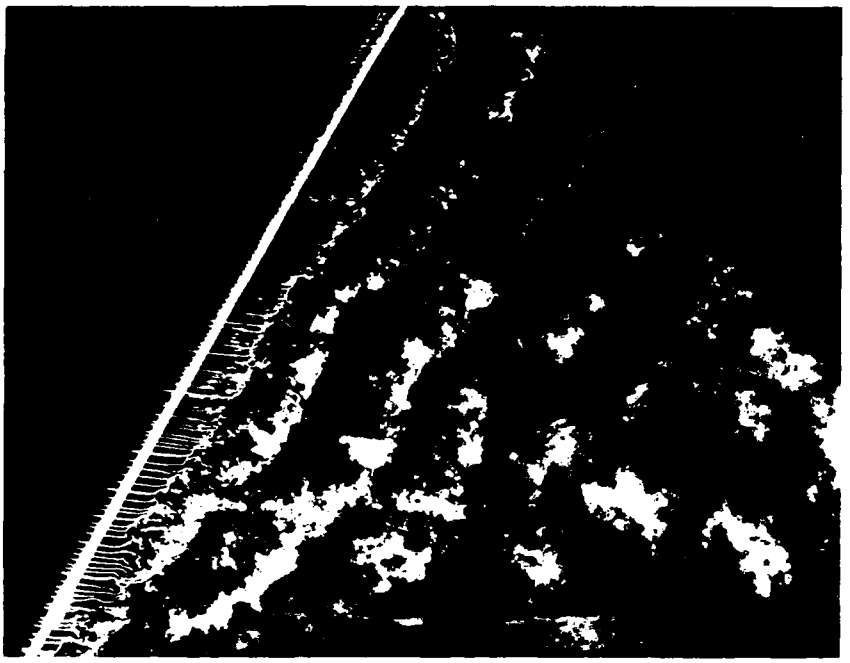

CYLINDER, 60° CABLE ANGLE, 18.7 FPS, PLAN VIEW

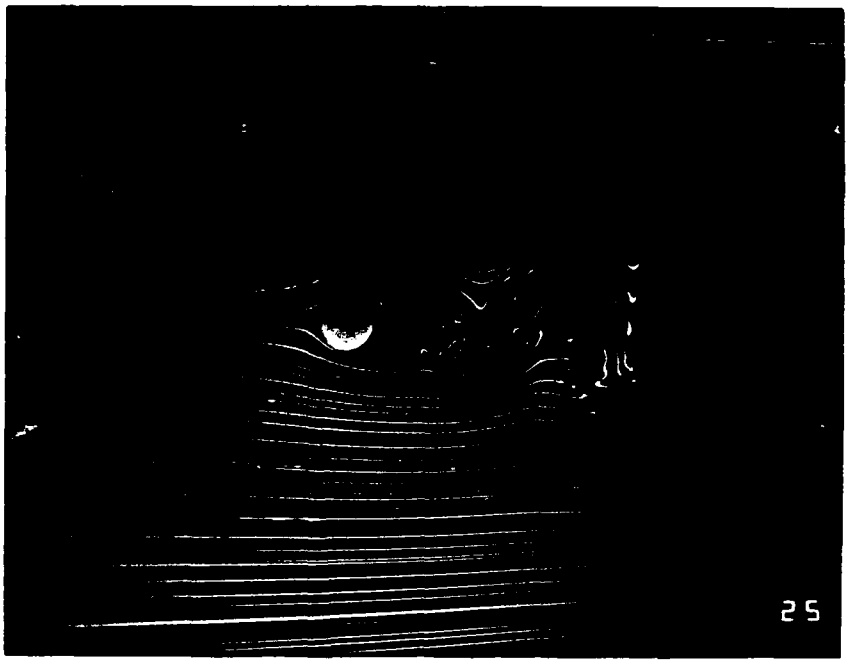

CYLINDER, 60° CABLE ANGLE, 18.7 FPS, AXIAL VIEW

Figure 15. Plan and Axial Views of the Cylinder, $\beta = 60°$

CYLINDER, 20° CABLE ANGLE, 18.7 FPS, PLAN VIEW

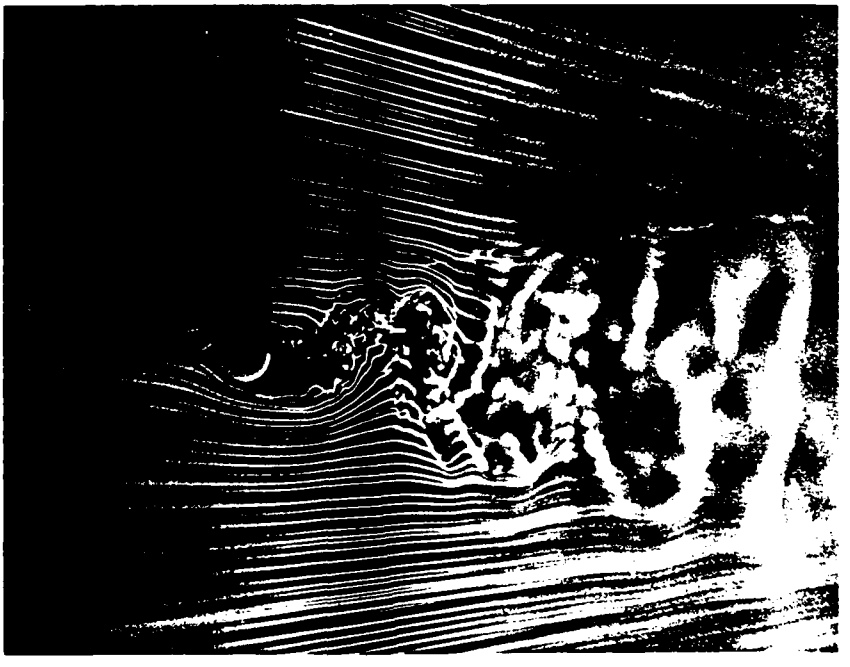

CYLINDER, 20° CABLE ANGLE, 18.7 FPS, AXIAL VIEW

Figure 16. Plan and Axial Views of the Cylinder, $\beta = 20°$

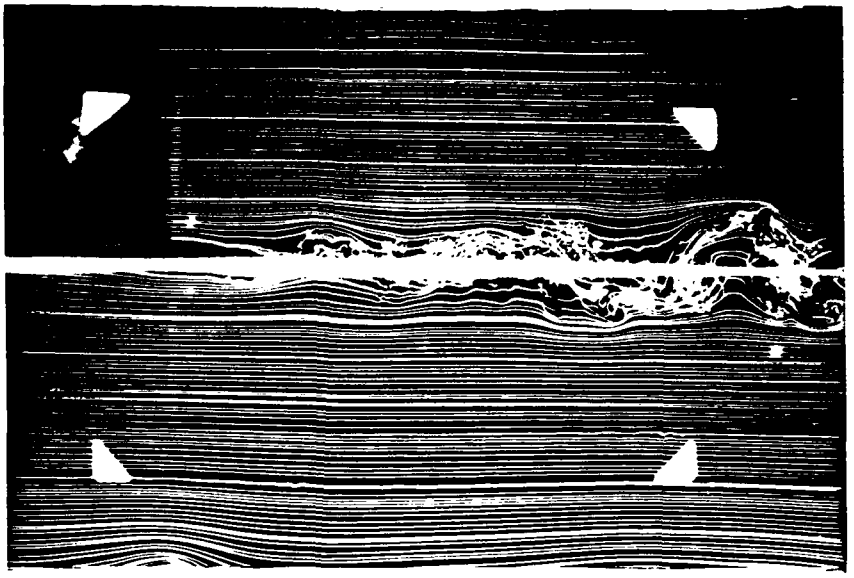

CYLINDER, 20° CABLE ANGLE, 18.7 FPS, SIDE VIEW

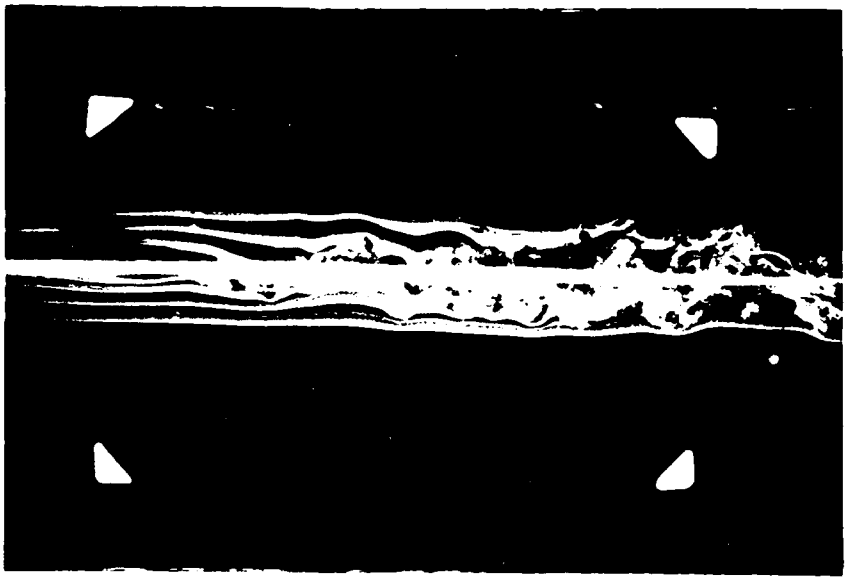

CYLINDER, 20° CABLE ANGLE, 44.9 FPS, SIDE VIEW

Figure 19. Side Views of the Cylinder, $\beta = 20°$, V=18.7 and 44.9 FPS

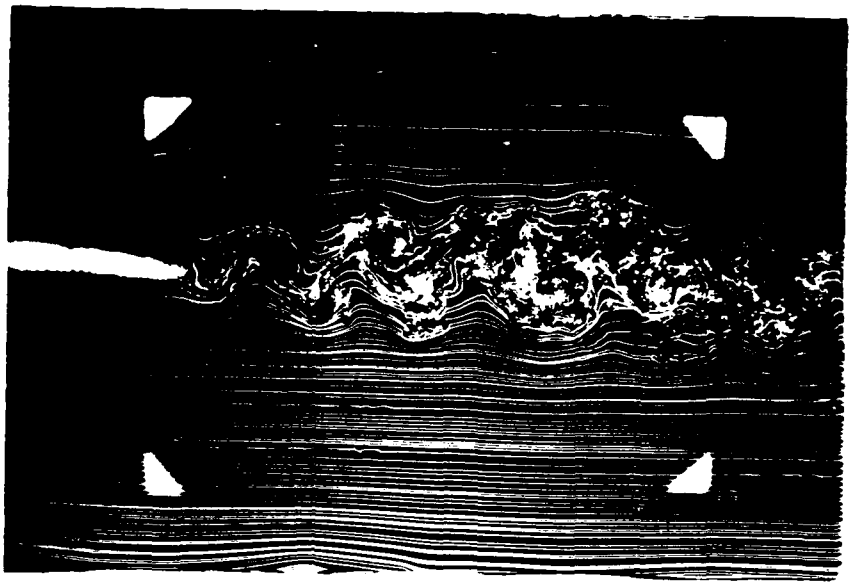

6X25 CABLE, 90° CABLE ANGLE, 18.7 FPS, SIDE VIEW

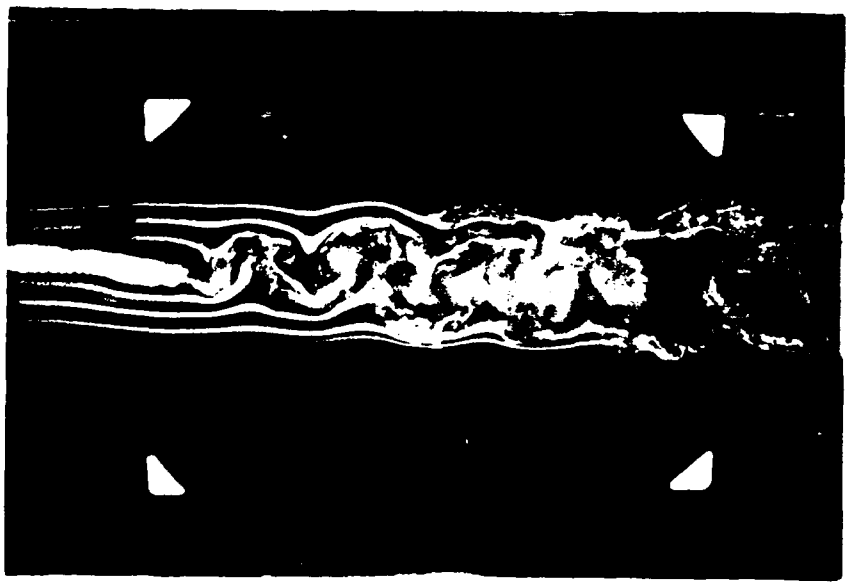

6X25 CABLE, 90° CABLE ANGLE, 44.9 FPS, SIDE VIEW

Figure 20. Side Views of the 6X25 Cable, $\beta = 90°$, V=18.7 and 44.9 FPS

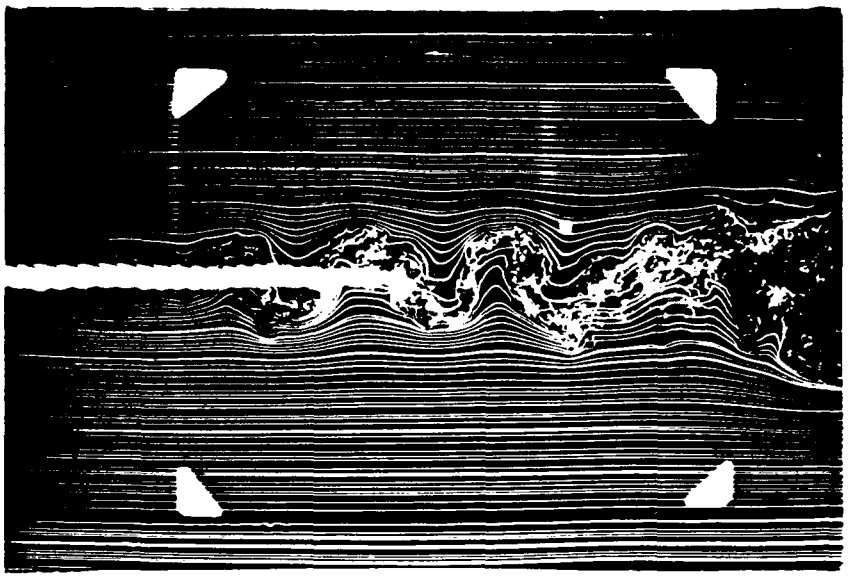

6X25 CABLE, 60° CABLE ANGLE, 18.7 FPS, SIDE VIEW

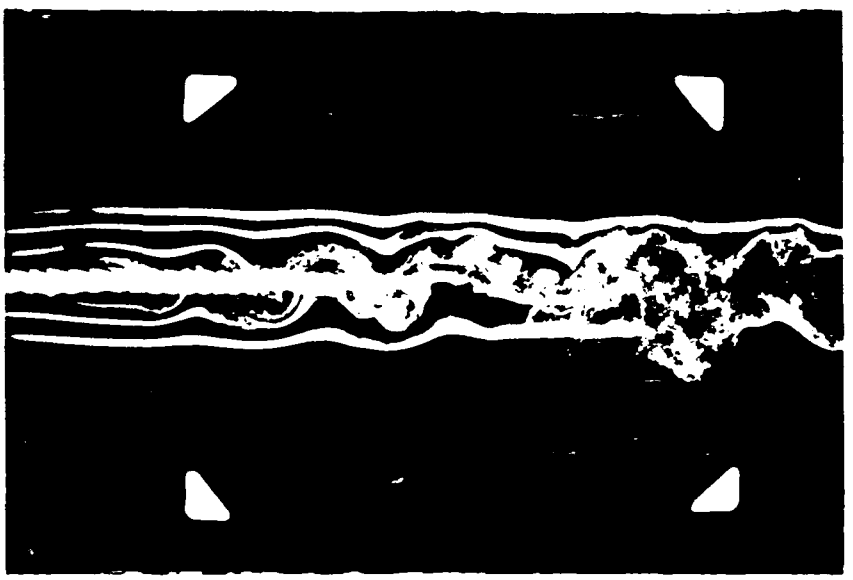

6X25 CABLE, 60° CABLE ANGLE, 44.9 FPS, SIDE VIEW

Figure 21. Side Views of the 6X25 Cable, $\beta = 60°$, V=18.7 and 44.9 FPS

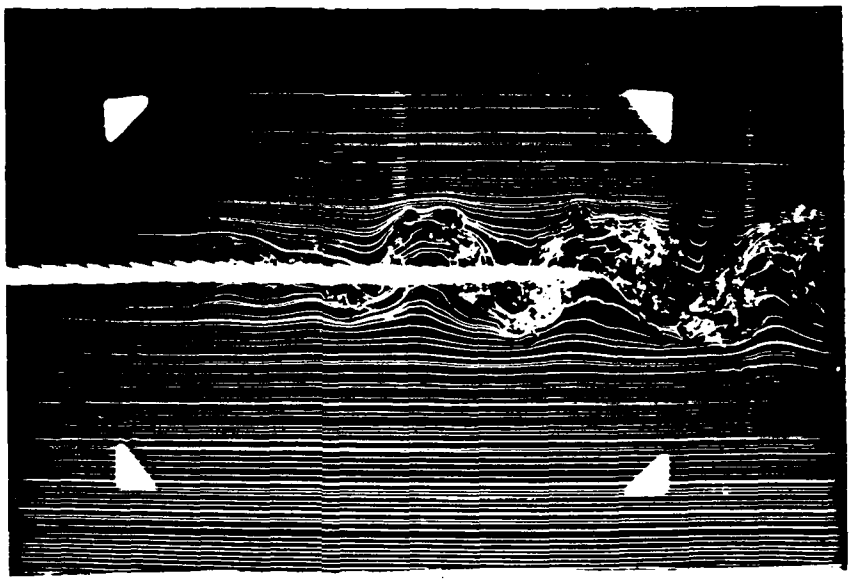

6X25 CABLE, 40° CABLE ANGLE, 18.7 FPS, SIDE VIEW

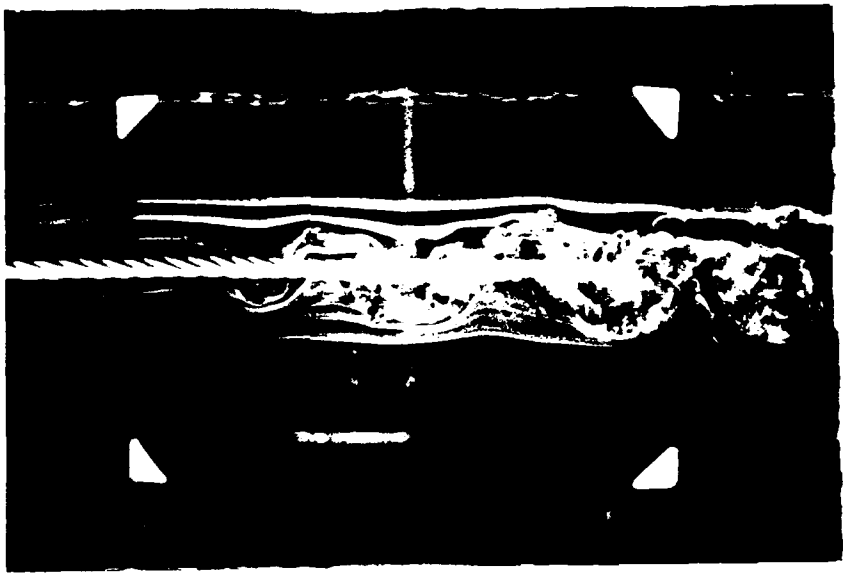

6X25 CABLE, 40° CABLE ANGLE, 44.9 FPS, SIDE VIEW

Figure 22. Side Views of the 6X25 Cable, $\beta = 40°$, V=18.7 and 44.9 FPS

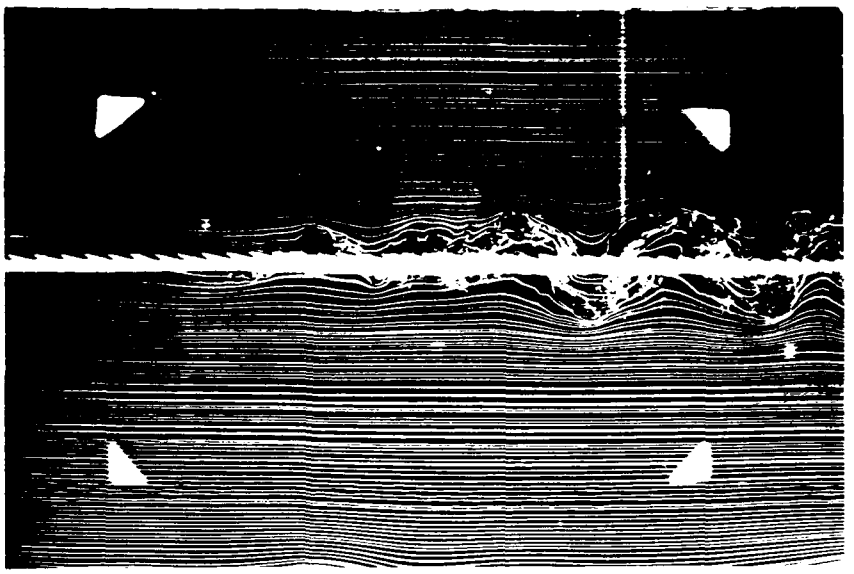

6X25 CABLE, 20° CABLE ANGLE, 18.7 FPS, SIDE VIEW

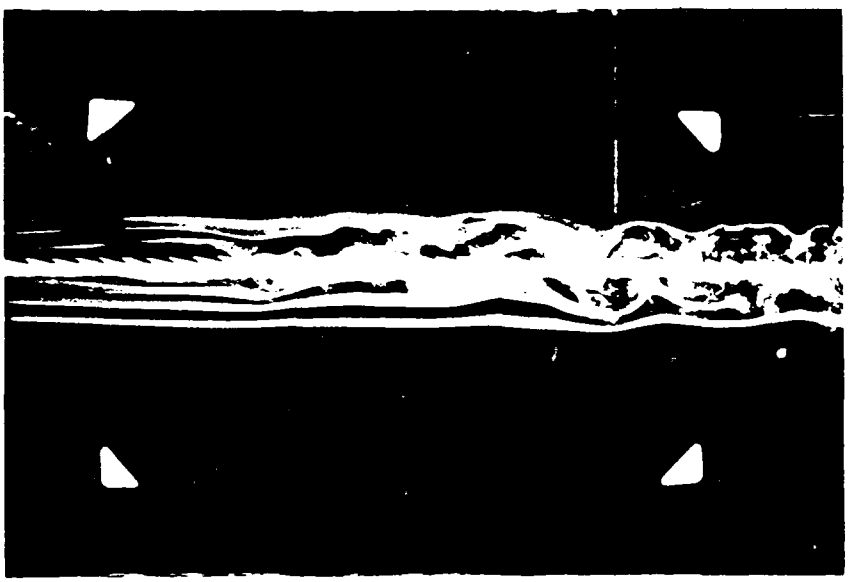

6X25 CABLE, 20° CABLE ANGLE, 44.9 FPS, SIDE VIEW

Figure 23. Side Views of the 6X25 Cable, $\beta = 20°$, V=18.7 and 44.9 FPS

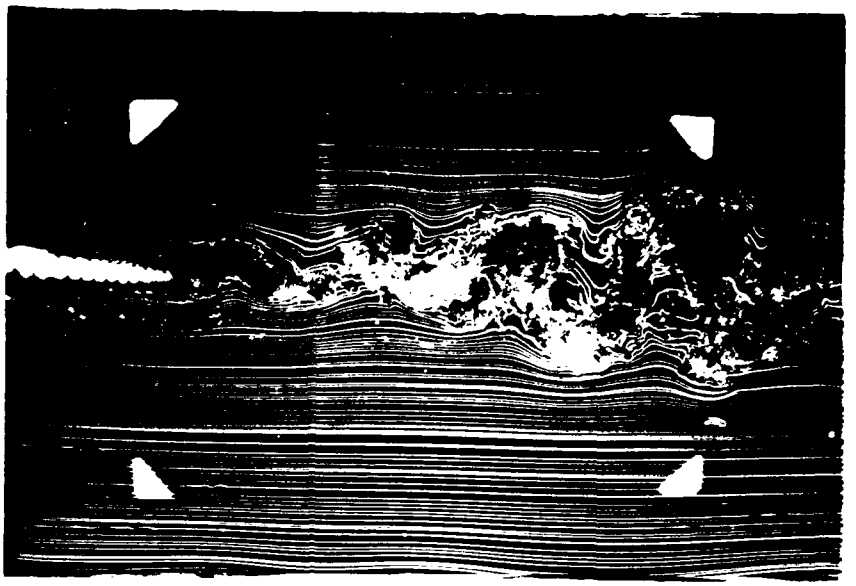

4X7 CABLE, 90° CABLE ANGLE, 18.7 FPS, SIDE VIEW

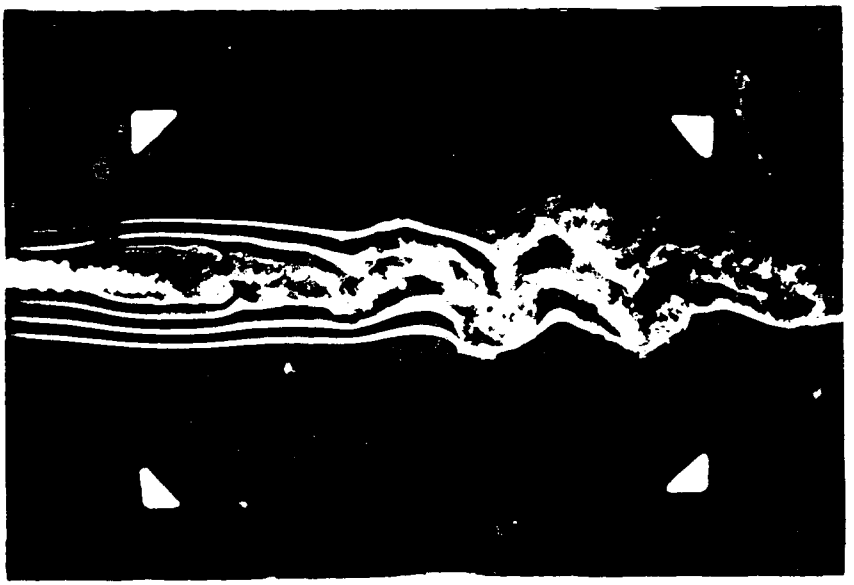

4X7 CABLE, 90° CABLE ANGLE, 44.9 FPS, SIDE VIEW

Figure 24. Side Views of the 4X7 Cable, $\beta = 90^{\circ}$, V=18.7 and 44.9 FPS

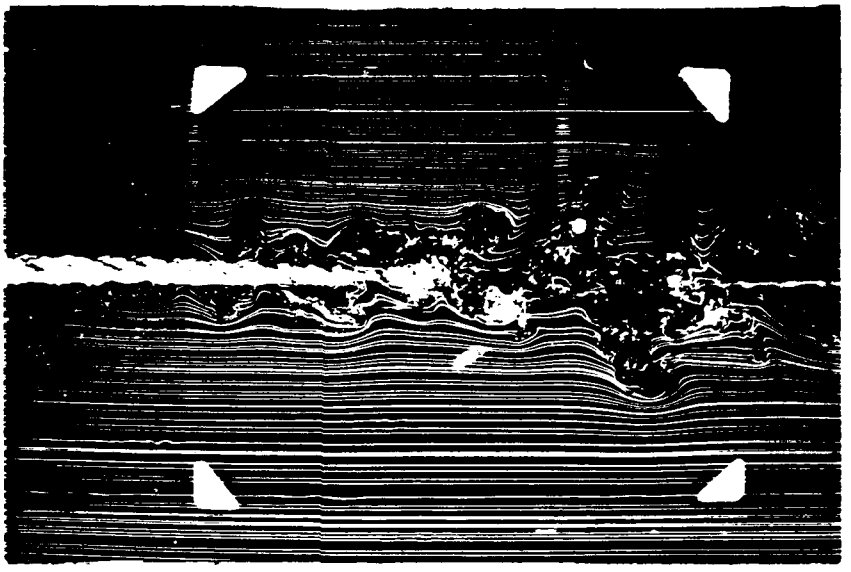

4X7 CABLE, 60° CABLE ANGLE, 18.7 FPS, SIDE VIEW

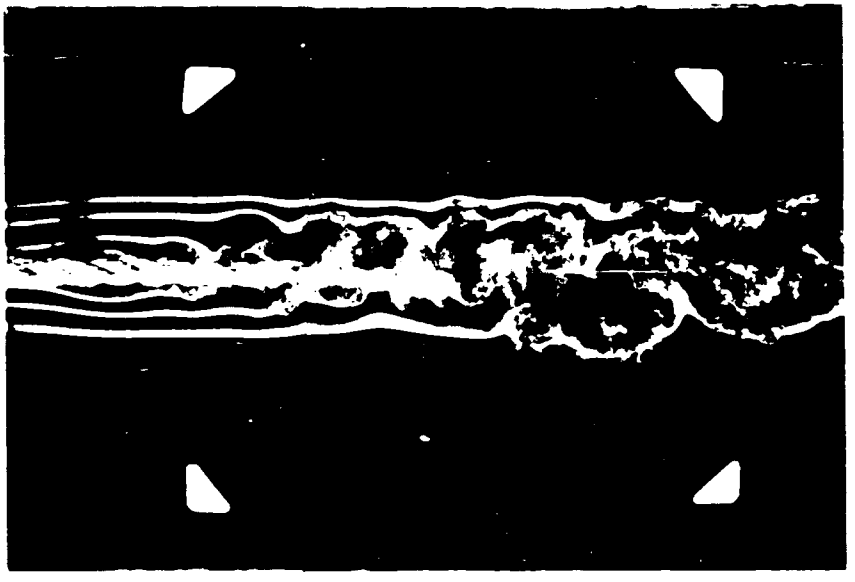

4X7 CABLE, 60° CABLE ANGLE, 44.9 FPS, SIDE VIEW

Figure 25. Side Views of the 4X7 Cable, $\beta = 60^{\circ}$, V=18.7 and 44.9 FPS

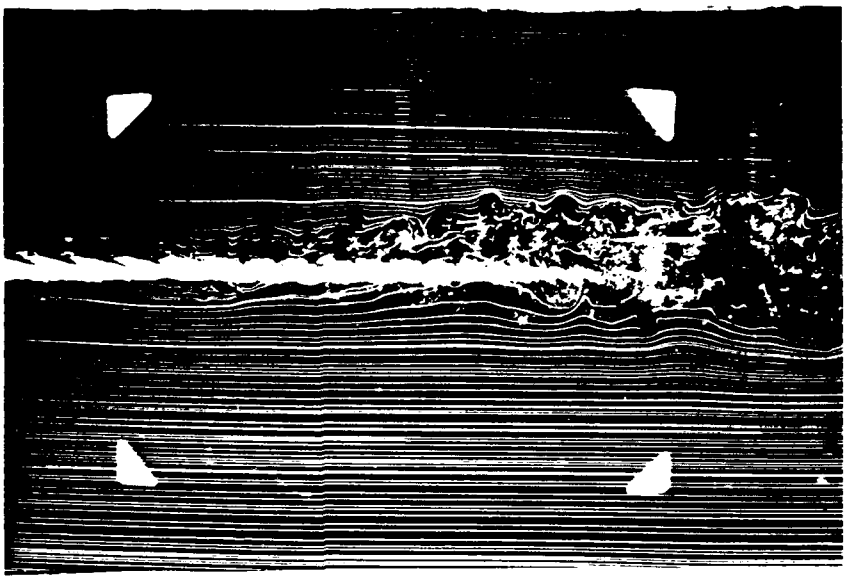

4X7 CABLE, 40° CABLE ANGLE, 18.7 FPS, SIDE VIEW

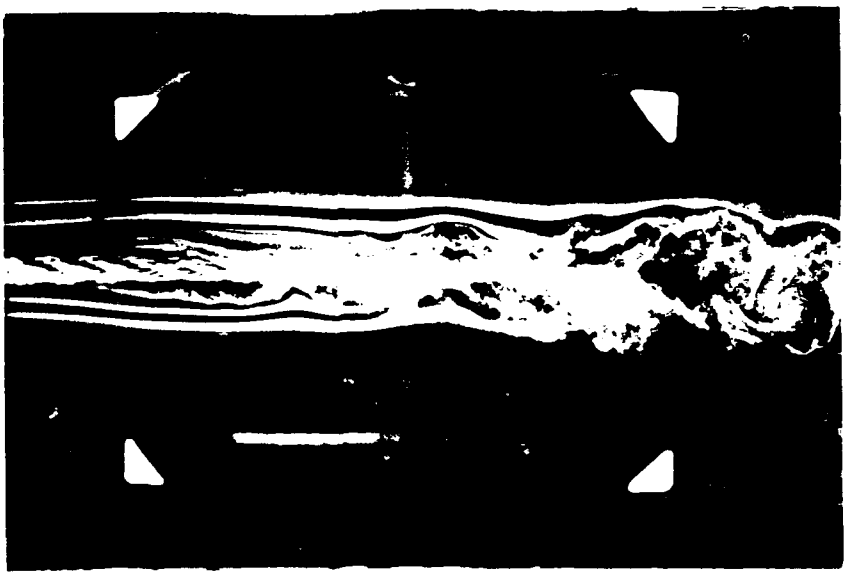

4X7 CABLE, 40° CABLE ANGLE, 44.9 FPS, SIDE VIEW

Figure 26. Side Views of the 4X7 Cable, $\beta = 40°$, V=18.7 and 44.9 FPS

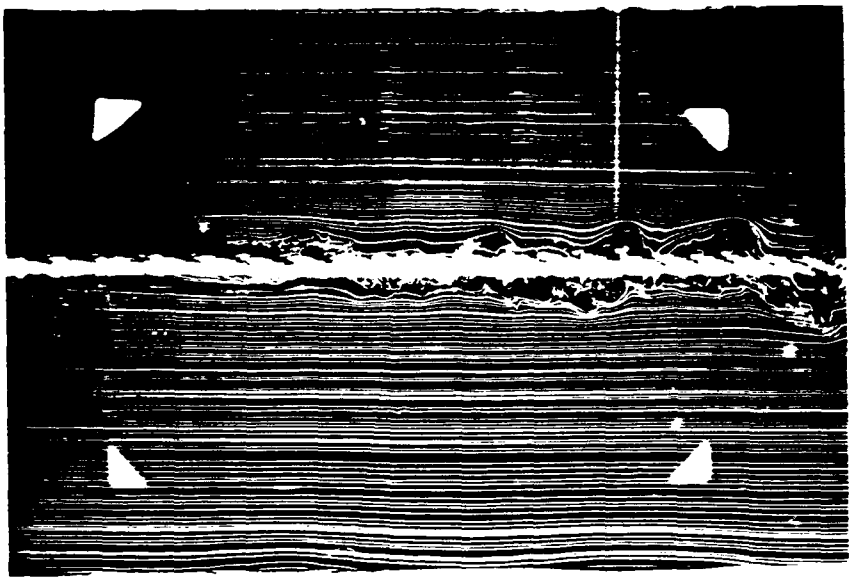

4X7 CABLE, 20° CABLE ANGLE, 18.7 FPS, SIDE VIEW

4X7 CABLE, 20° CABLE ANGLE, 44.9 FPS, SIDE VIEW

Figure 27. Side Views of the 4X7 Cable, $\beta = 20°$, V=18.7 and 44.9 FPS

REFERENCE SYSTEM AND NOTATION

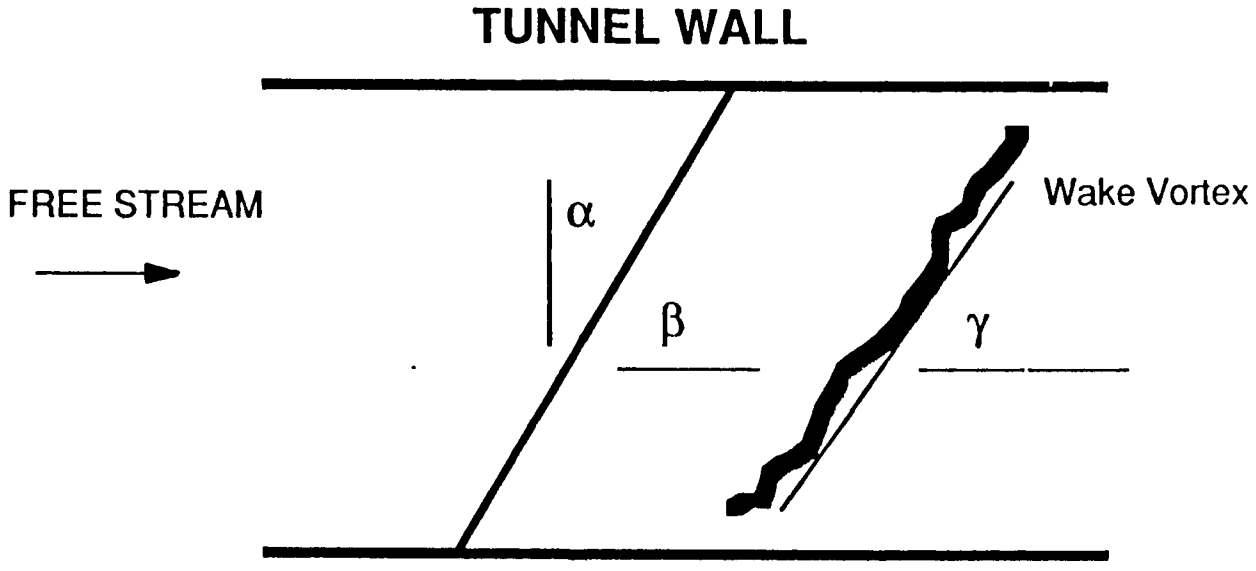

α - Yaw angle

β - Cable angle

γ - Shedding angle

Figure 28. Reference System and Notation.

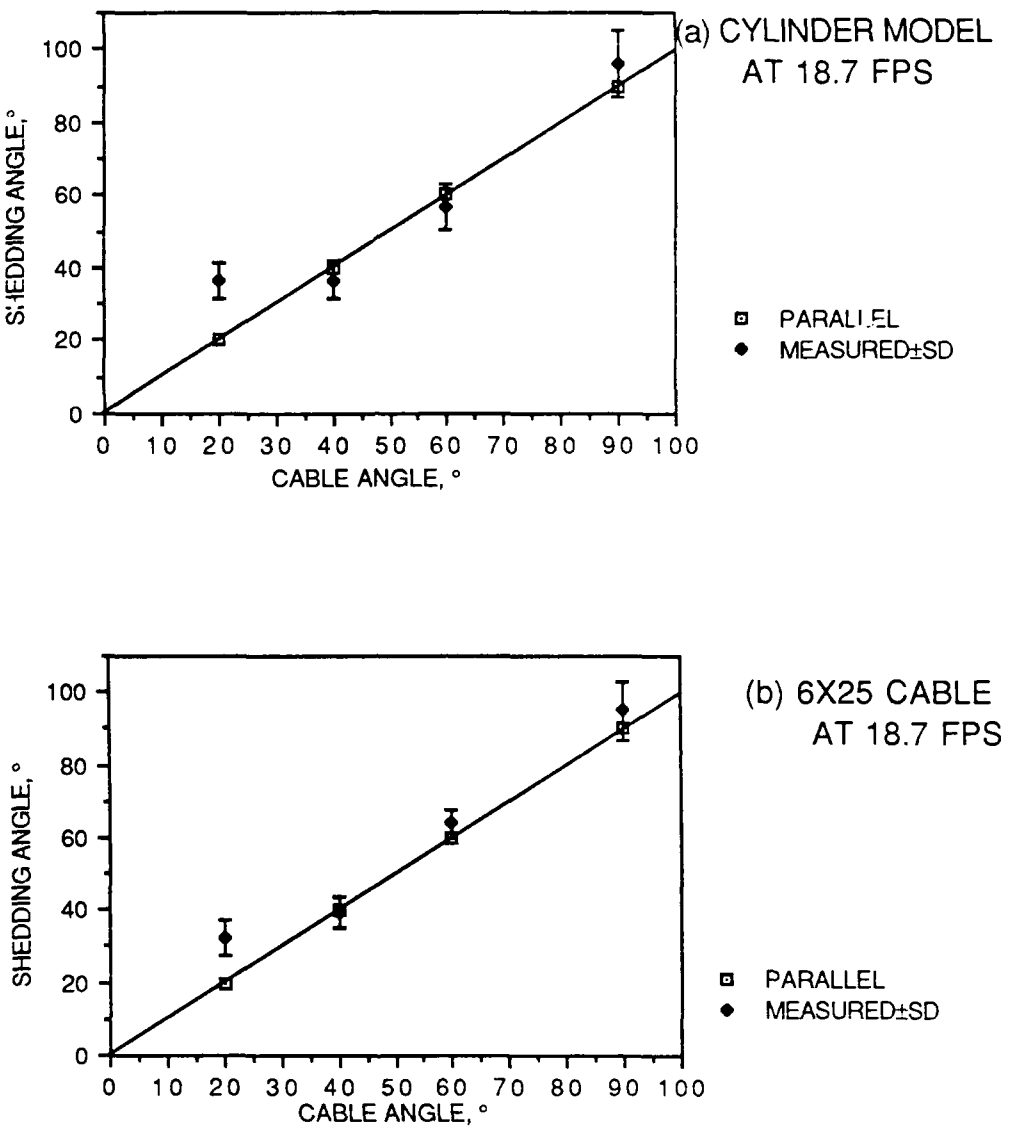

Figure 29. Shedding Angle Versus Yaw Angle From Digitized Plan View Photographs.

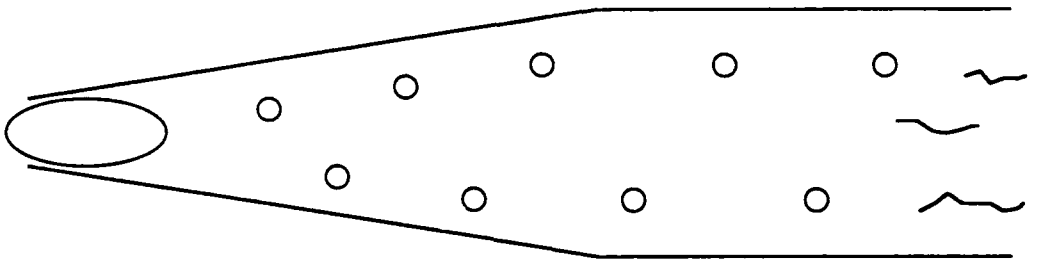

(a) CYLINDER WAKE PROFILE

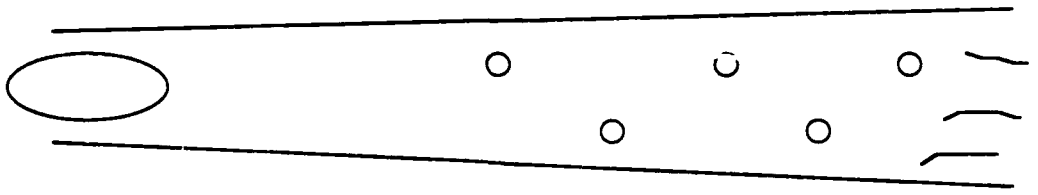

(b) 4X7 SERRATED CABLE WAKE PROFILE

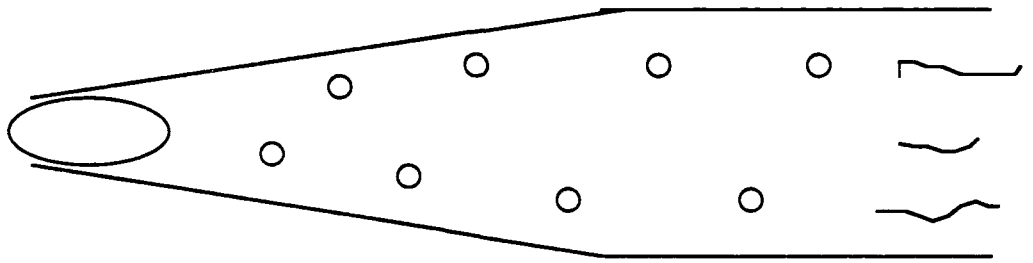

(c) 6X25 LANG LAY CABLE WAKE PROFILE

Figure 30. Typical Wake Profiles Illustrating Differences in Wake Width.

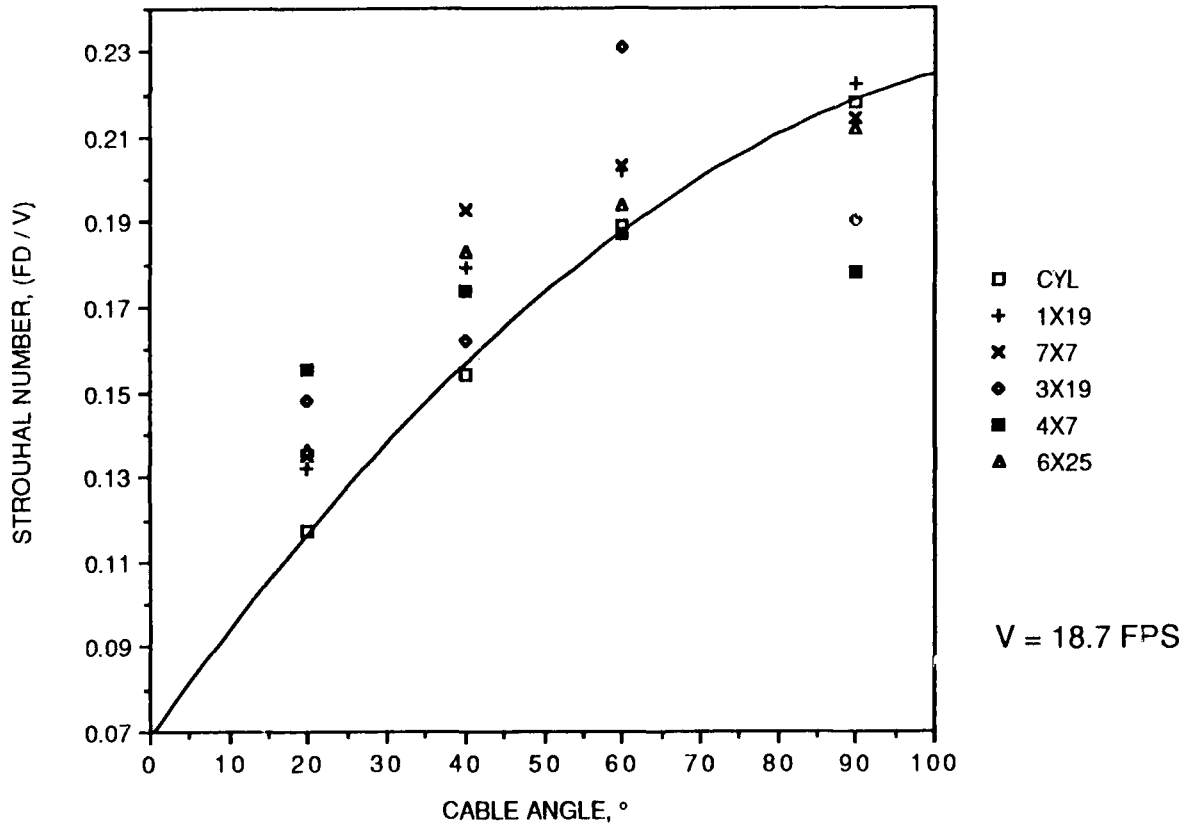

Figure 31. Strouhal Number Versus Cable Angle Based on Freestream Velocity

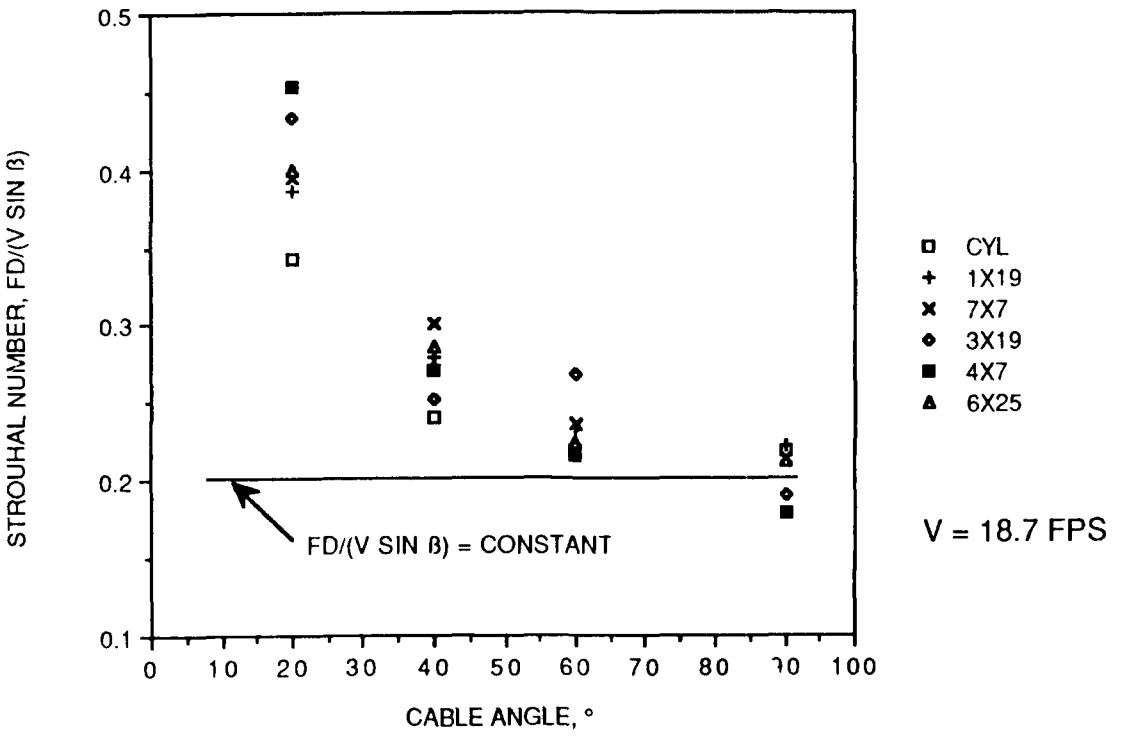

Figure 32. Strouhal Number Versus Yaw Angle Based on Normal Velocity

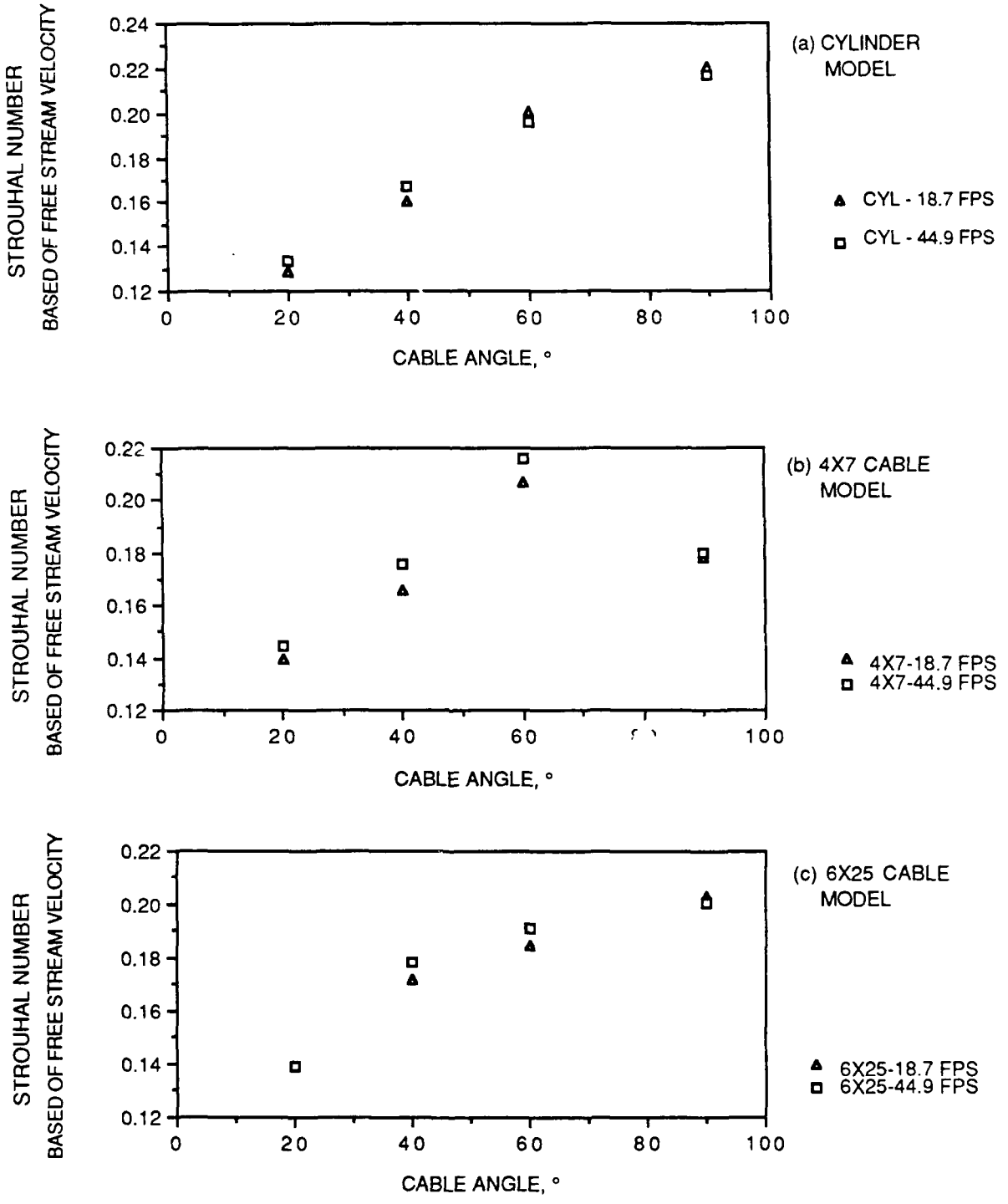

Figure 33. Effect of Velocity on Strouhal Number

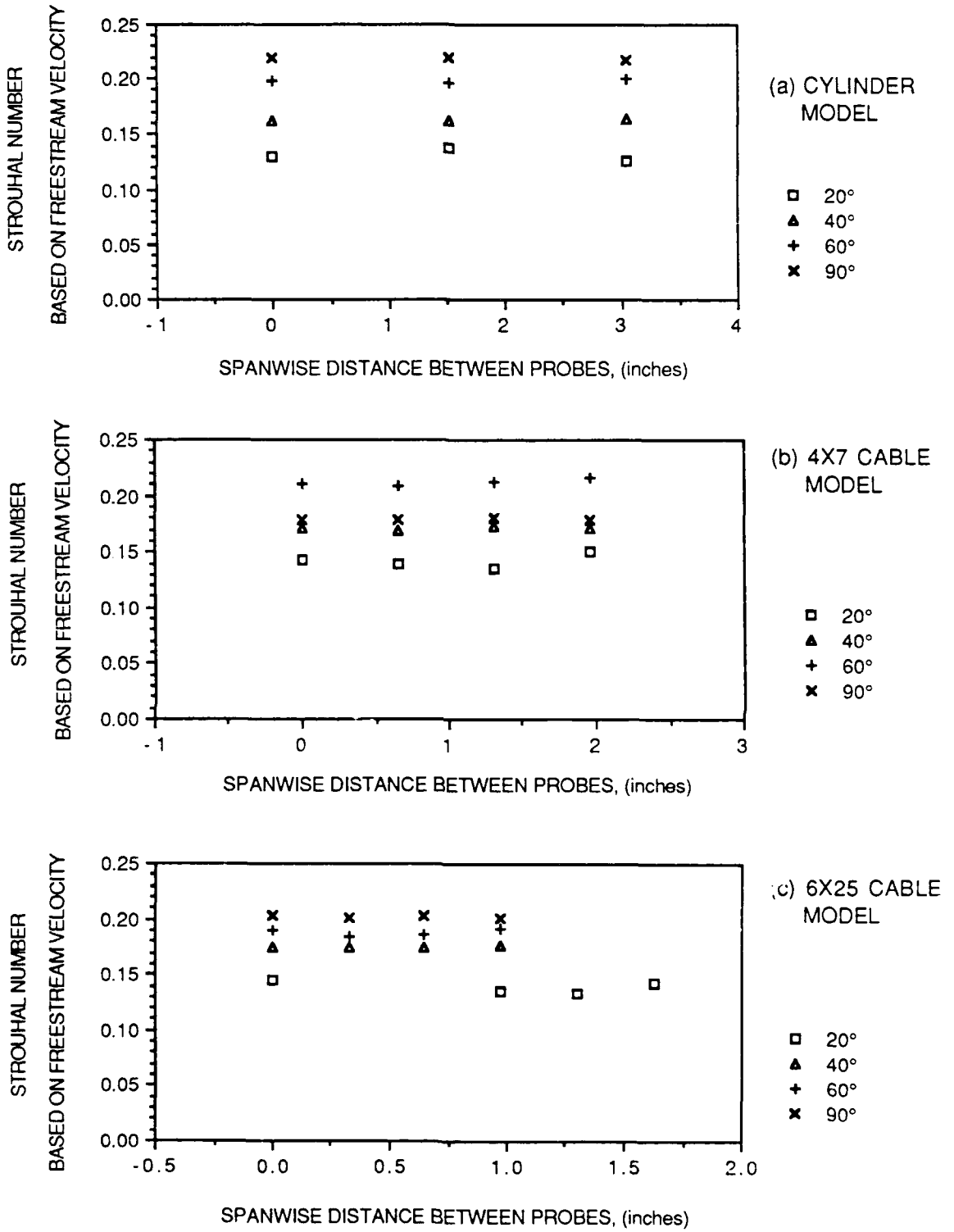

Figure 34. Average Strouhal Number Versus Spanwise Location for Velocity Range Tested

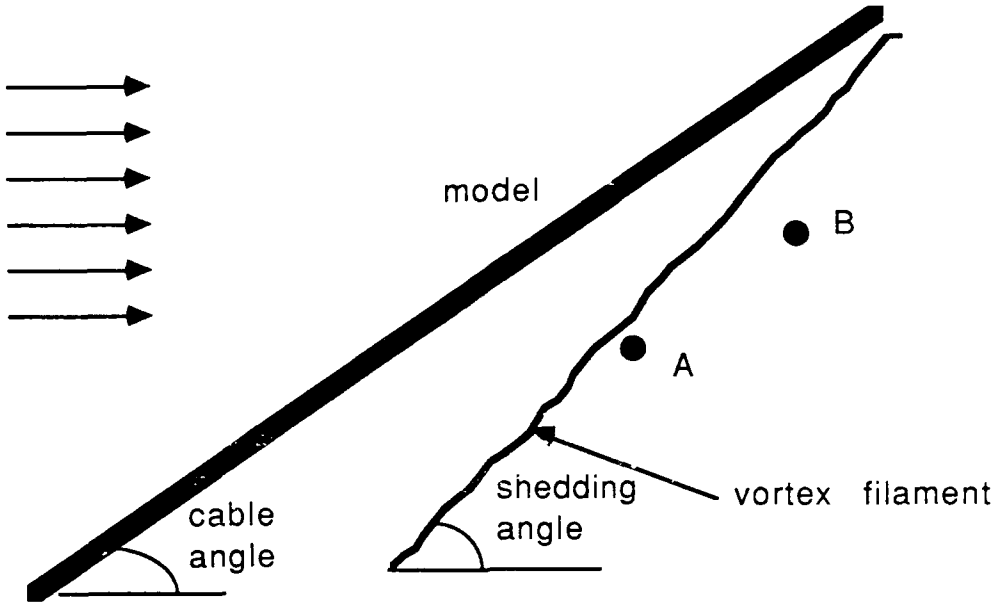

(a) SIGNAL B IS LAGGING, CORRESPONDS TO POSITIVE TIME SHIFT

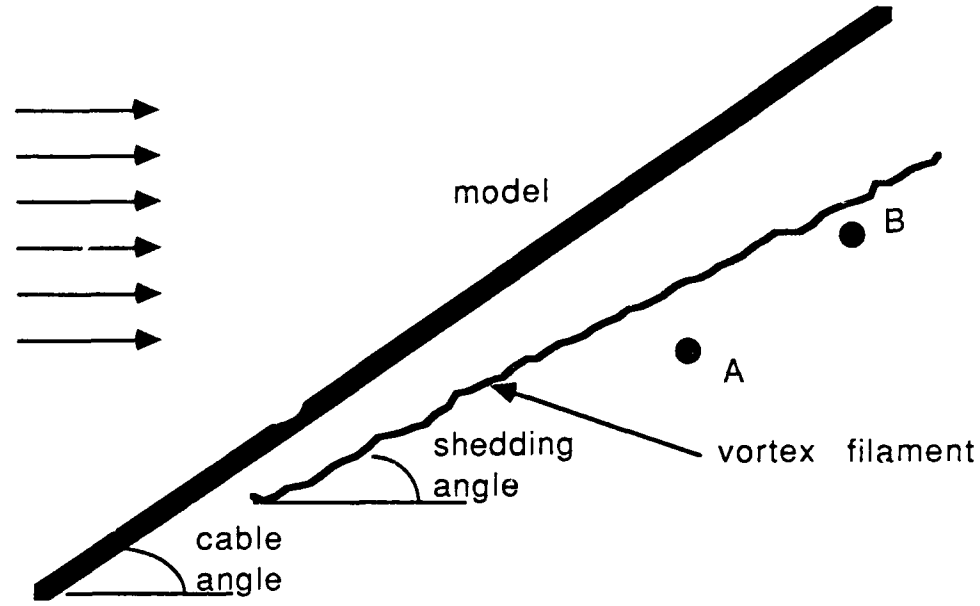

(b) SIGNAL B IS LEADING, CORRESPONDS TO NEGATIVE TIME SHIFT

Figure 35. Hypothetical Cases of Shedding Angles of Vortex Filaments

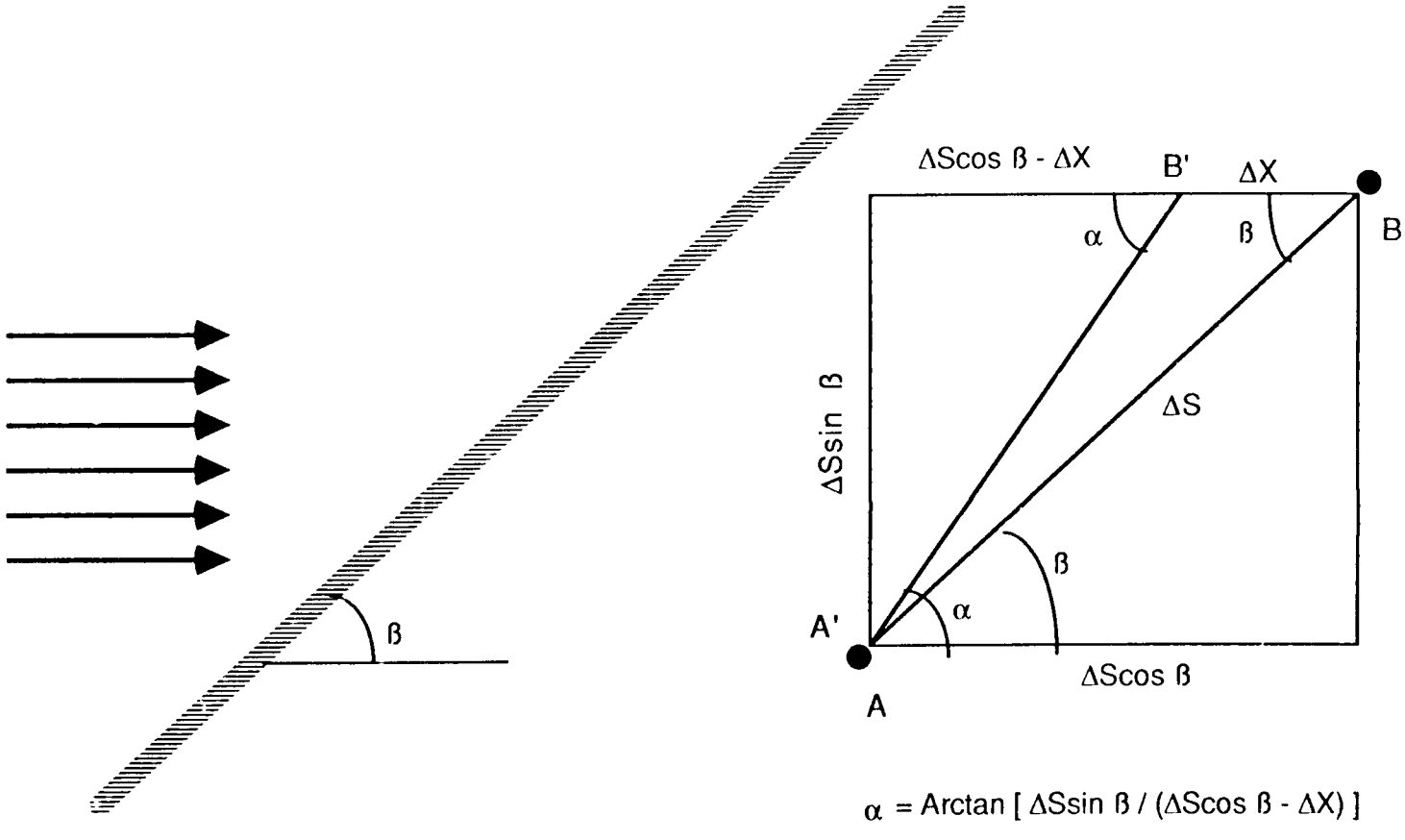

Figure 36. Calculation of the Shedding Angle.

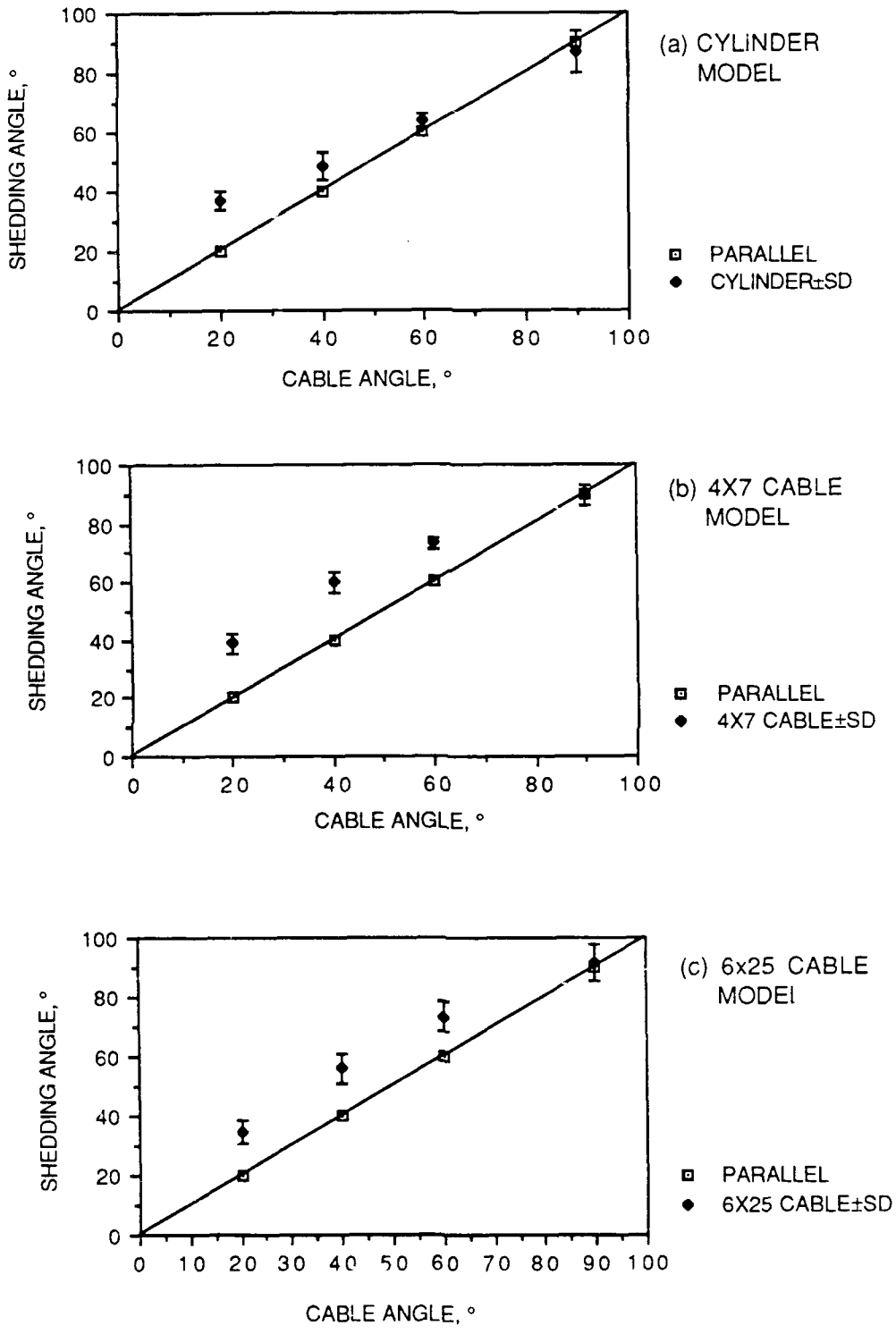

Figure 37. Shedding Angle Versus Cable Angle from Cross Correlation Data

APPENDIX A - Photographic Data

The following contains photographic data from the preliminary phase flow visualization study for each of the cable models and the circular cylinder. All the data is for a flow speed of 18.7 ft/sec and both plan view and side view data are presented.

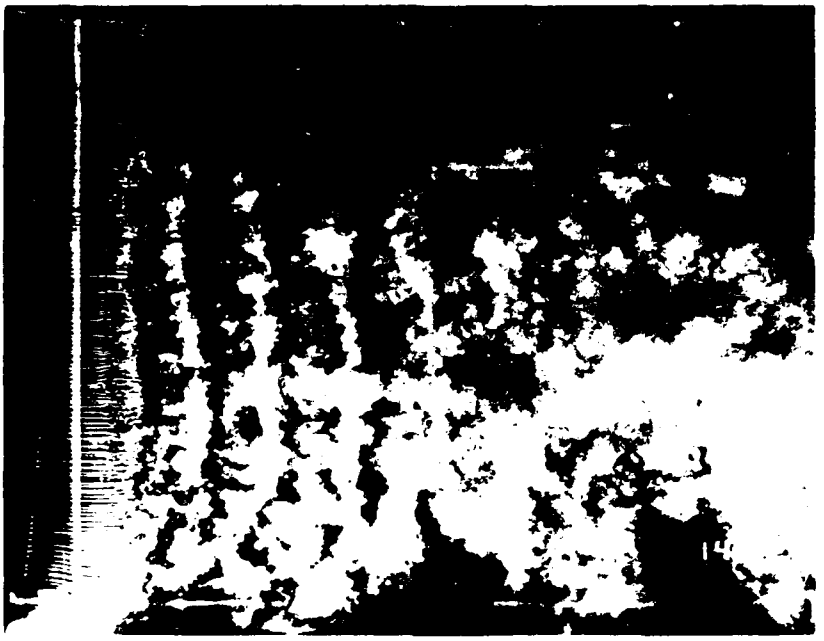

CYLINDER, 90° CABLE ANGLE, 18.7 FPS, PLAN VIEW

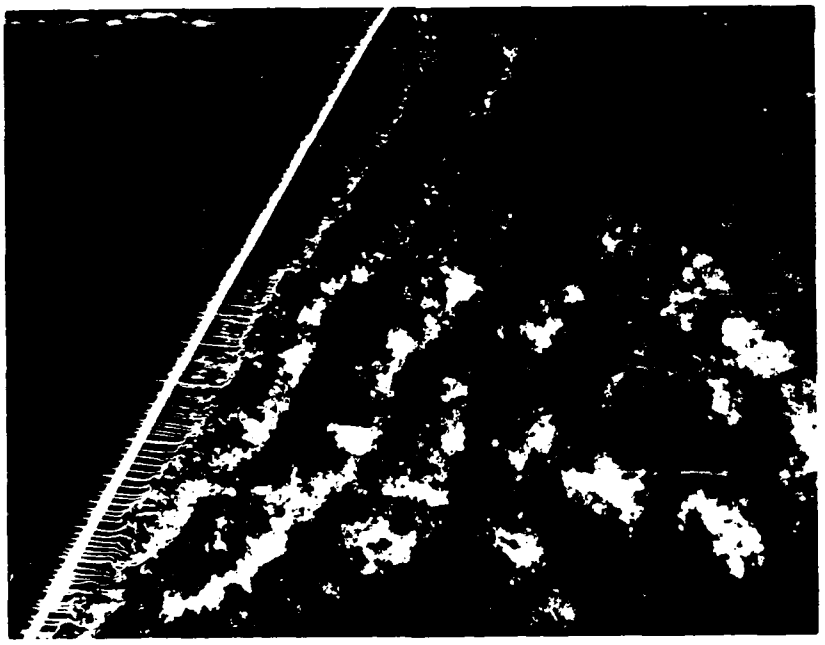

CYLINDER, 60° CABLE ANGLE, 18.7 FPS, PLAN VIEW

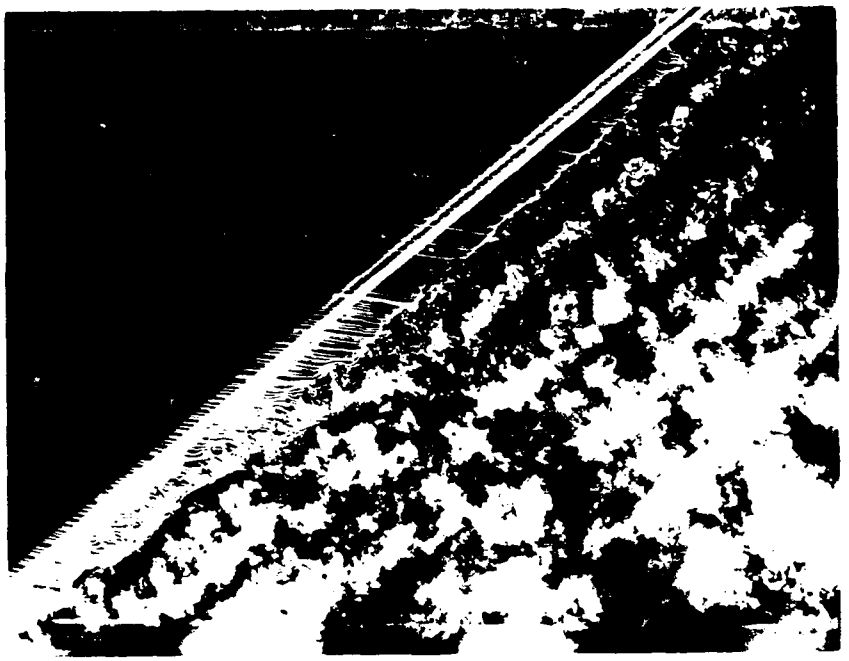

CYLINDER, 40° CABLE ANGLE, 18.7 FPS, PLAN VIEW

CYLINDER, 20° CABLE ANGLE, 18.7 FPS, PLAN VIEW

1X19 CABLE, 90° CABLE ANGLE, 18.7 FPS, PLAN VIEW

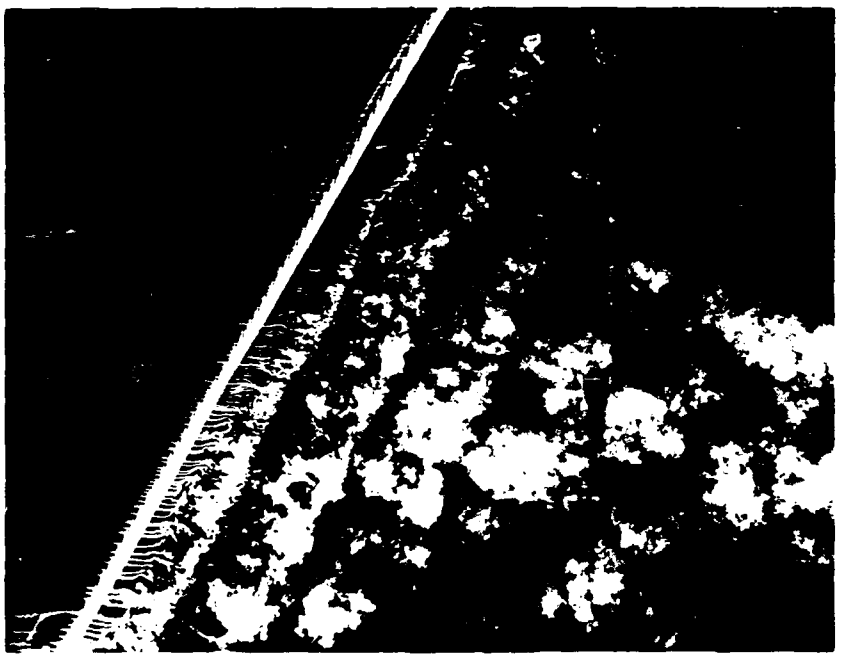

1X19 CABLE, 60° CABLE ANGLE, 18.7 FPS, PLAN VIEW

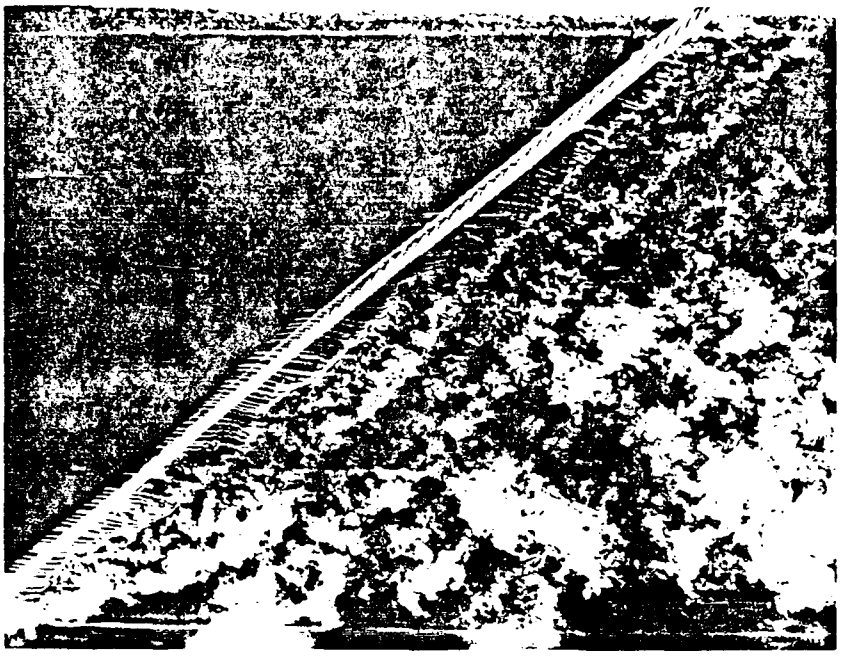

1X19 CABLE, 40° CABLE ANGLE, 18.7 FPS, PLAN VIEW

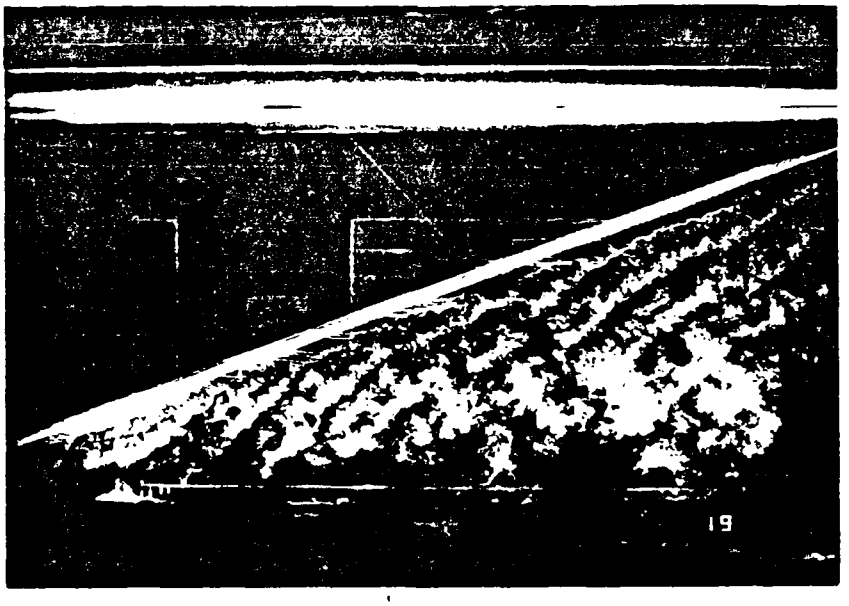

1X19 CABLE, 20° CABLE ANGLE, 18.7 FPS, PLAN VIEW

7X7 CABLE, 90° CABLE ANGLE, 18.7 FPS, PLAN VIEW

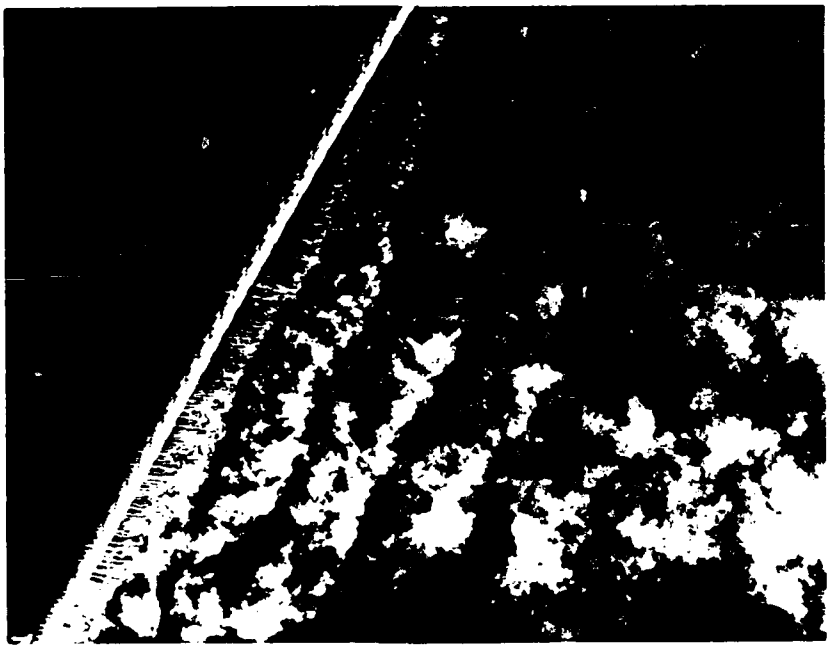

7X7 CABLE, 60° CABLE ANGLE, 18.7 FPS, PLAN VIEW

7X7 CABLE, 40° CABLE ANGLE, 18.7 FPS, PLAN VIEW

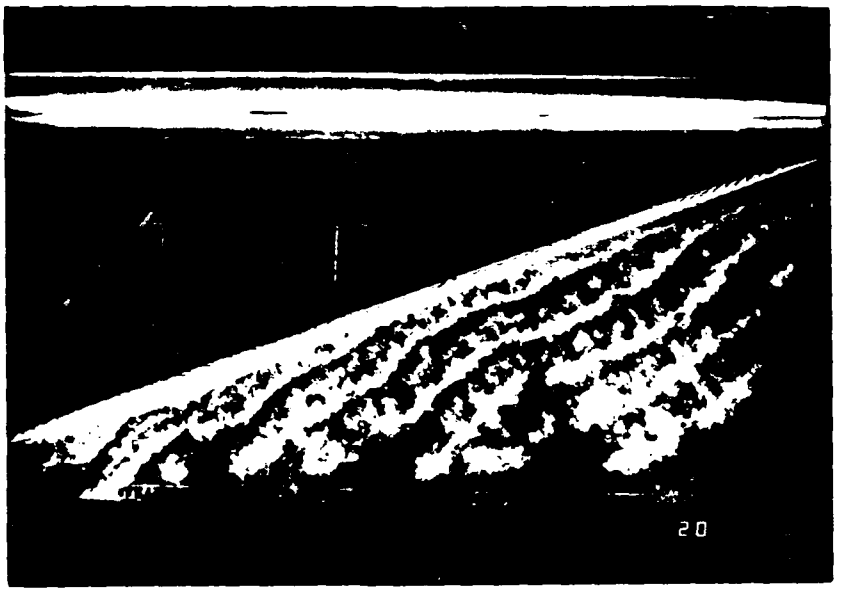

7X7 CABLE, 20° CABLE ANGLE, 18.7 FPS, PLAN VIEW

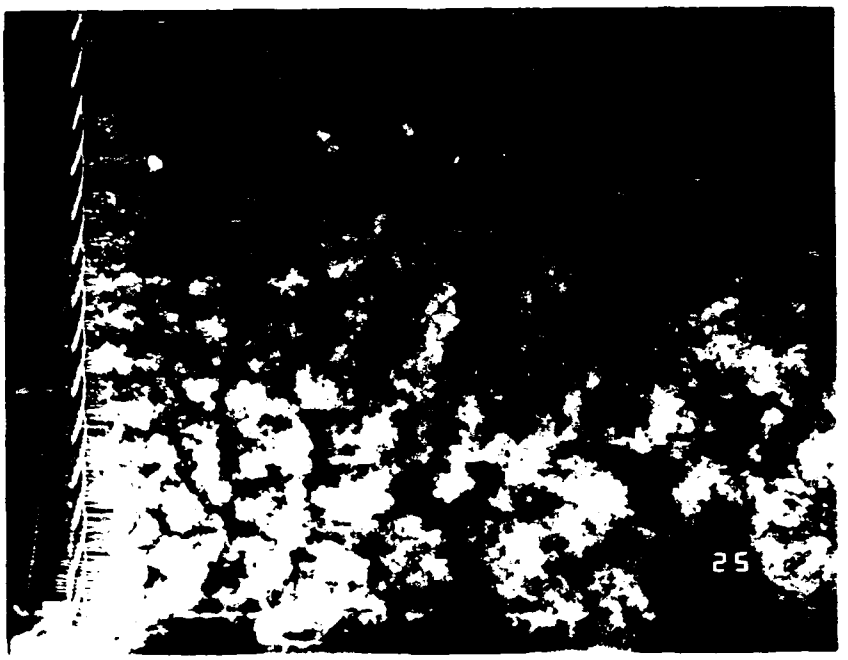

3X19 CABLE, 90° CABLE ANGLE, 18.7 FPS, PLAN VIEW

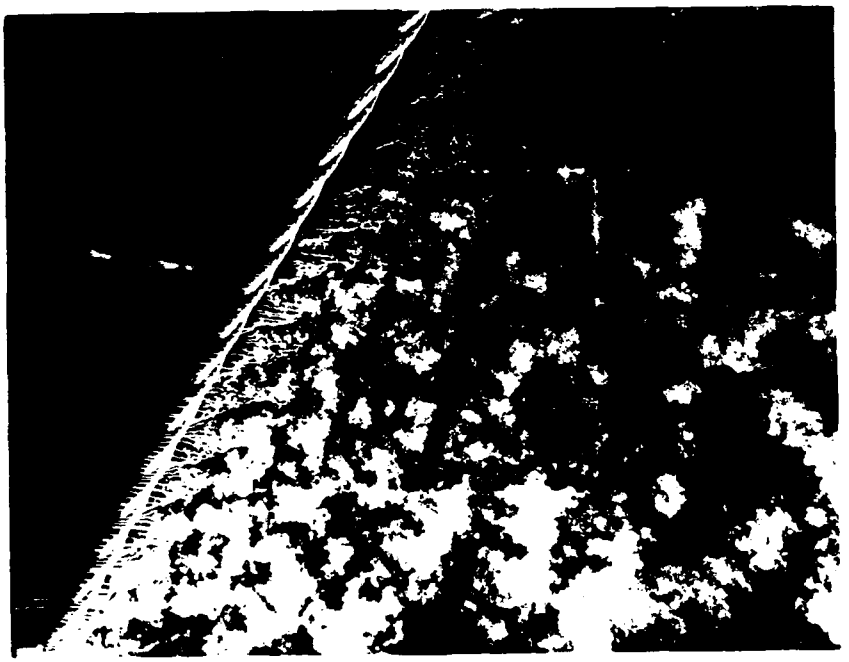

3X19 CABLE, 60° CABLE ANGLE, 18.7 FPS, PLAN VIEW

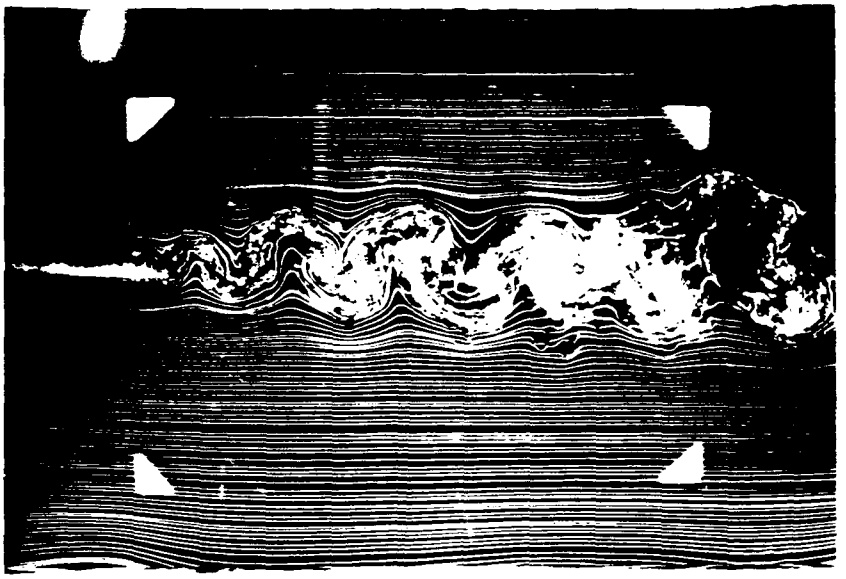

CYLINDER, 90° CABLE ANGLE, 18.7 FPS, SIDE VIEW

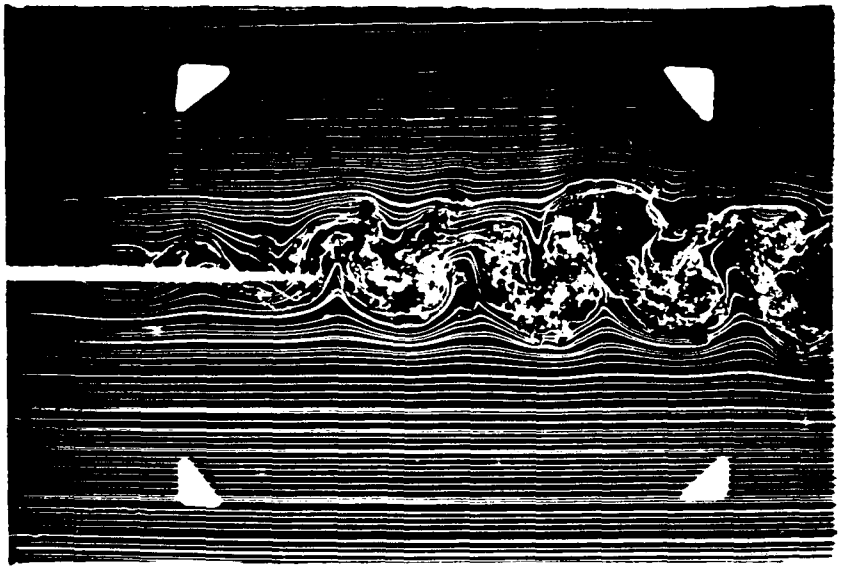

CYLINDER, 60° CABLE ANGLE, 18.7 FPS, SIDE VIEW

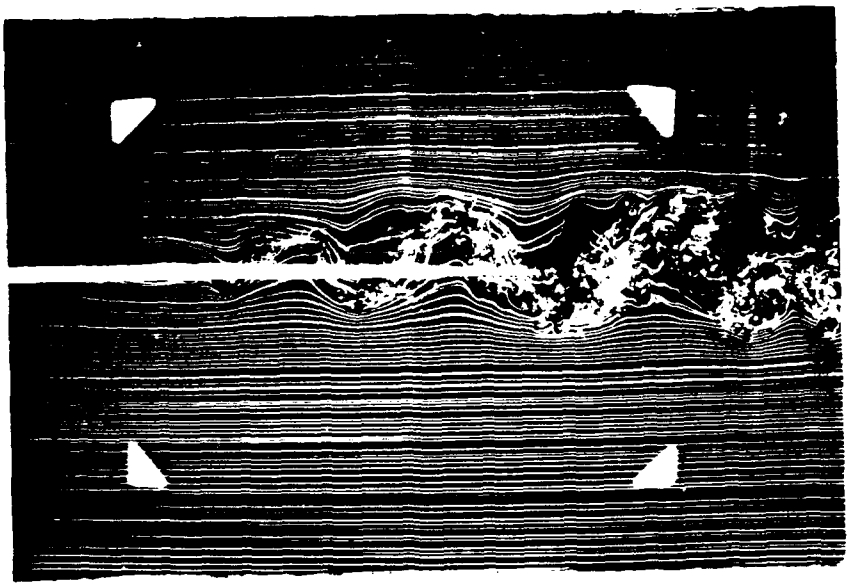

CYLINDER, 40° CABLE ANGLE, 18.7 FPS, SIDE VIEW

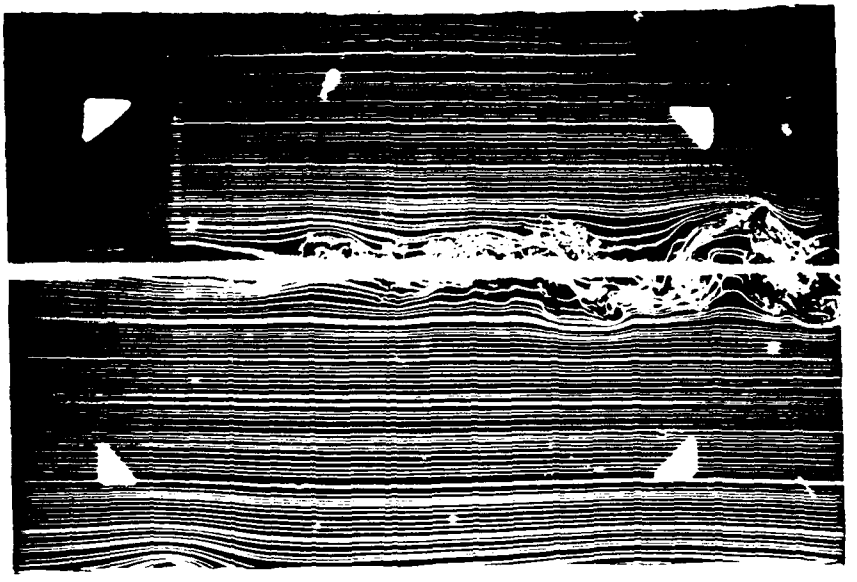

CYLINDER, 20° CABLE ANGLE, 18.7 FPS, SIDE VIEW

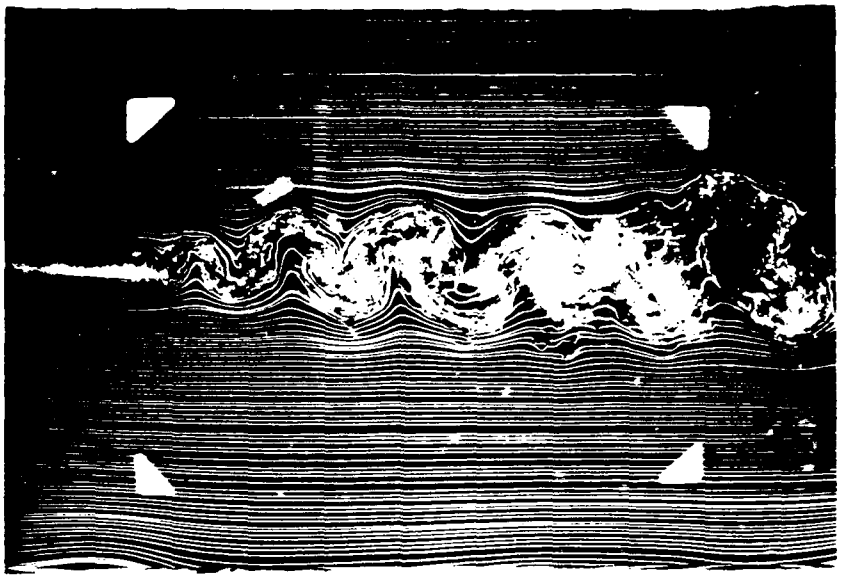

CYLINDER, 90° CABLE ANGLE, 18.7 FPS, SIDE VIEW

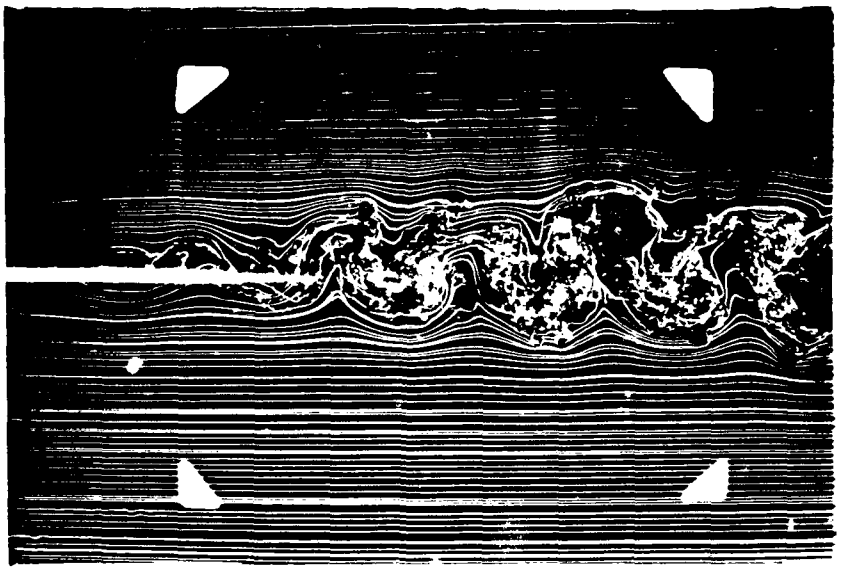

CYLINDER, 60° CABLE ANGLE, 18.7 FPS, SIDE VIEW

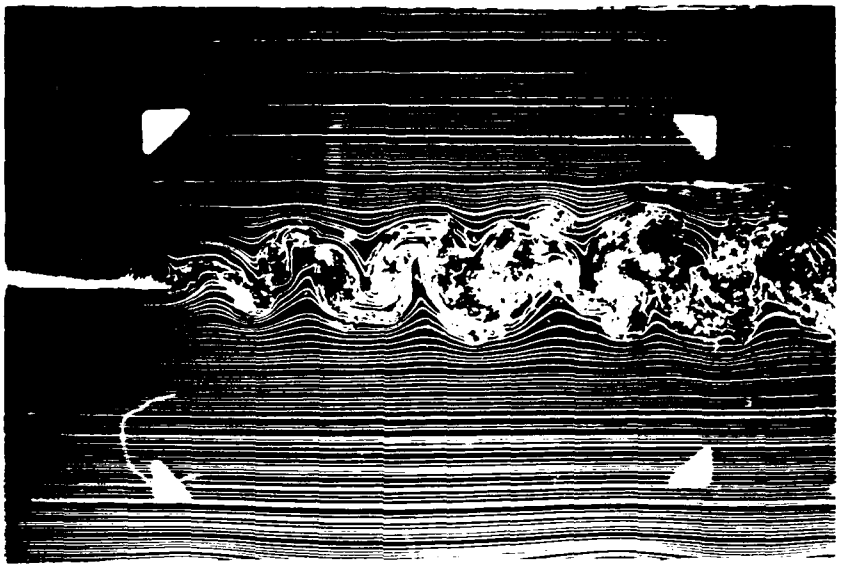

1X19 CABLE, 90° CABLE ANGLE, 18.7 FPS, SIDE VIEW

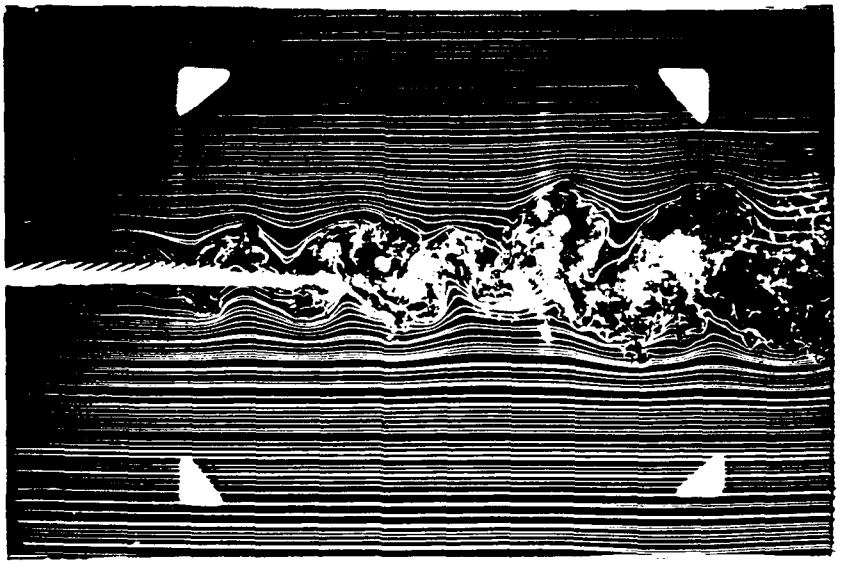

1X19 CABLE, 60° CABLE ANGLE, 18.7 FPS, SIDE VIEW

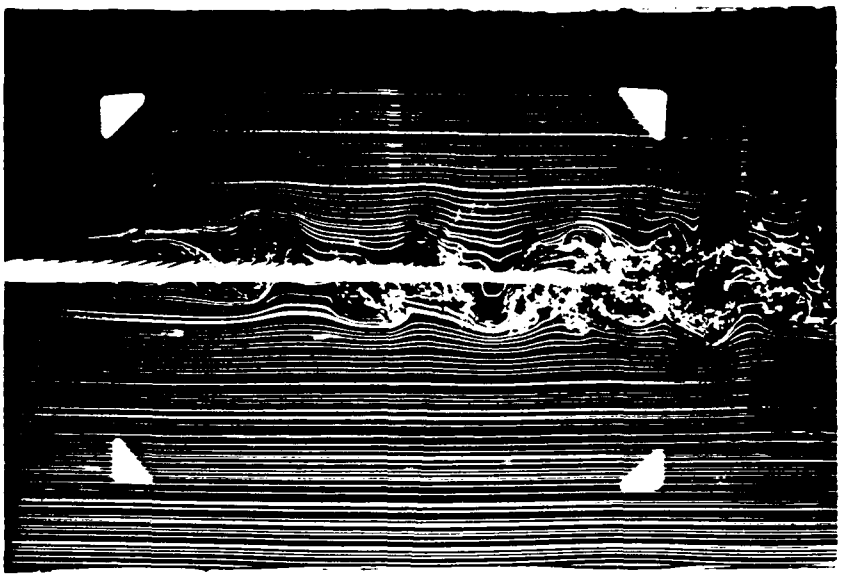

1X19 CABLE, 40° CABLE ANGLE, 18.7 FPS, SIDE VIEW

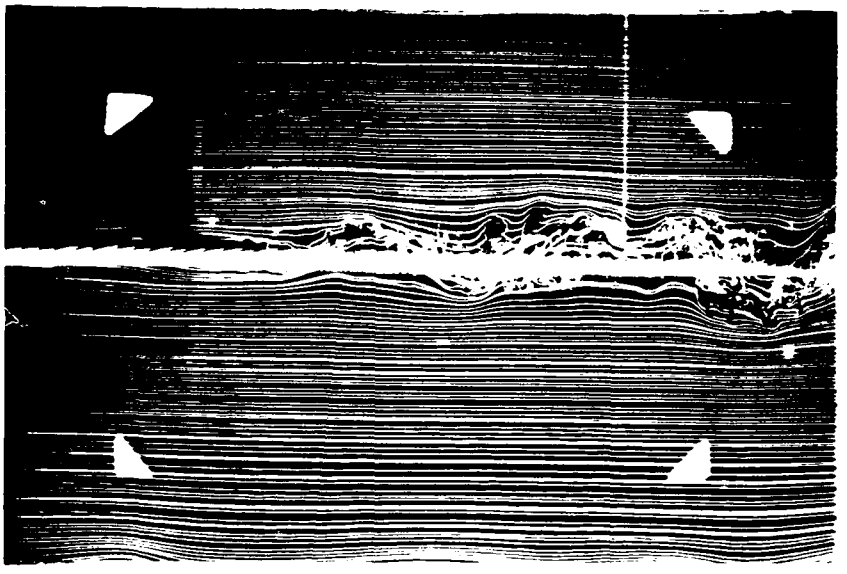

1X19 CABLE, 20° CABLE ANGLE, 18.7 FPS, SIDE VIEW

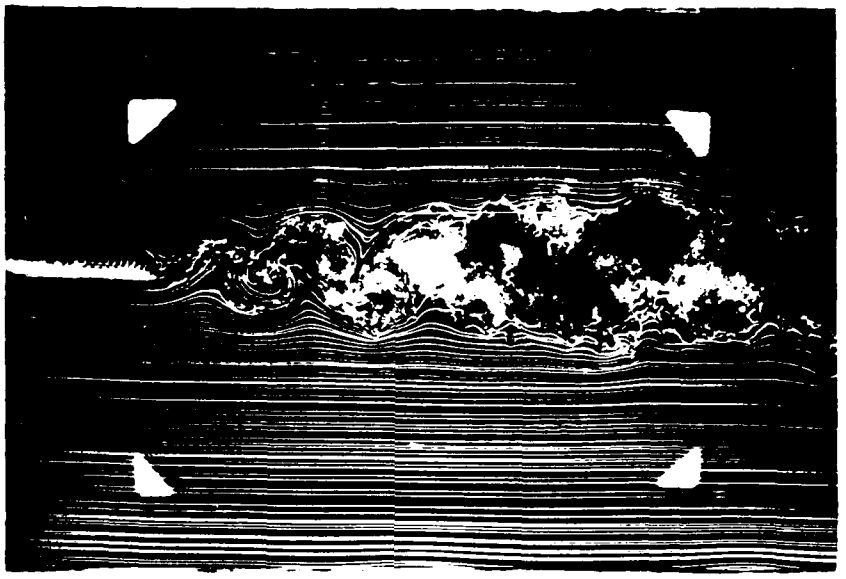

7X7 CABLE, 90° CABLE ANGLE, 18.7 FPS, SIDE VIEW

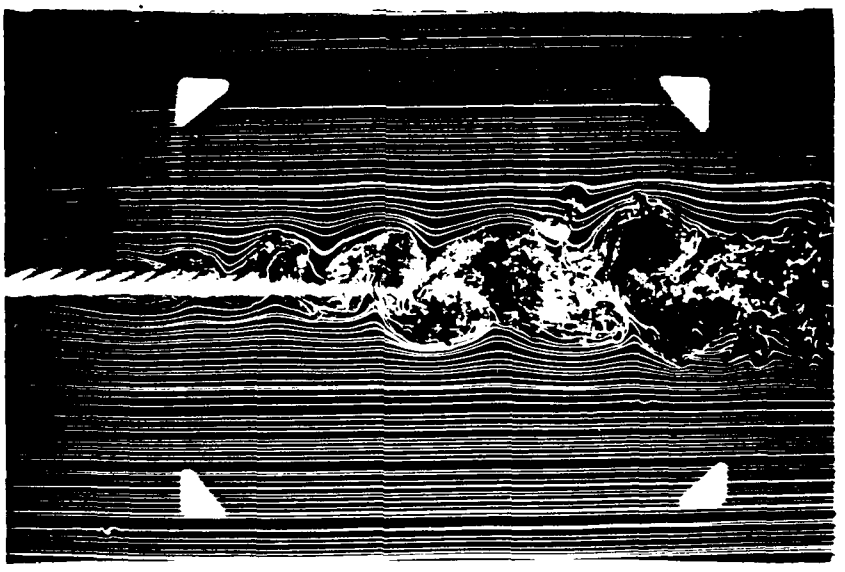

7X7 CABLE, 60° CABLE ANGLE, 18.7 FPS, SIDE VIEW

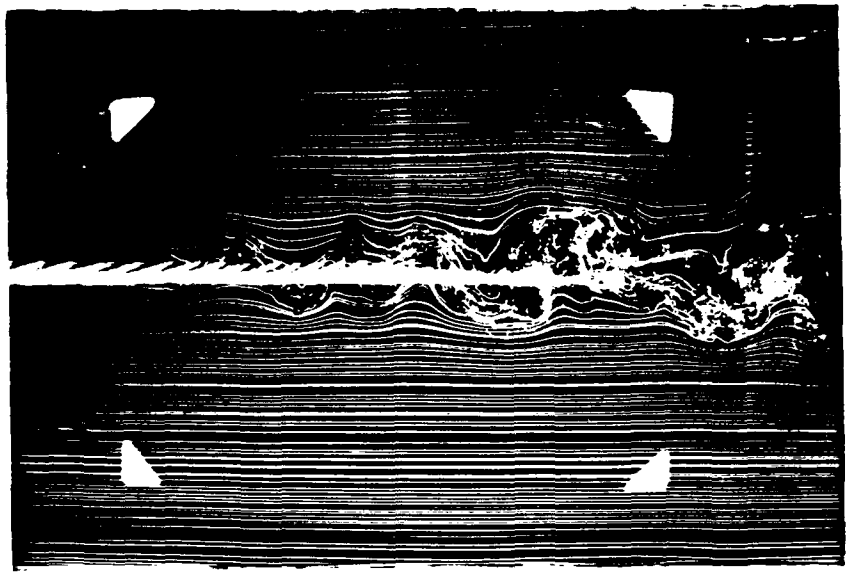

7X7 CABLE 40° CABLE ANGLE, 18.7 FPS, SIDE VIEW

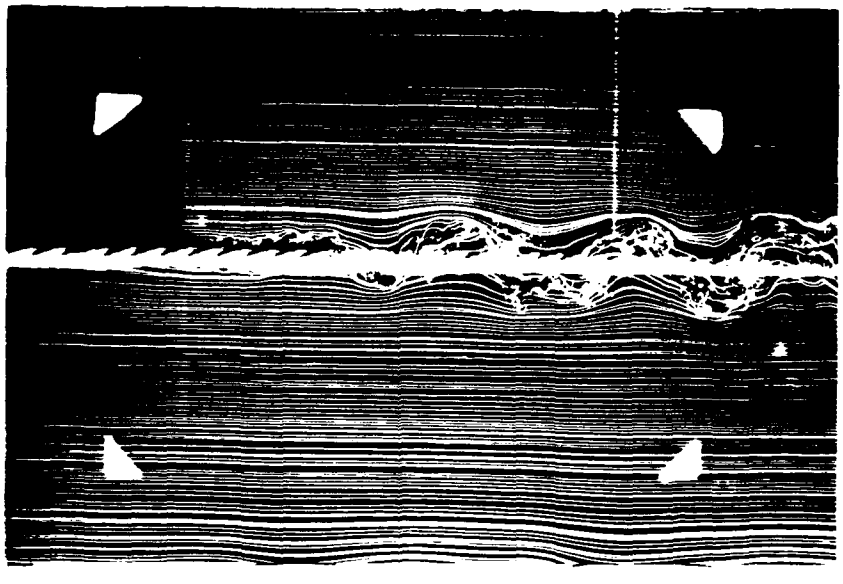

7X7 CABLE, 20° CABLE ANGLE, 18.7 FPS, SIDE VIEW

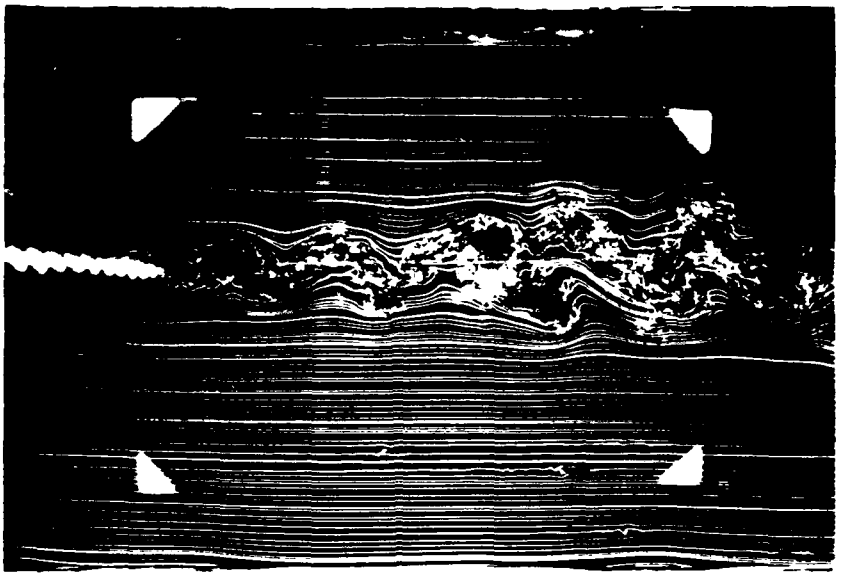

3X19 CABLE, 90° CABLE ANGLE, 18.7 FPS, SIDE VIEW

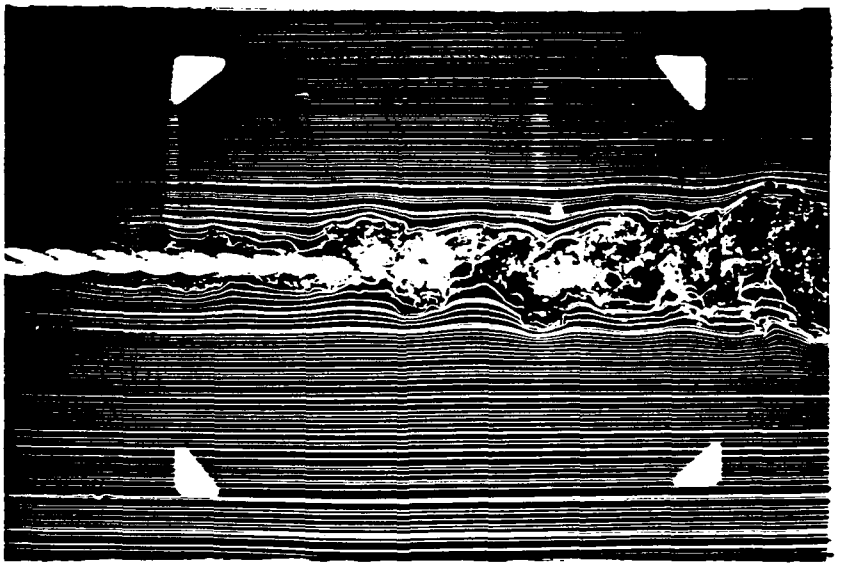

3X19 CABLE, 60° CABLE ANGLE, 18.7 FPS, SIDE VIEW

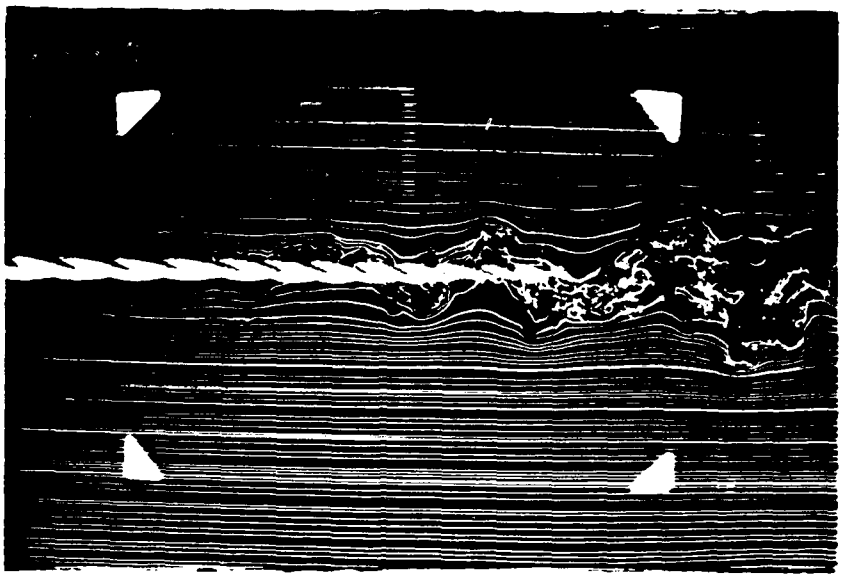

3X19 CABLE, 40° CABLE ANGLE, 18.7 FPS, SIDE VIEW

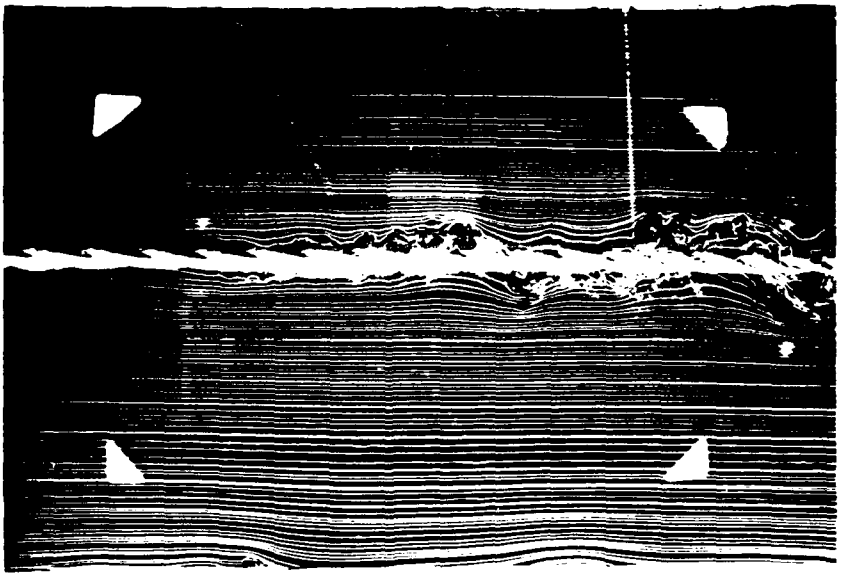

3X19 CABLE, 20° CABLE ANGLE, 18.7 FPS, SIDE VIEW

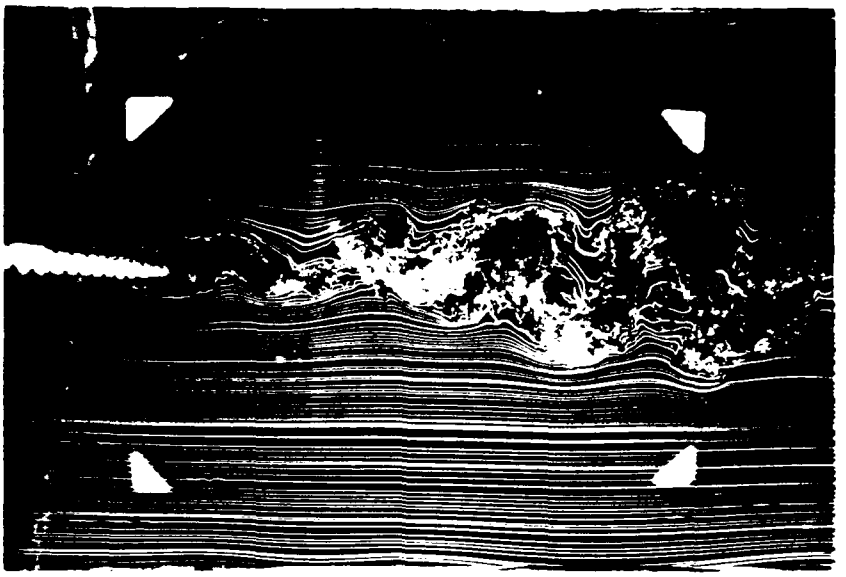

4X7 CABLE, 90° CABLE ANGLE, 18.7 FPS, SIDE VIEW

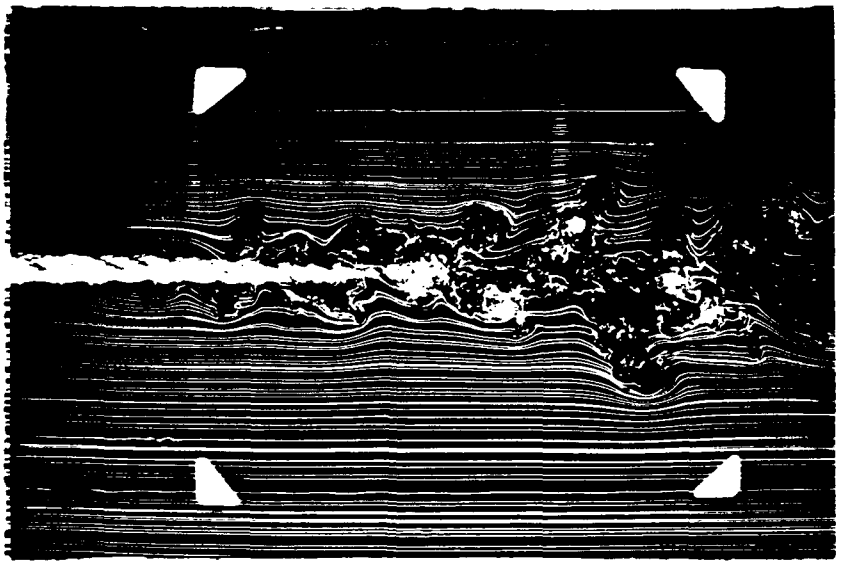

4X7 CABLE, 60° CABLE ANGLE, 18.7 FPS, SIDE VIEW

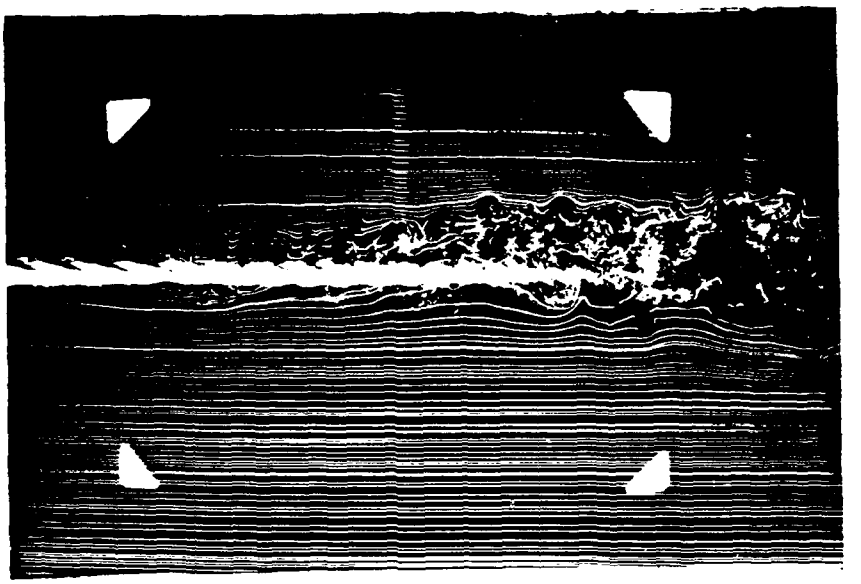

4X7 CABLE, 40° CABLE ANGLE, 18.7 FPS, SIDE VIEW

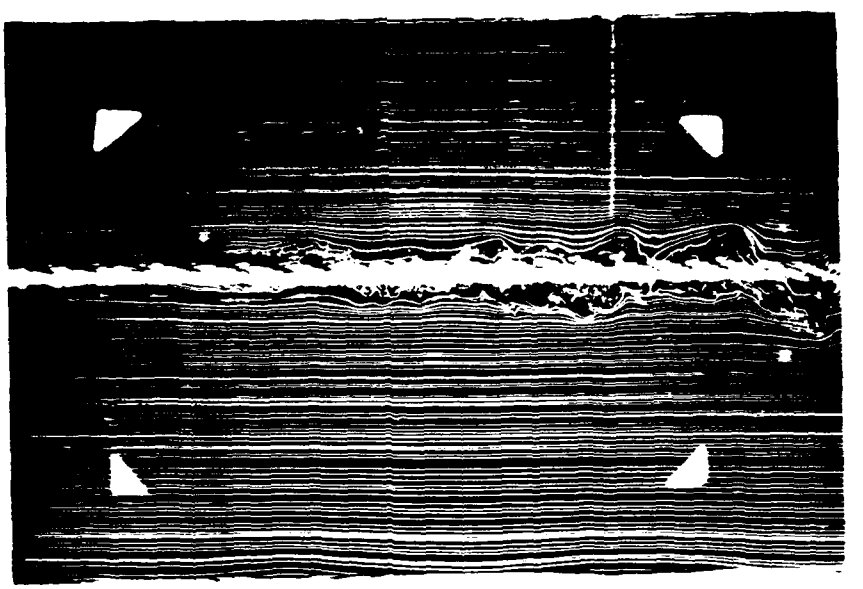

4X7 CABLE, 20° CABLE ANGLE, 18.7 FPS, SIDE VIEW

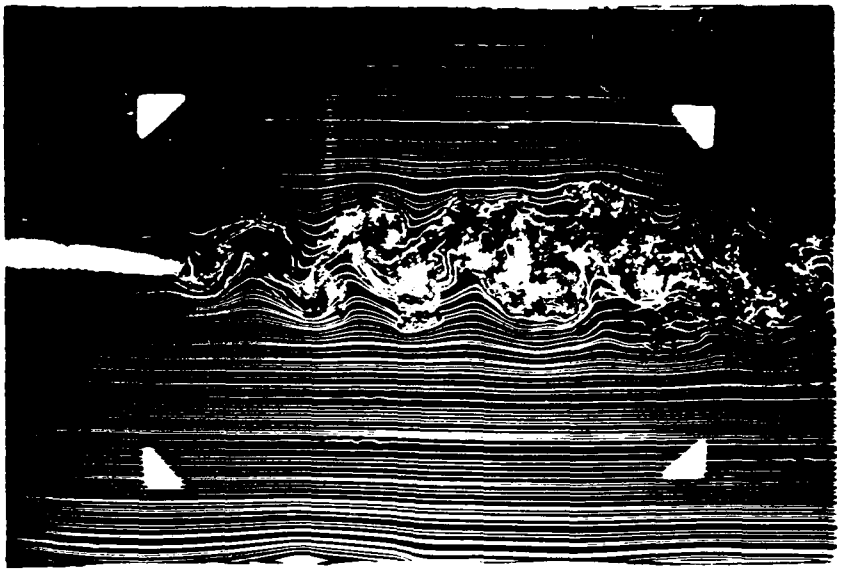

6X25 CABLE, 90° CABLE ANGLE, 18.7 FPS, SIDE VIEW

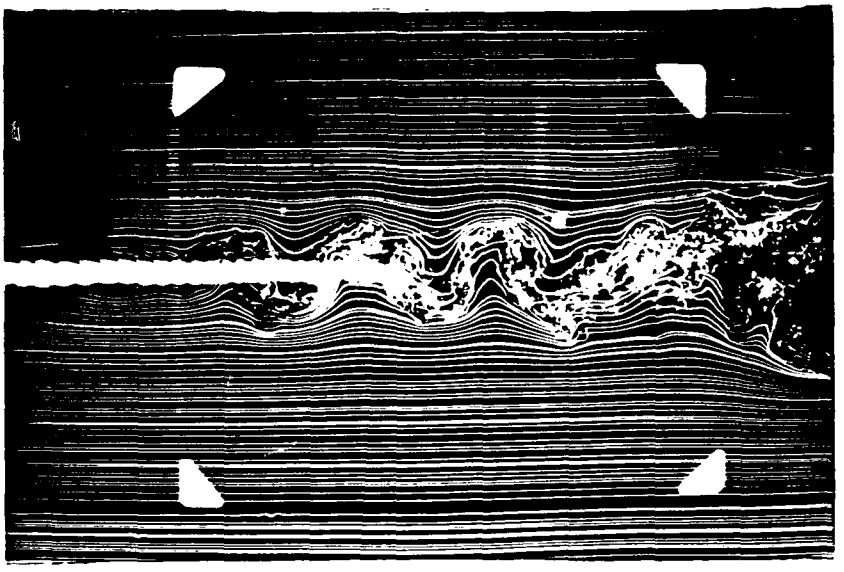

6X25 CABLE, 60° CABLE ANGLE, 18.7 FPS, SIDE VIEW

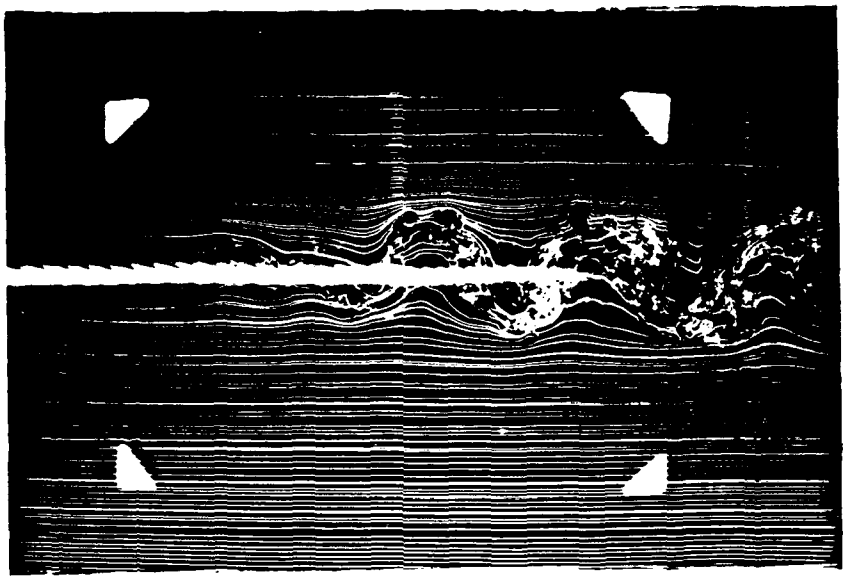

6X25 CABLE, 40° CABLE ANGLE, 18.7 FPS, SIDE VIEW

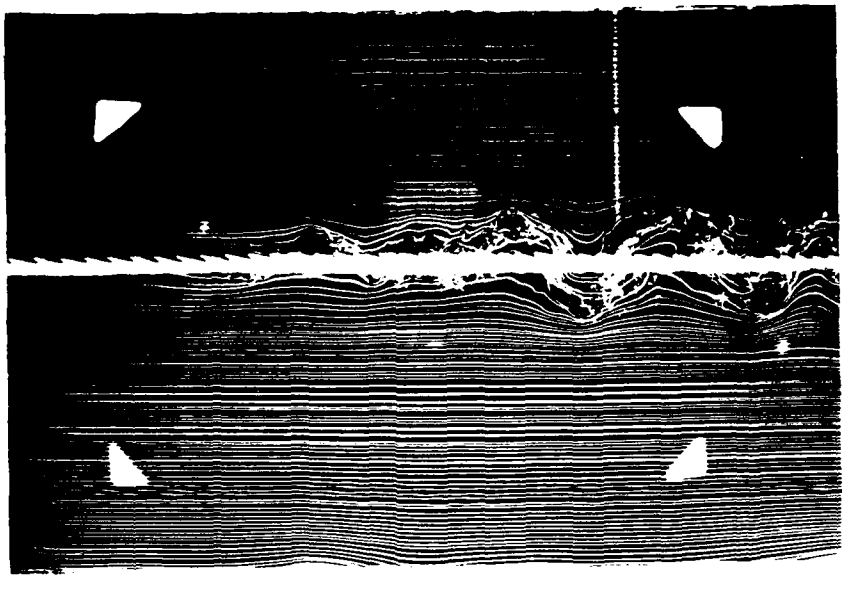

6X25 CABLE, 20° CABLE ANGLE, 18.7 FPS, SIDE VIEW

APPENDIX B - Wake Spectra

The following contains wake spectrum data for each of the 4X7 and 6X25 cable models and the circular cylinder. The data is for both flow speeds of 18.7 ft/sec and 45 ft/sec for each of the cable angles tested.

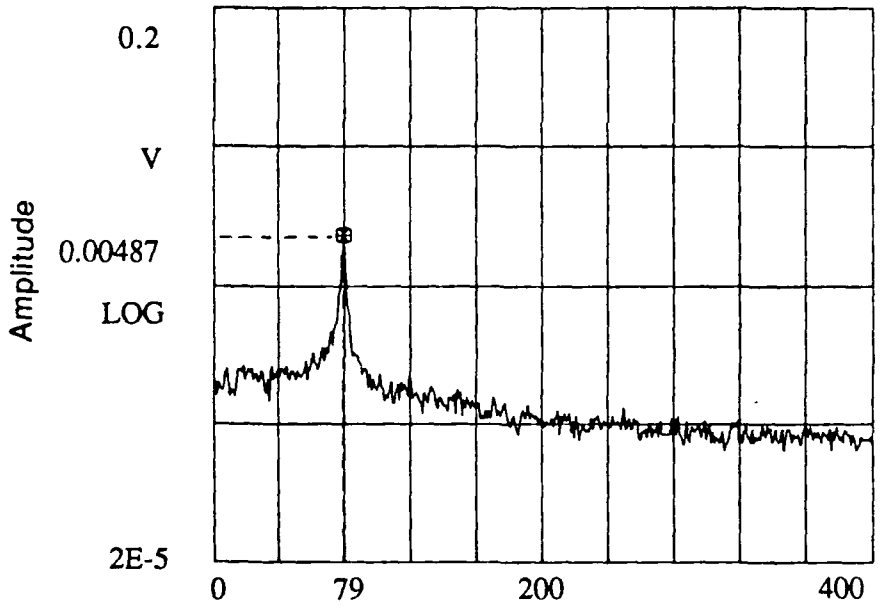

Frequency, HZ

Cylinder, 90° Cable Angle, 18 FPS

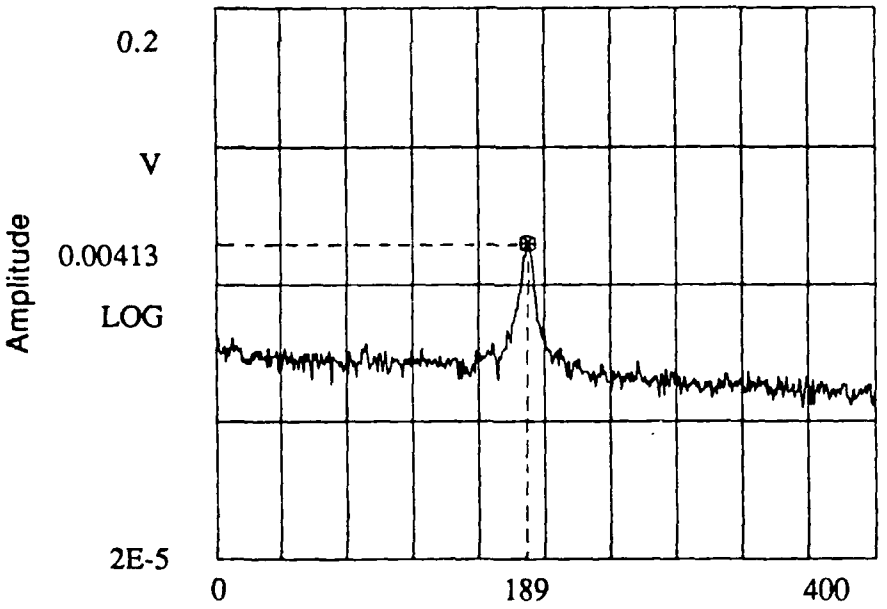

Frequency, HZ

Cylinder, 90° Cable Angle, 45 FPS

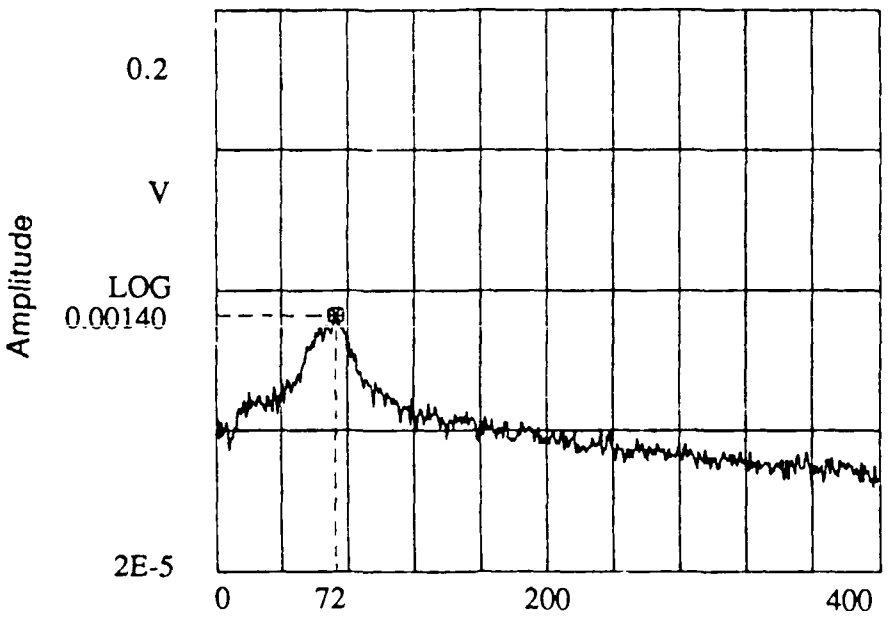

Frequency, HZ

Cylinder, 60° Cable Angle, 18 FPS

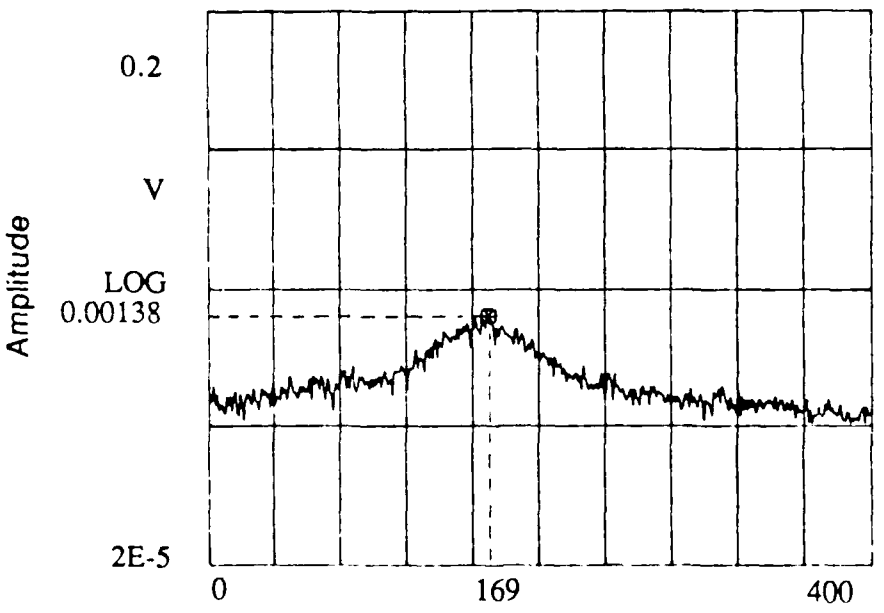

Frequency, HZ

Cylinder, 60° Cable Angle, 45 FPS

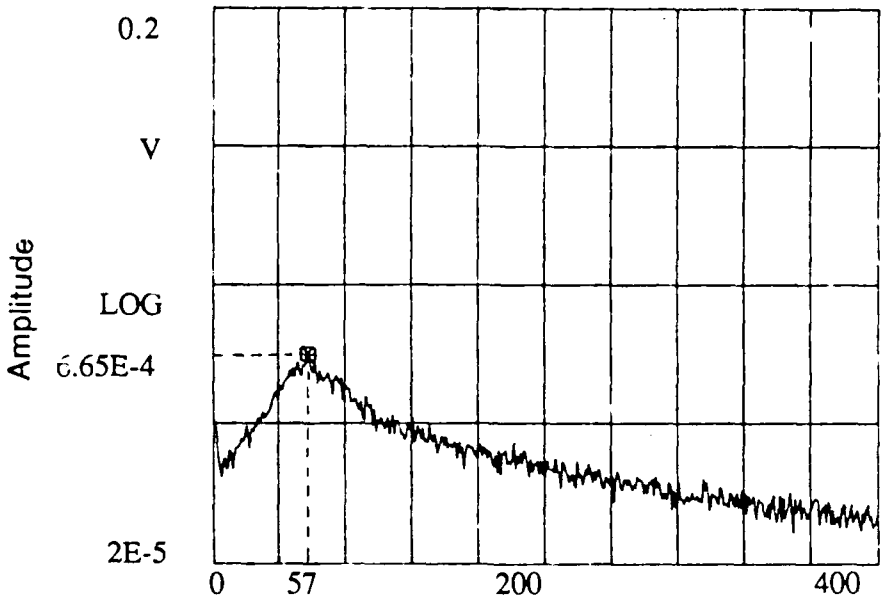

Frequency, HZ

Cylinder, 40° Cable Angle, 18 FPS

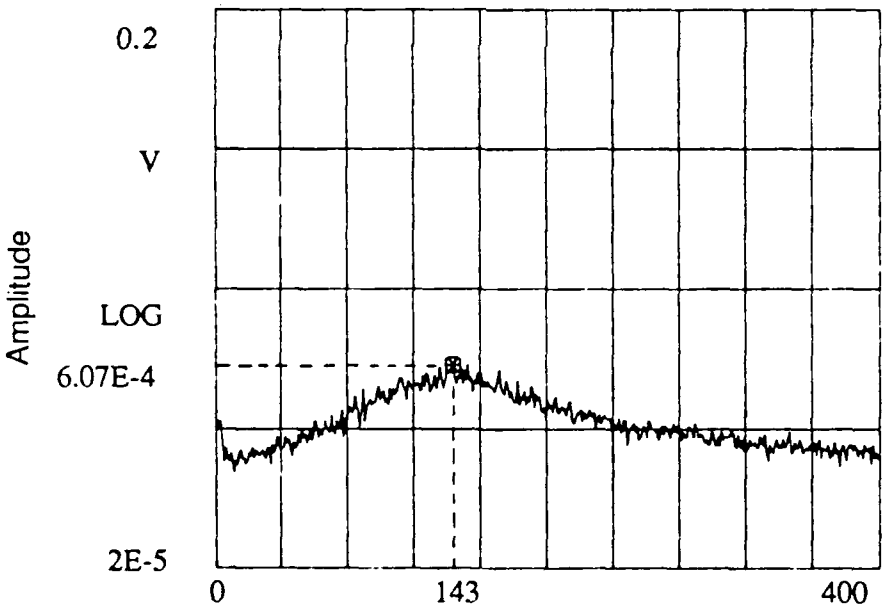

Frequency, HZ

Cylinder, 40° Cable Angle, 45 FPS

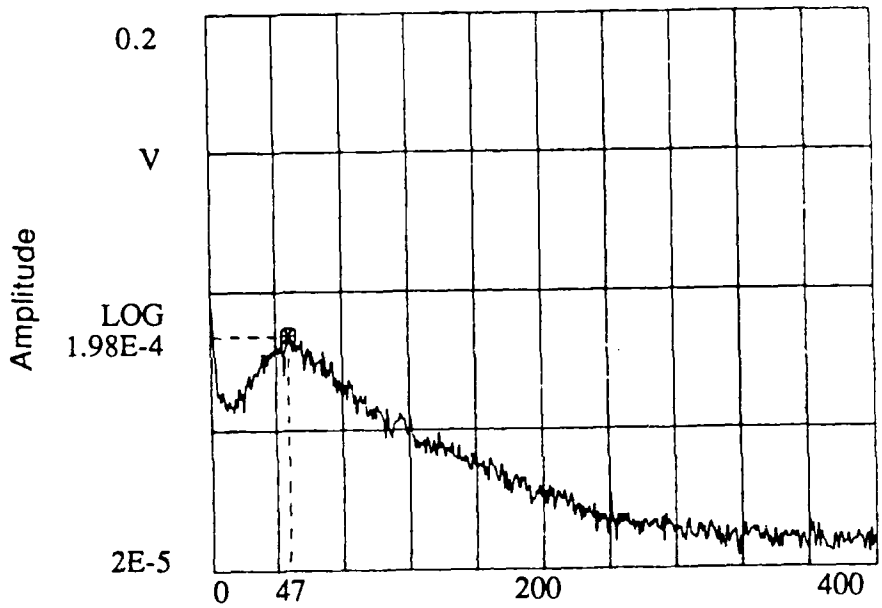

Frequency, HZ

Cylinder, 20° Cable Angle, 18 FPS

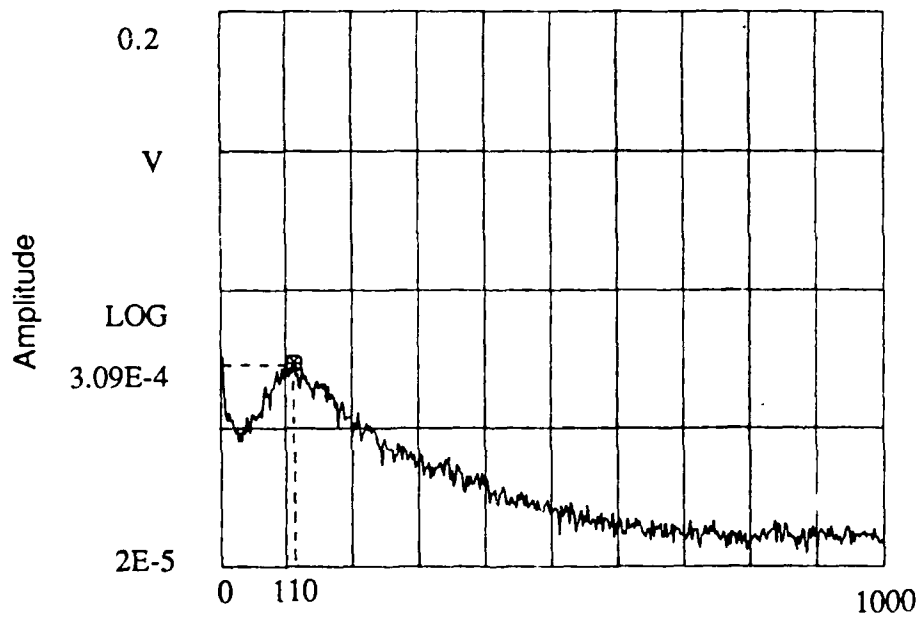

Frequency, HZ

Cylinder, 20° Cable Angle, 45 FPS

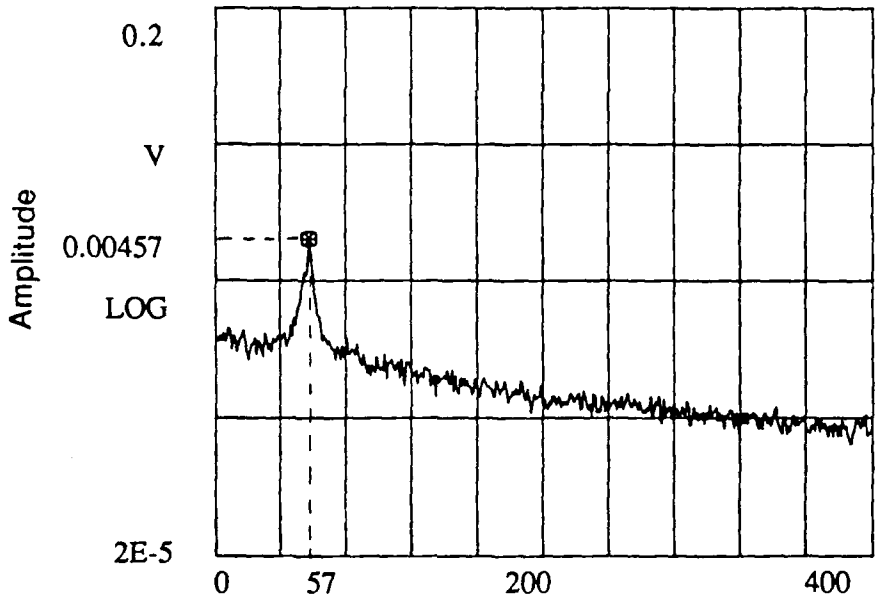

Frequency, HZ

4 x 7, 90° Cable Angle, 18 FPS

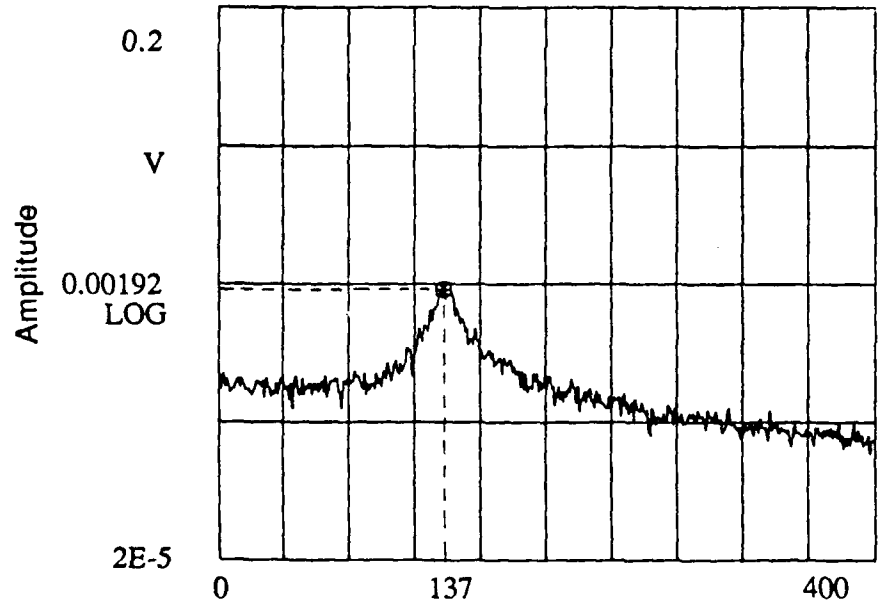

Frequency, HZ

4 x 7, 90° Cable Angle, 45 FPS

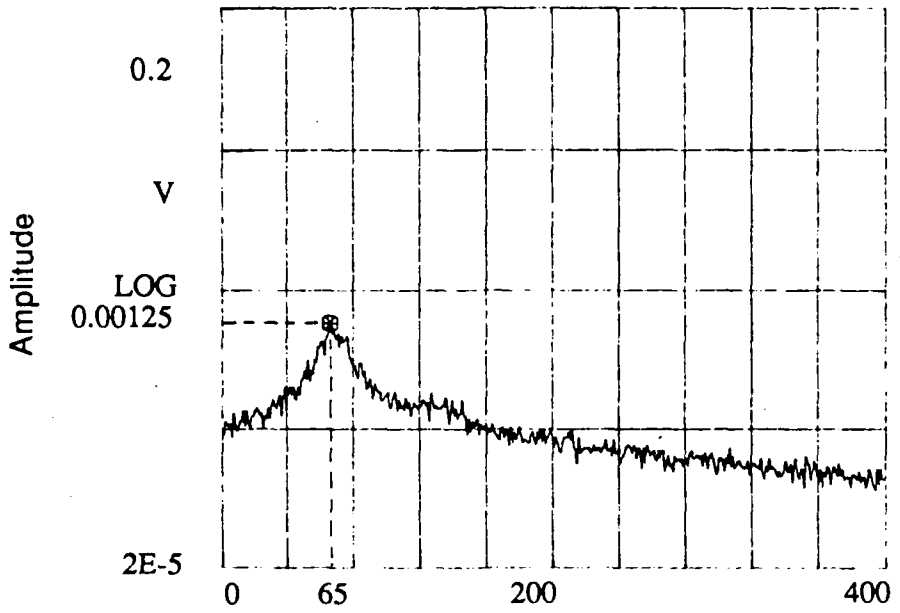

4 x 7, 60° Cable Angle, 18 FPS

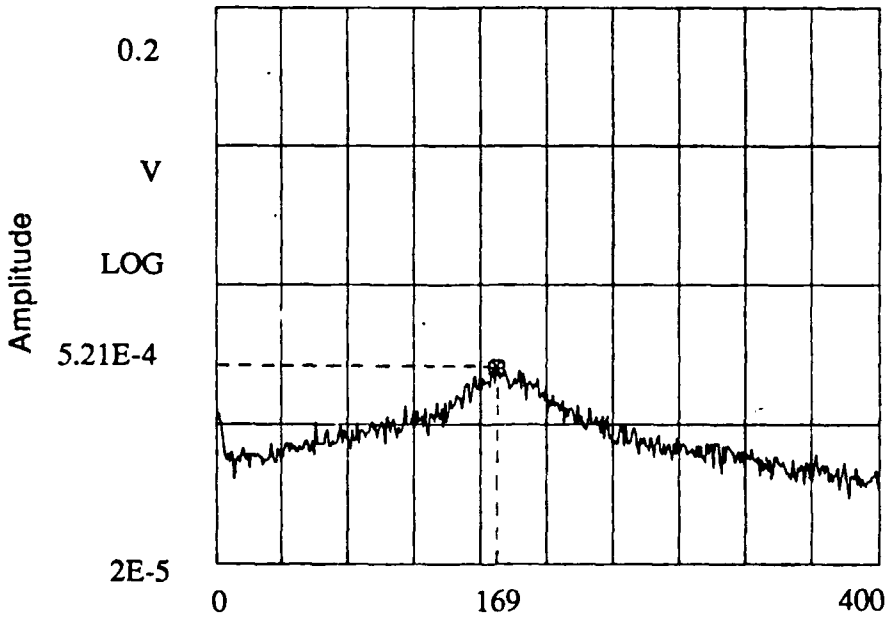

4 x 7, 60° Cable Angle, 45 FPS

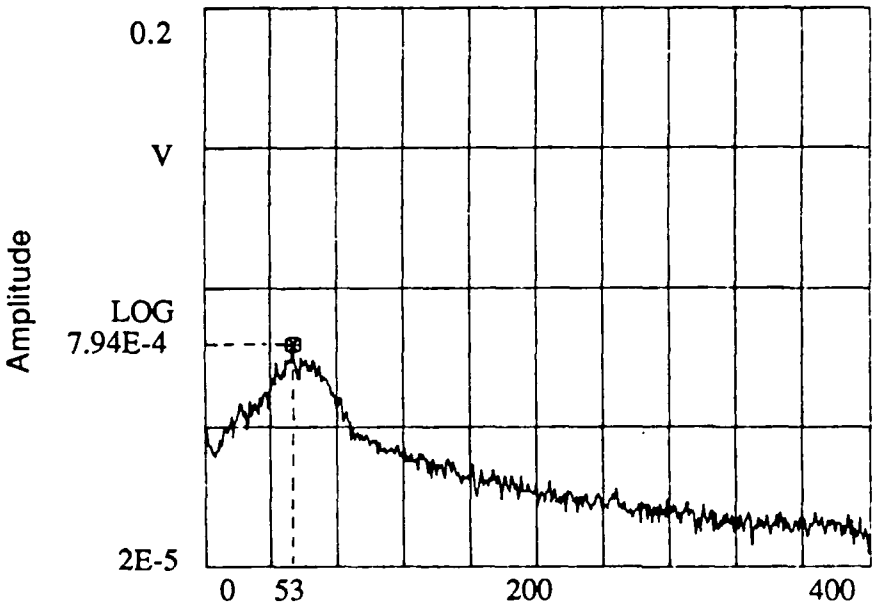

Frequency, HZ

4 x 7, 40° Cable Angle, 18 FPS

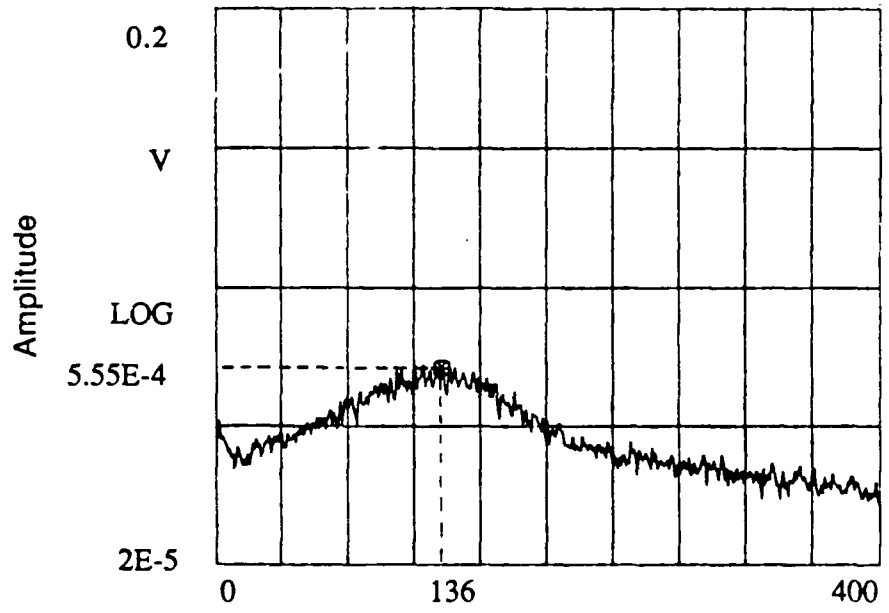

Frequency, HZ

4 x 7, 40° Cable Angle, 45 FPS

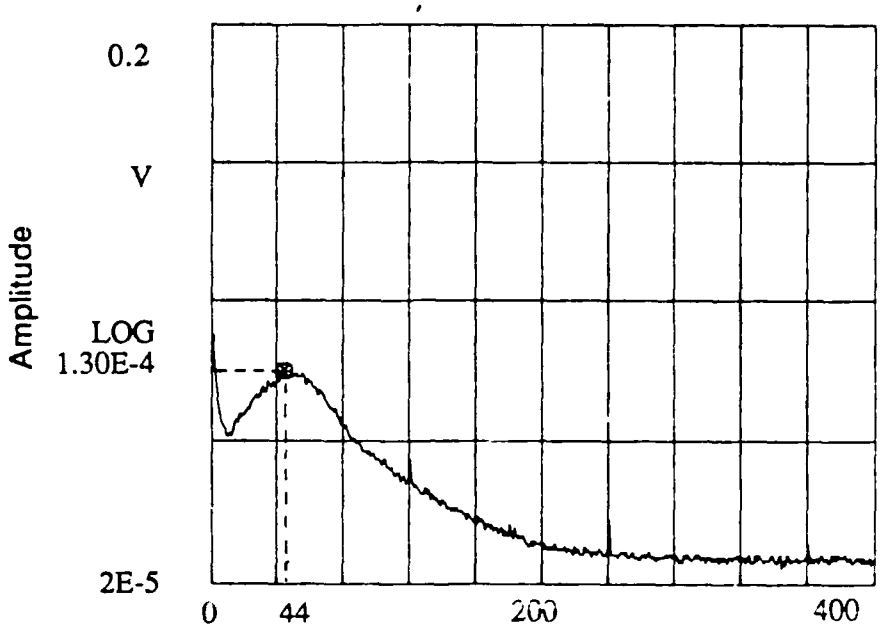

Frequency, HZ

4 x 7, 20° Cable Angle, 18 FPS

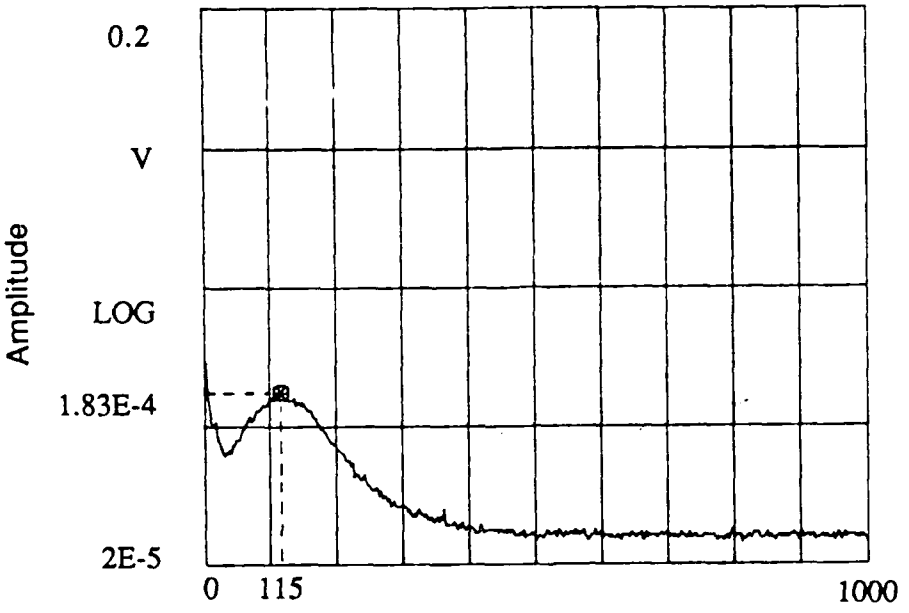

Frequency, HZ

4 x 7, 20° Cable Angle, 45 FPS

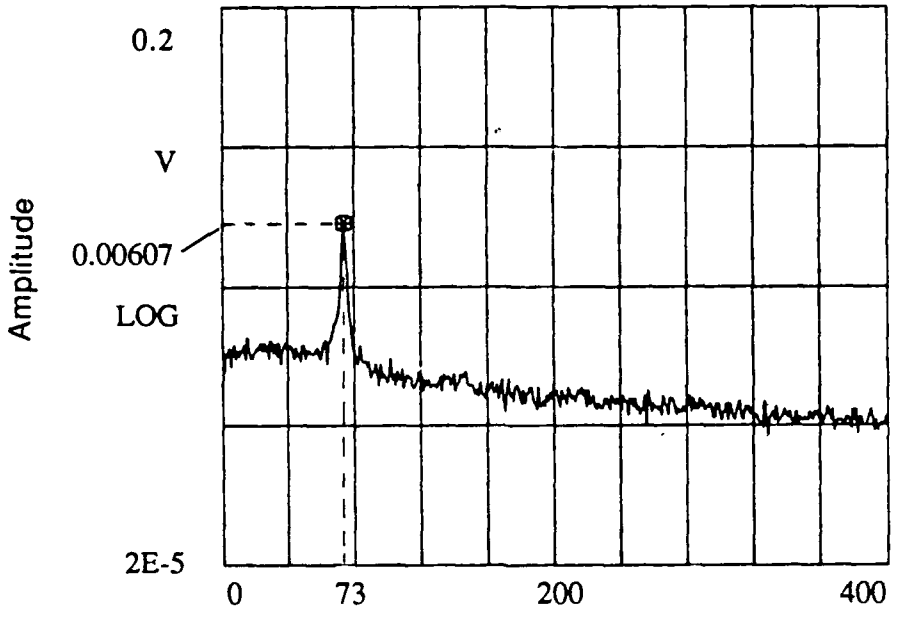

Frequency, HZ

6 x 25, 90° Cable Angle, 18 FPS

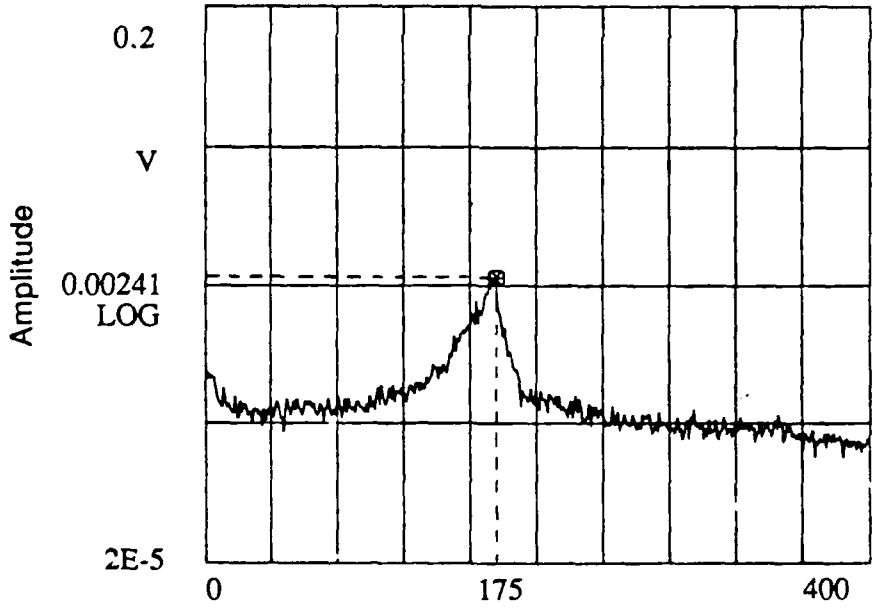

Frequency, HZ

6 x 25, 90° Cable Angle, 45 FPS

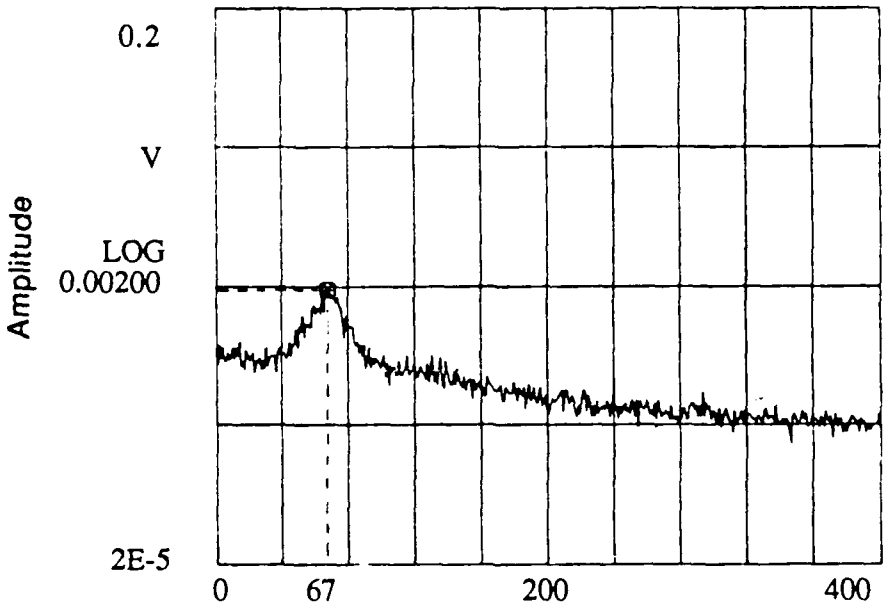

Frequency, HZ

6 x 25, 60° Cable Angle, 18 FPS

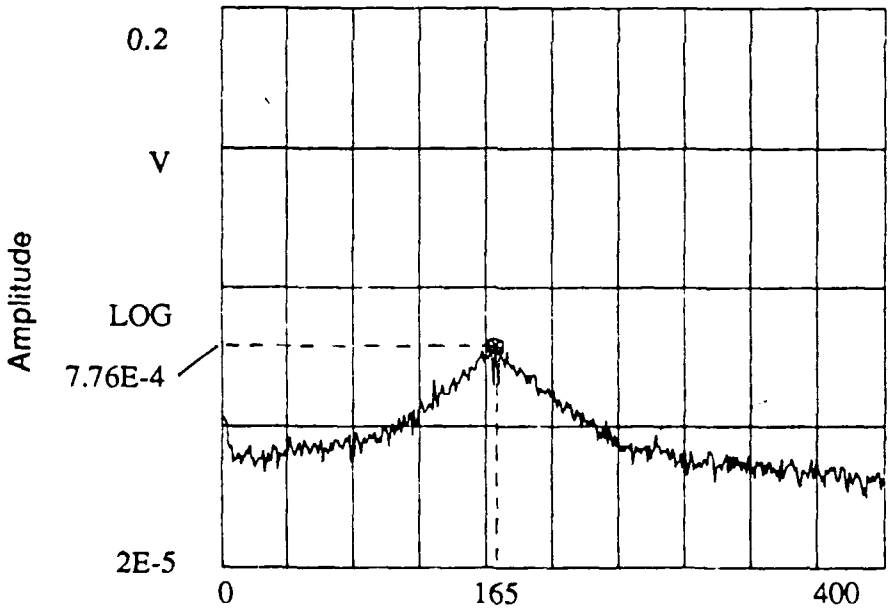

Frequency, HZ

6 x 25, 60° Cable Angle, 45 FPS

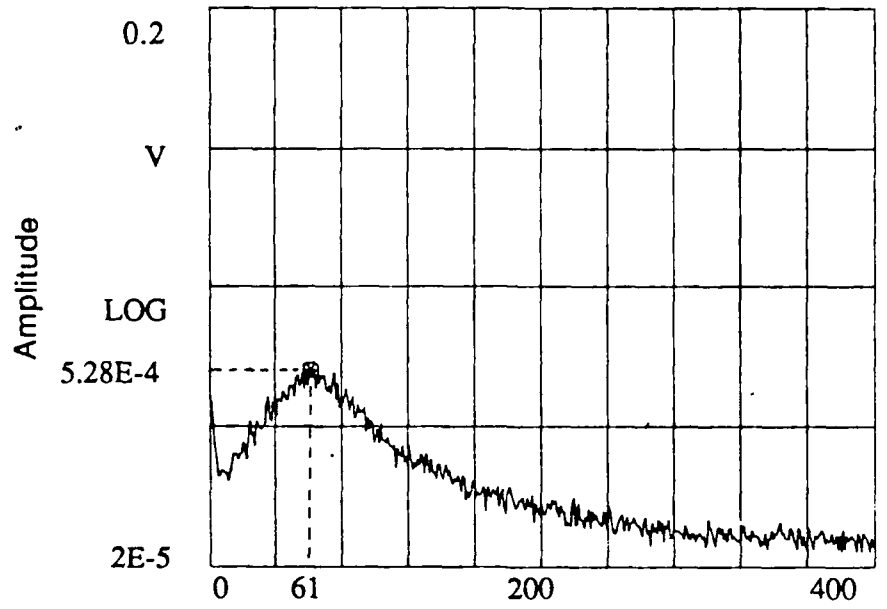

Frequency, HZ

6 x 25, 40° Cable Angle, 18 FPS

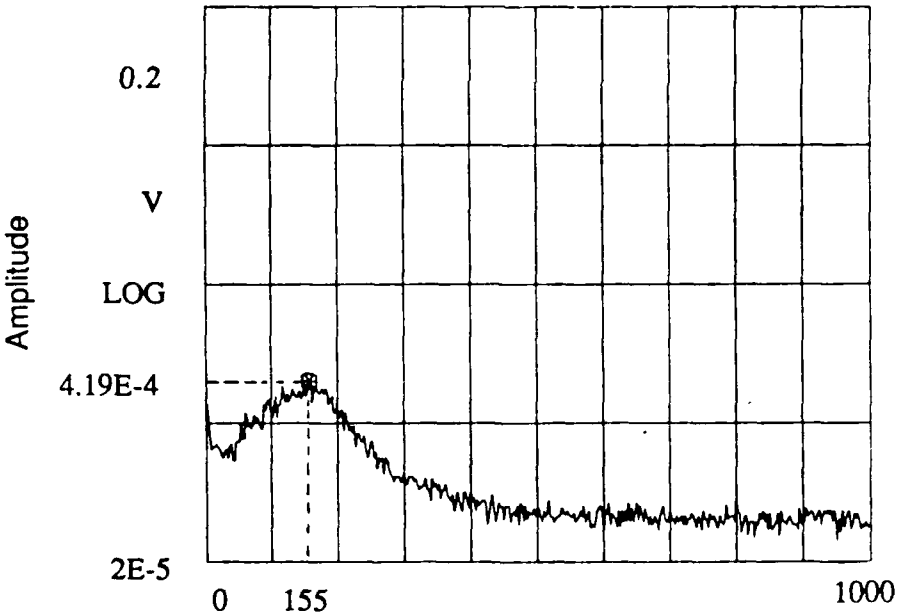

Frequency, HZ

6 x 25, 40° Cable Angle, 45 FPS

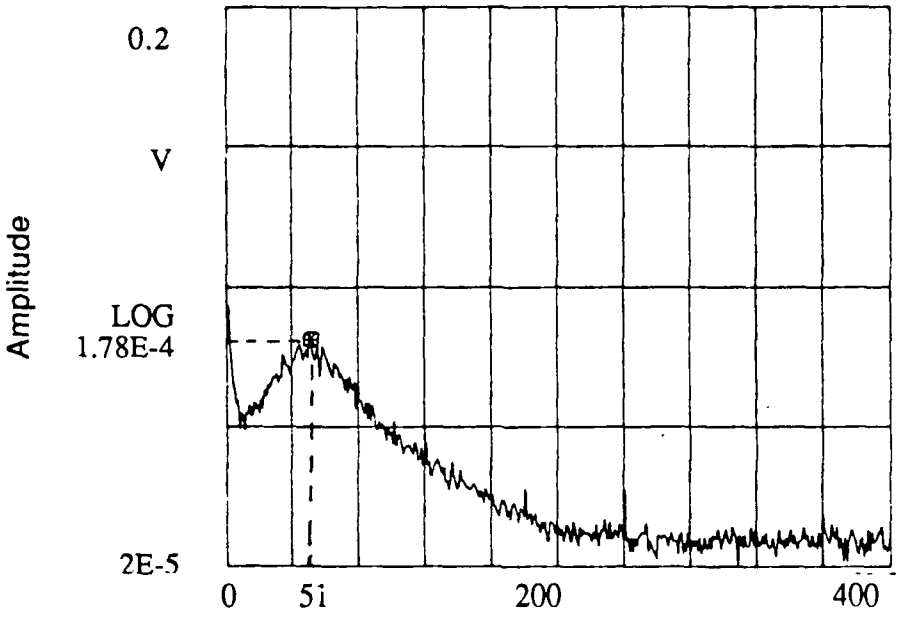

Frequency, HZ

6 x 25, 20° Cable Angle, 18 FPS

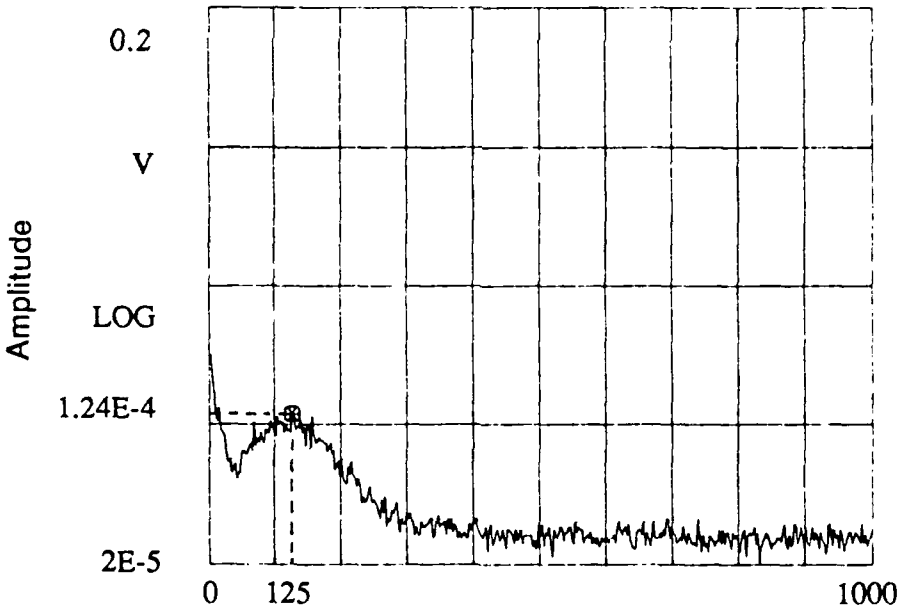

Frequency, HZ

6 x 25, 20° Cable Angle, 45 FPS

APPENDIX C - Correlation Results

The following contains wake correlation data for each of the 4X7 and 6X25 cable models and the circular cylinder. The data is for both flow speeds of 18.7 ft/sec and 45 ft/sec for each of the cable angles tested and for various probe spacings.

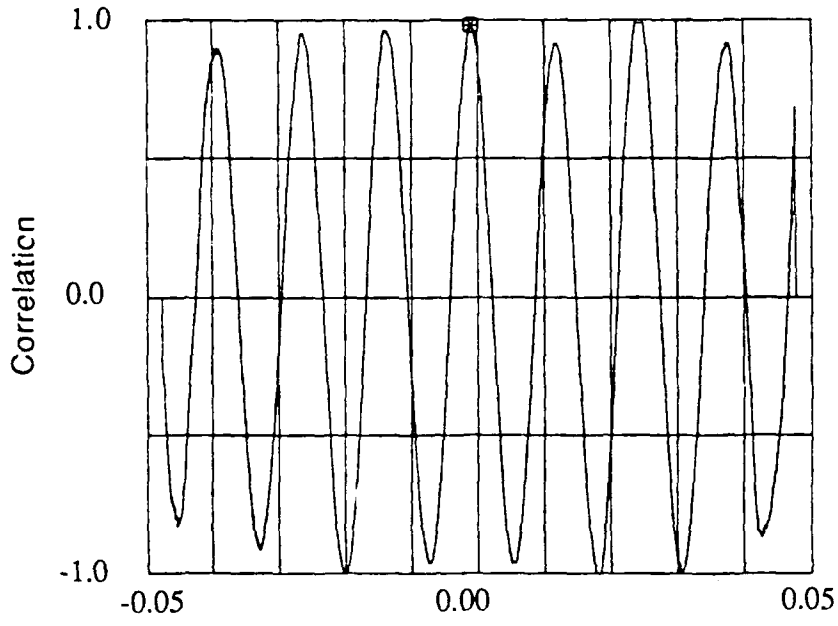

Time Shift, Sec
Cylinder Model, 90° Cable Angle, 18 FPS
Spanwise Distance Between Probes = 1.52 in.

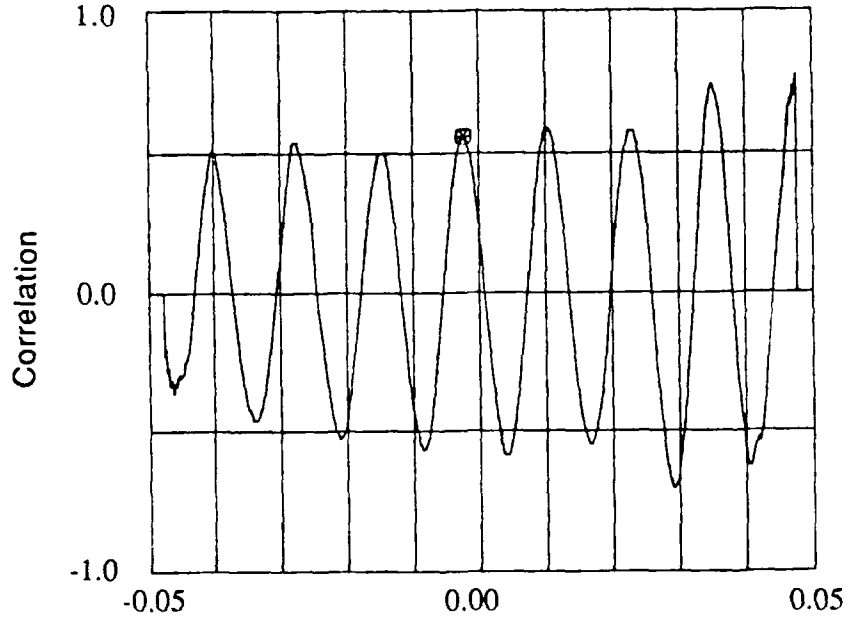

Time Shift, Sec
Cylinder Model, 90° Cable Angle, 18 FPS
Spanwise Distance Between Probes = 3.04 in.

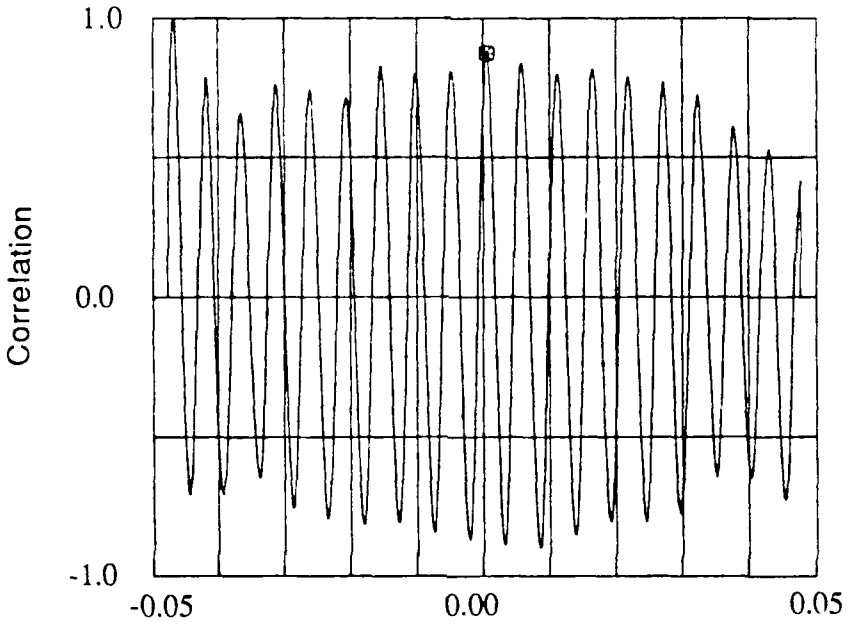

Time Shift, Sec
Cylinder Model, 90° Cable Angle, 45 FPS
Spanwise Distance Between Probes = 1.52 in.

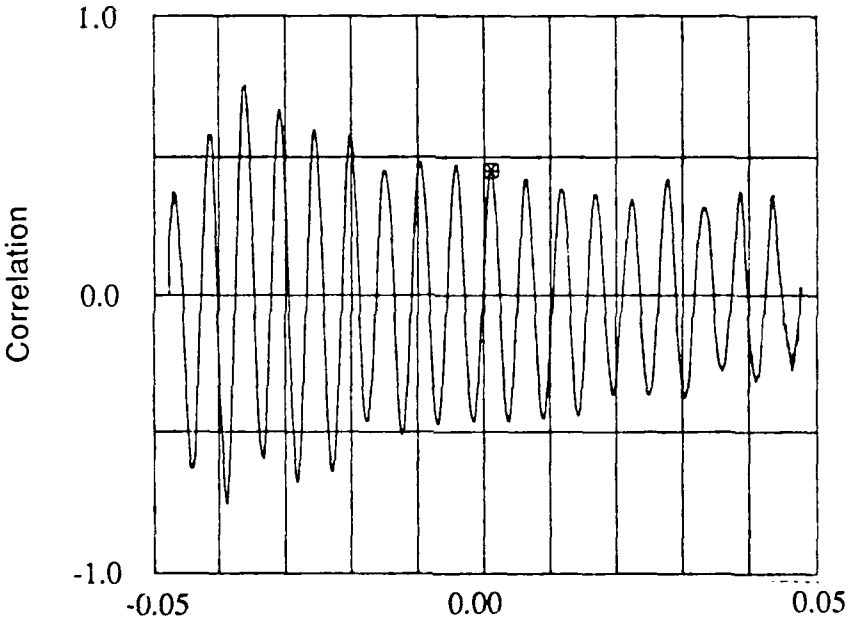

Time Shift, Sec
Cylinder Model, 90° Cable Angle, 45 FPS
Spanwise Distance Between Probes = 3.04 in.

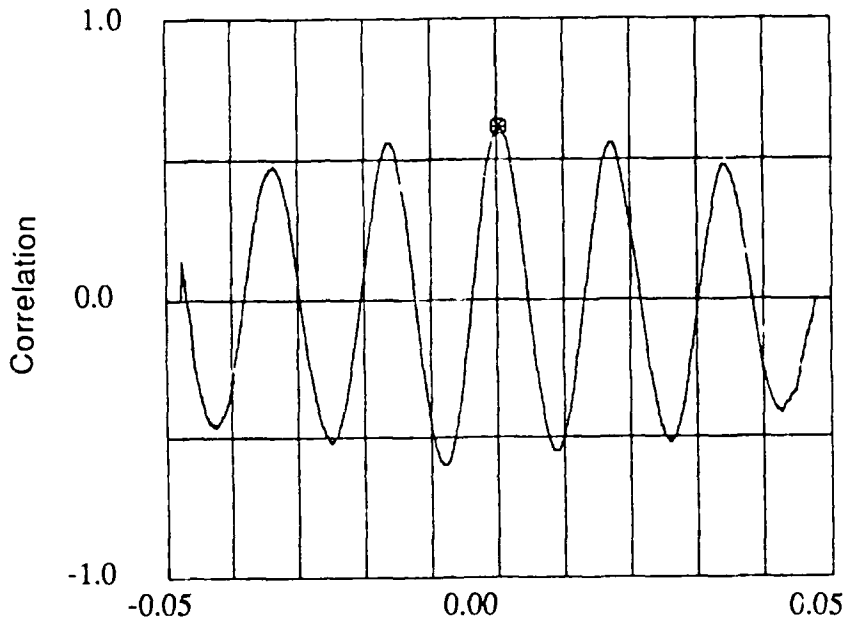

Time Shift, Sec
4 x 7, 90° Cable Angle, 18 FPS
Spanwise Distance Between Probes = 0.65 in.

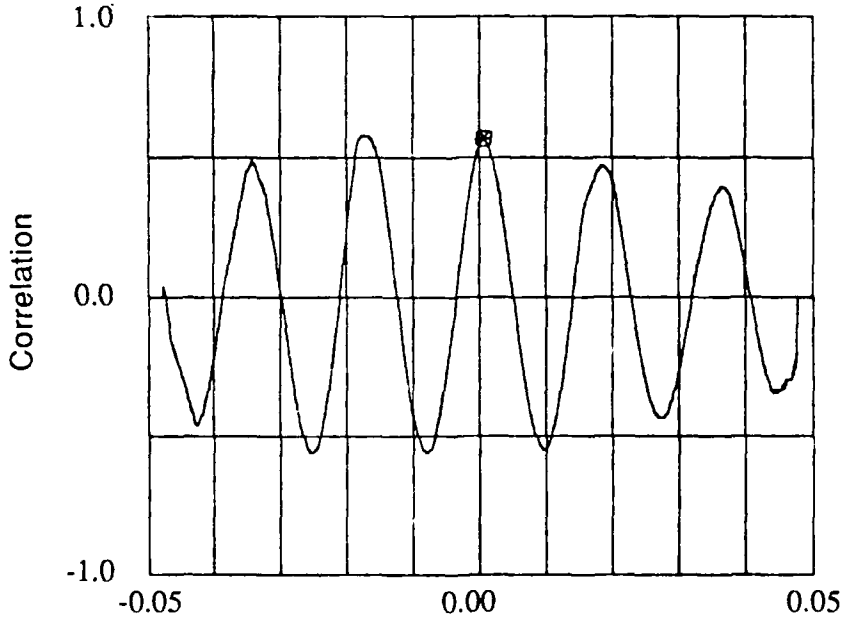

Time Shift, Sec
4 x 7, 90° Cable Angle, 18 FPS
Spanwise Distance Between Probes = 1.30 in.

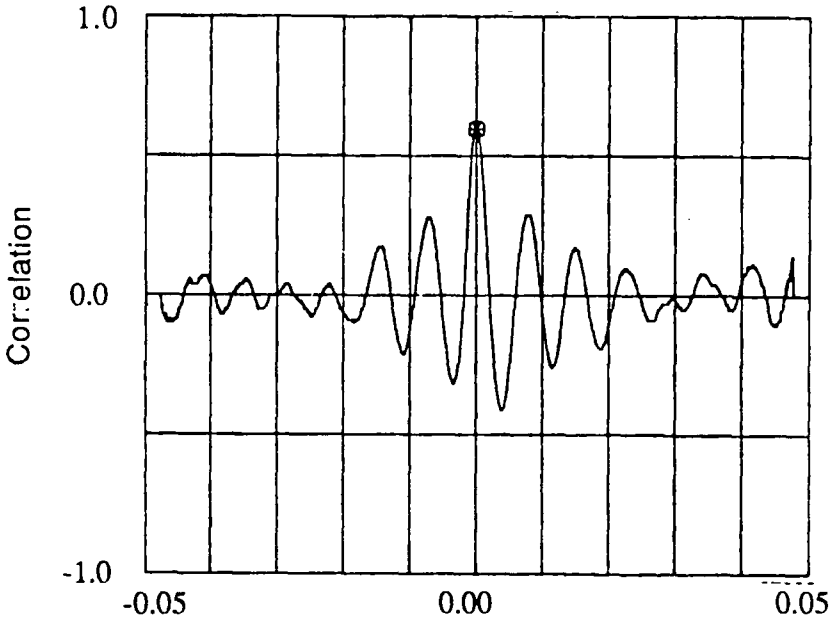

Time Shift, Sec
4 x 7, 90° Cable Angle, 45 FPS
Spanwise Distance Between Probes = 0.65 in.

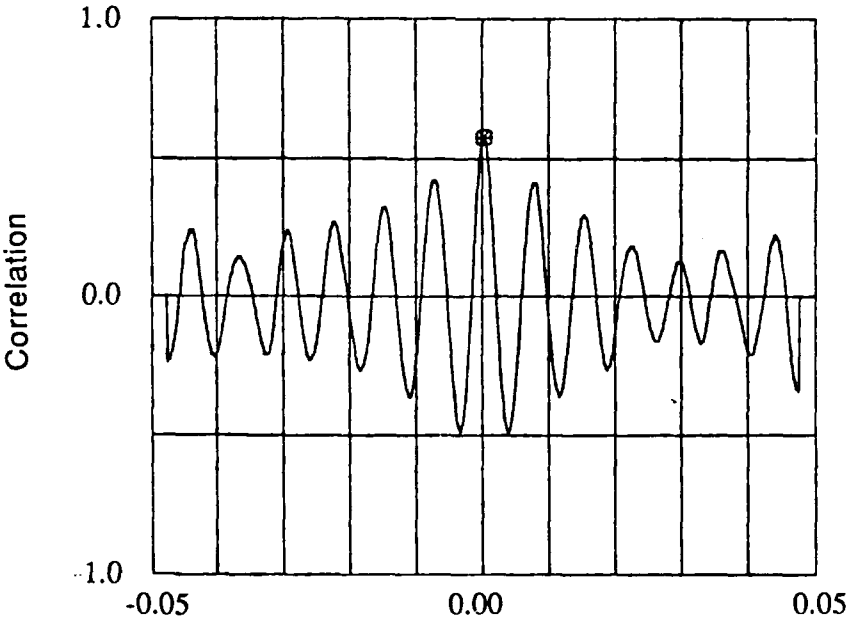

Time Shift, Sec
4 x 7, 90° Cable Angle, 45 FPS
Spanwise Distance Between Probes = 1.30 in.

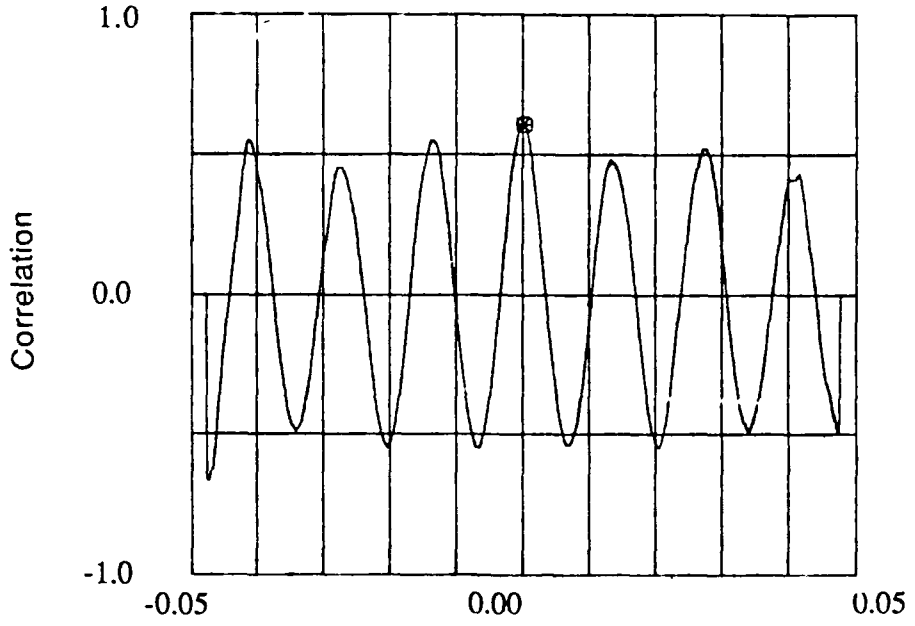

Time Shift, Sec
6 x 25, 90° Cable Angle, 18 FPS
Spanwise Distance Between Probes = 0.325 in.

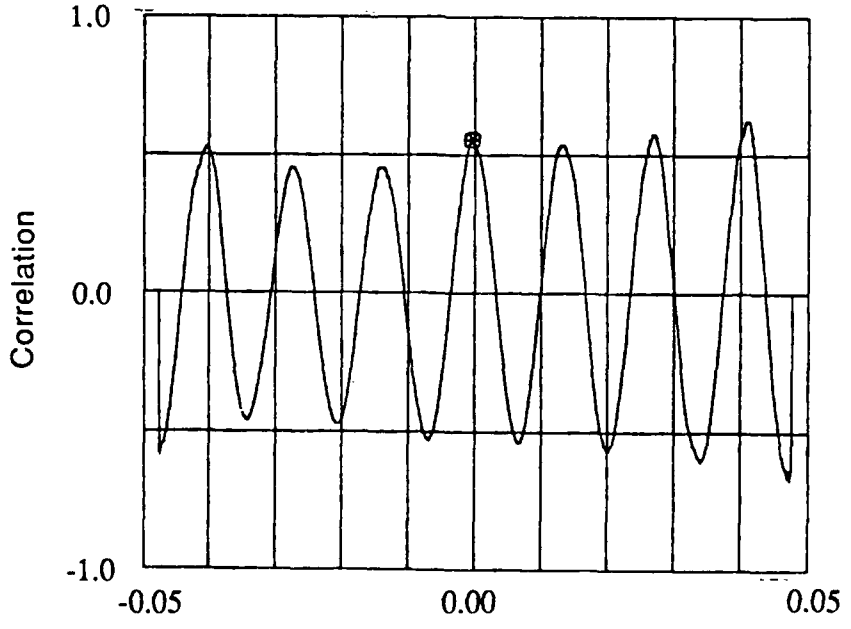

Time Shift, Sec
6 x 25, 90° Cable Angle, 18 FPS
Spanwise Distance Between Probes = 0.65 in.

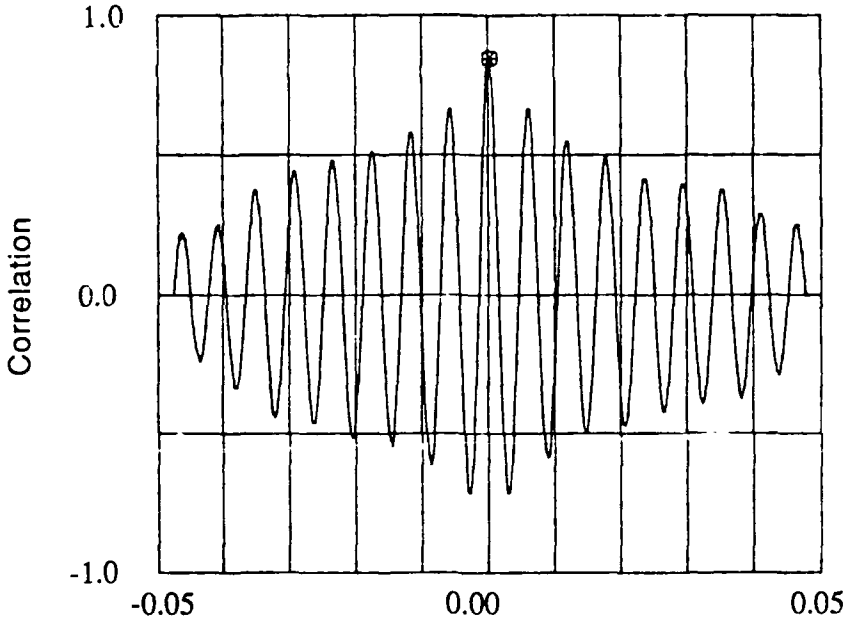

Time Shift, Sec
6 x 25, 90° Cable Angle, 45 FPS
Spanwise Distance Between Probes = 0.325 in.

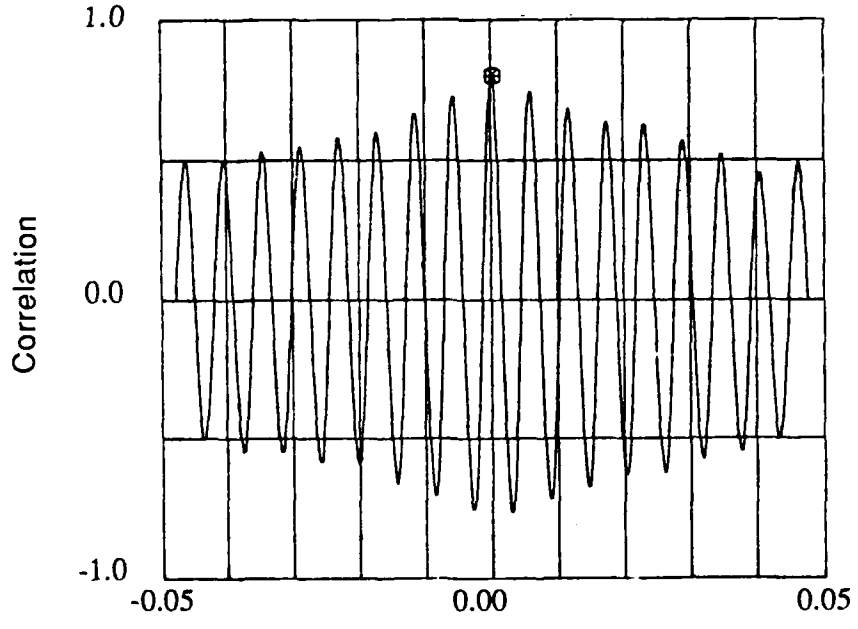

Time Shift, Sec
6 x 25, 90° Cable Angle, 45 FPS
Spanwise Distance Between Probes = 0.65 in.

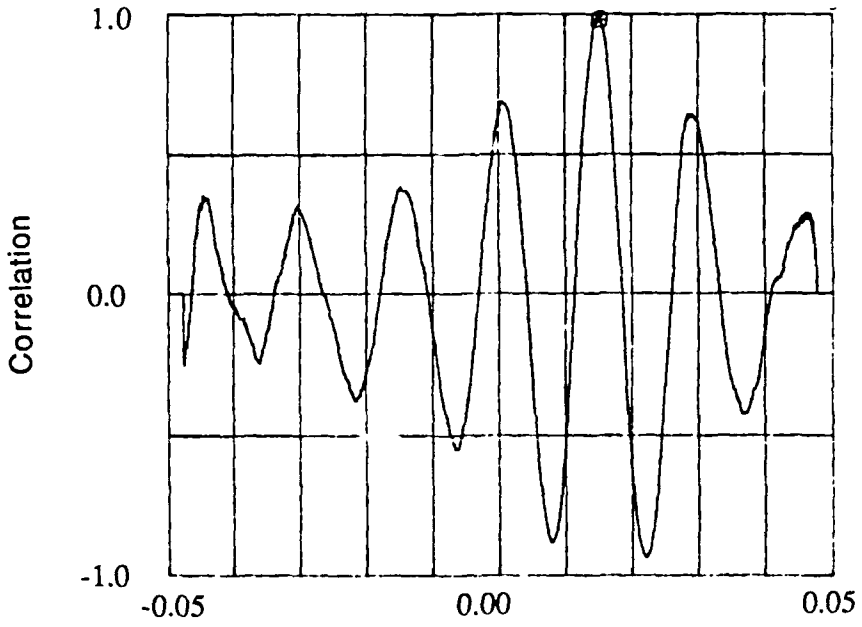

Time Shift, Sec
Cylinder Model, 60° Cable Angle, 18 FPS
Spanwise Distance Between Probes = 1.52 in.

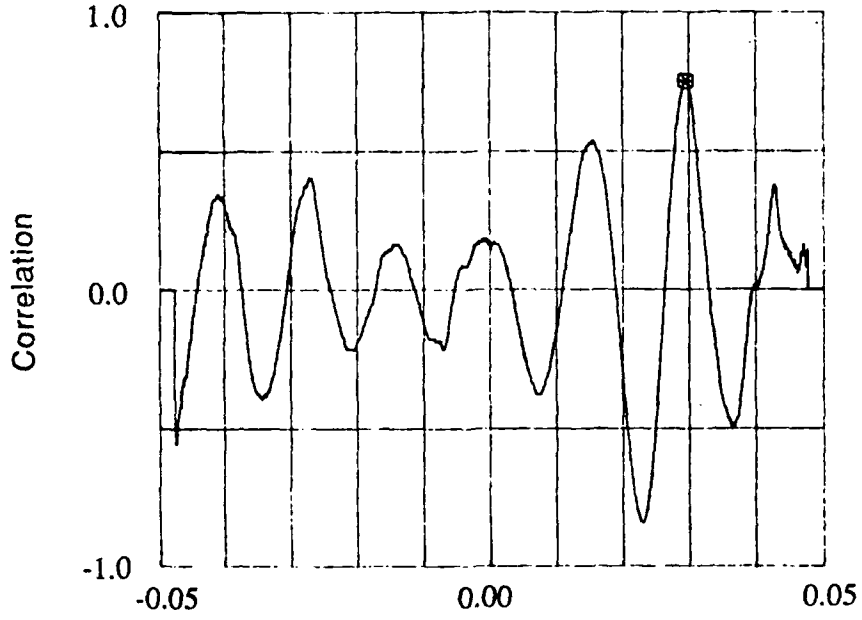

Time Shift, Sec
Cylinder Model, 60° Cable Angle, 18 FPS
Spanwise Distance Between Probes = 3.04 in.

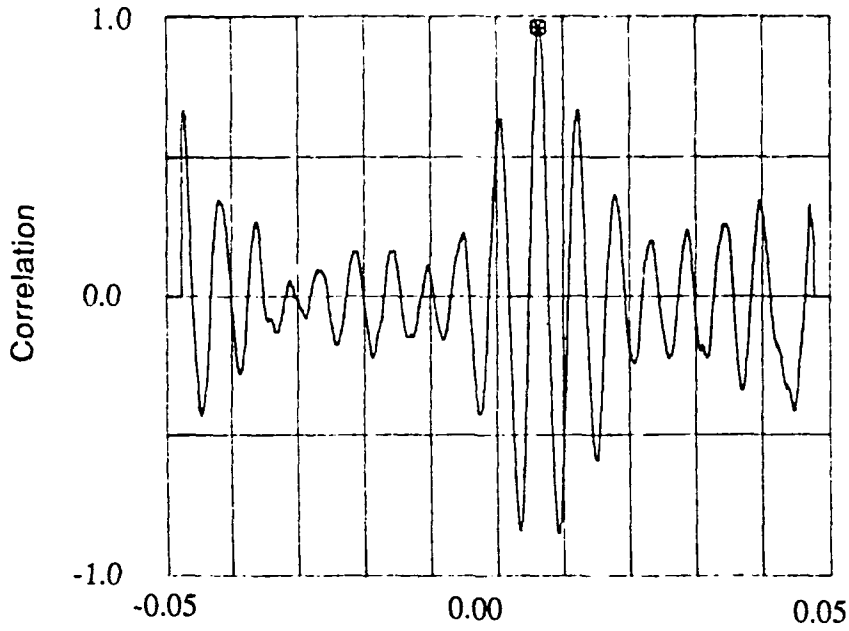

Time Shift, Sec
Cylinder Model, 60° Cable Angle, 45 FPS
Spanwise Distance Between Probes = 1.52 in.

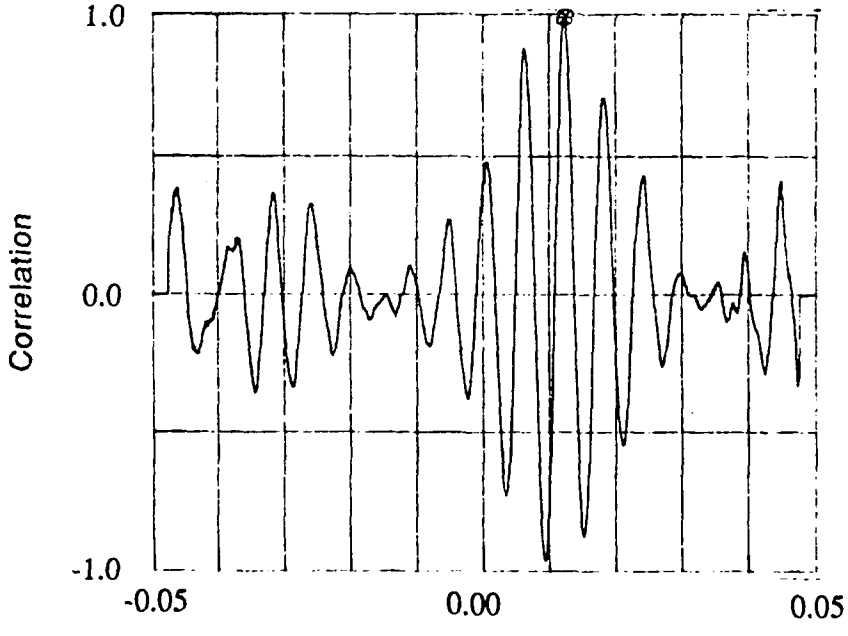

Time Shift, Sec
Cylinder Model, 60° Cable Angle, 45 FPS
Spanwise Distance Between Probes = 3.04 in.

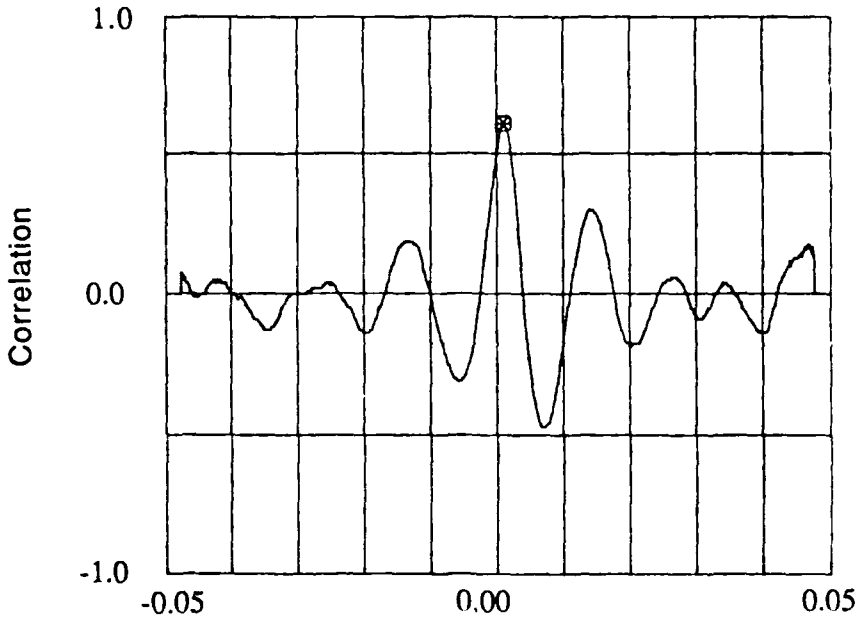

Time Shift, Sec
4 x 7, 60° Cable Angle, 18 FPS
Spanwise Distance Between Probes = 0.65 in.

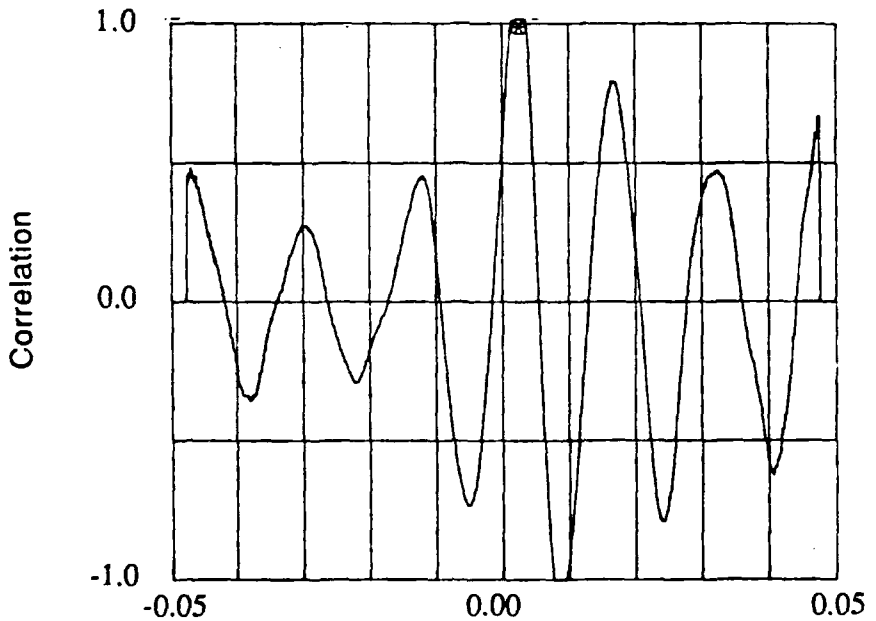

Time Shift, Sec
4 x 7, 60° Cable Angle, 18 FPS
Spanwise Distance Between Probes = 1.30 in.

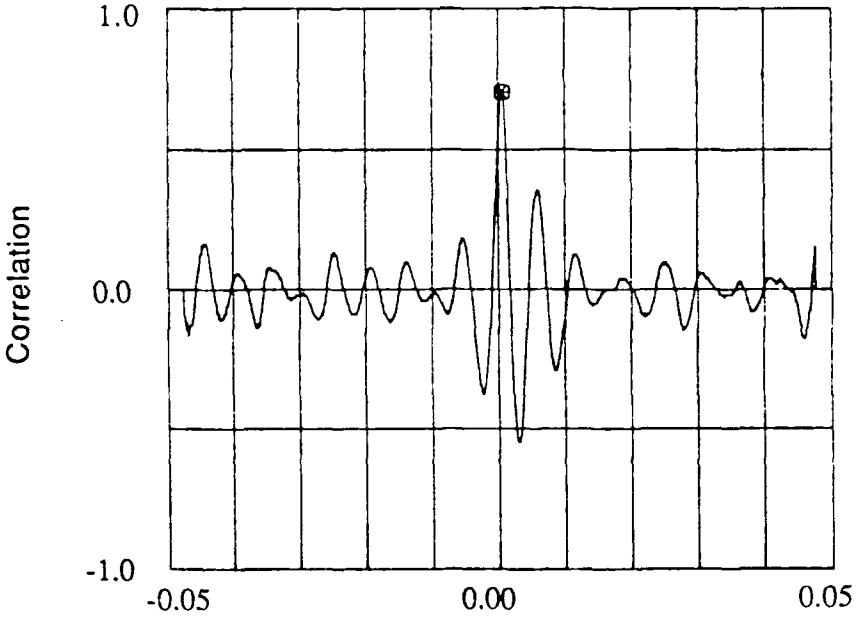

Time Shift, Sec
4 x 7, 60° Cable Angle, 45 FPS
Spanwise Distance Between Probes = 0.65 in.

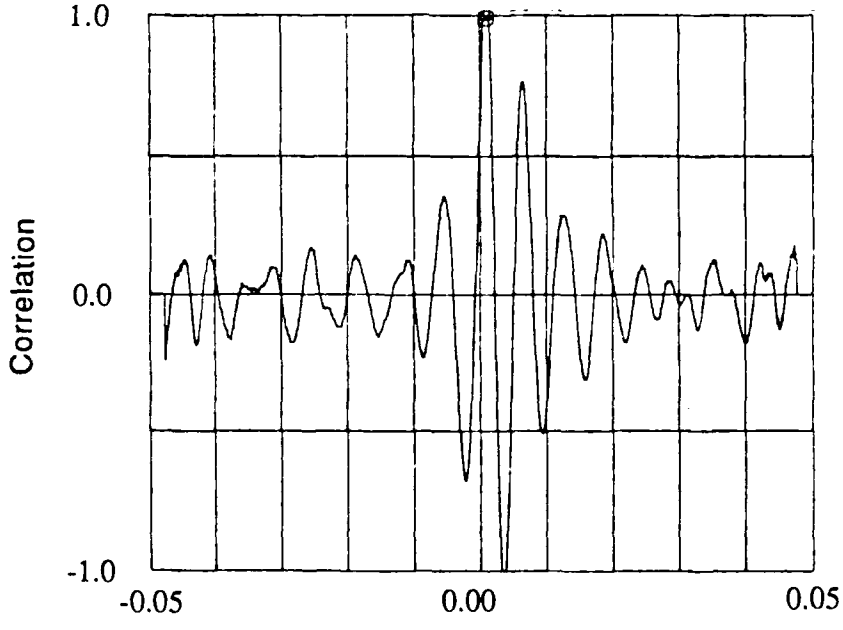

Time Shift, Sec
4 x 7, 60° Cable Angle, 45 FPS
Spanwise Distance Between Probes = 1.30 in.

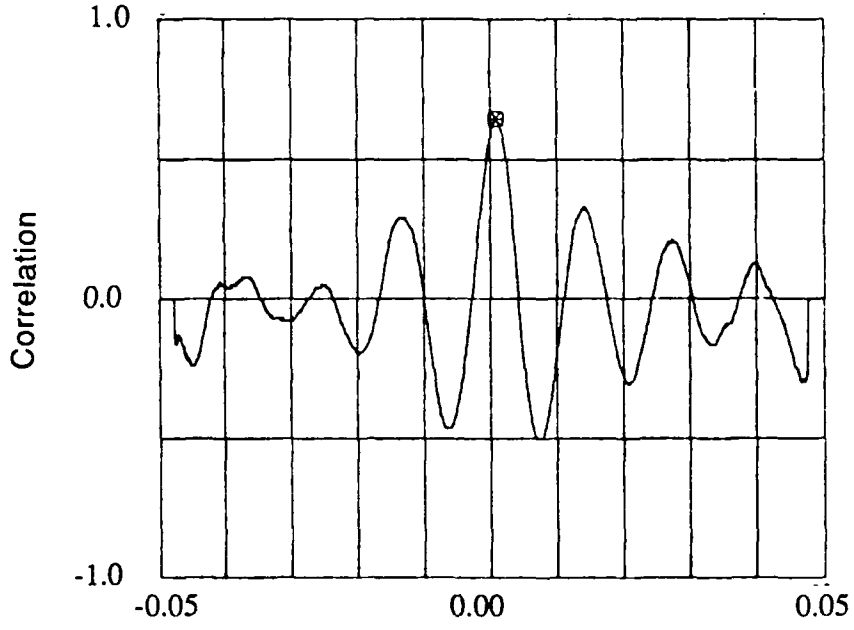

Time Shift, Sec
6 x 25, 60° Cable Angle, 18 FPS
Spanwise Distance Between Probes = 0.325 in.

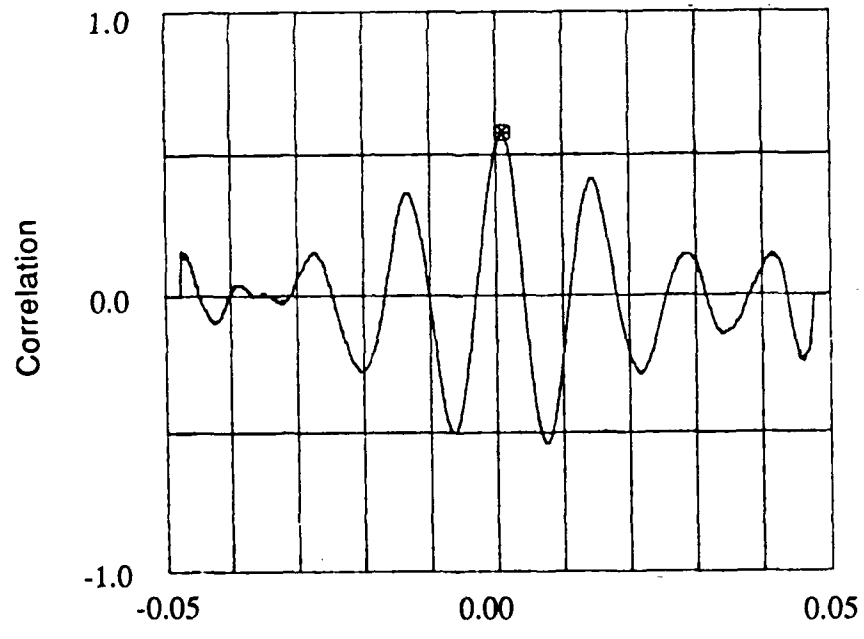

Time Shift, Sec
6 x 25, 60° Cable Angle, 18 FPS
Spanwise Distance Between Probes = 0.65 in.

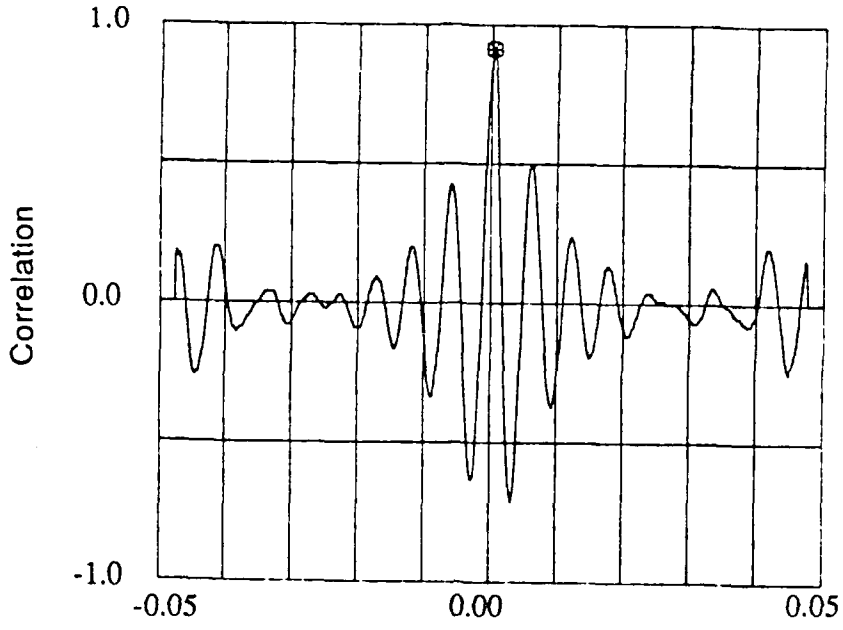

Time Shift, Sec
6 x 25, 60° Cable Angle, 45 FPS
Spanwise Distance Between Probes = 0.325 in.

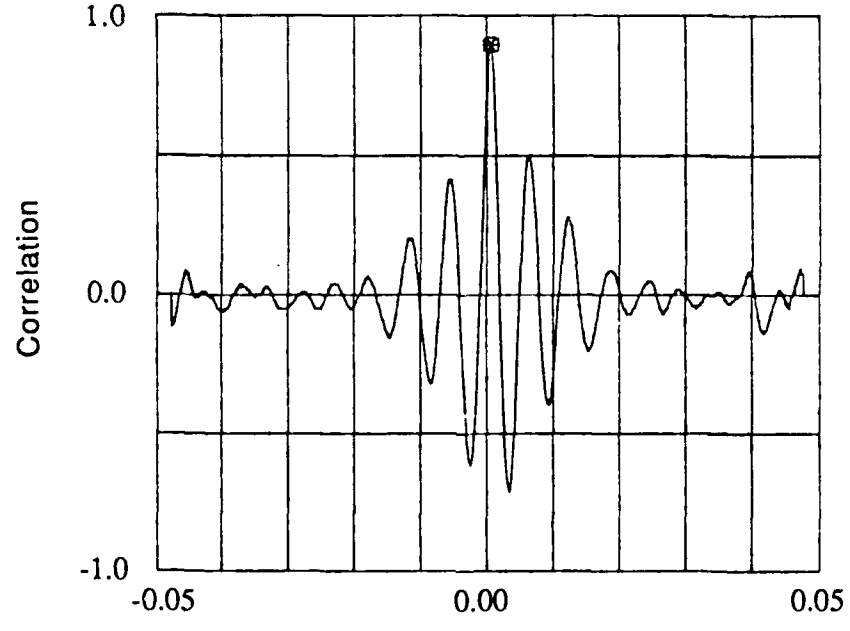

Time Shift, Sec
6 x 25, 60° Cable Angle, 45 FPS
Spanwise Distance Between Probes = 0.65 in.

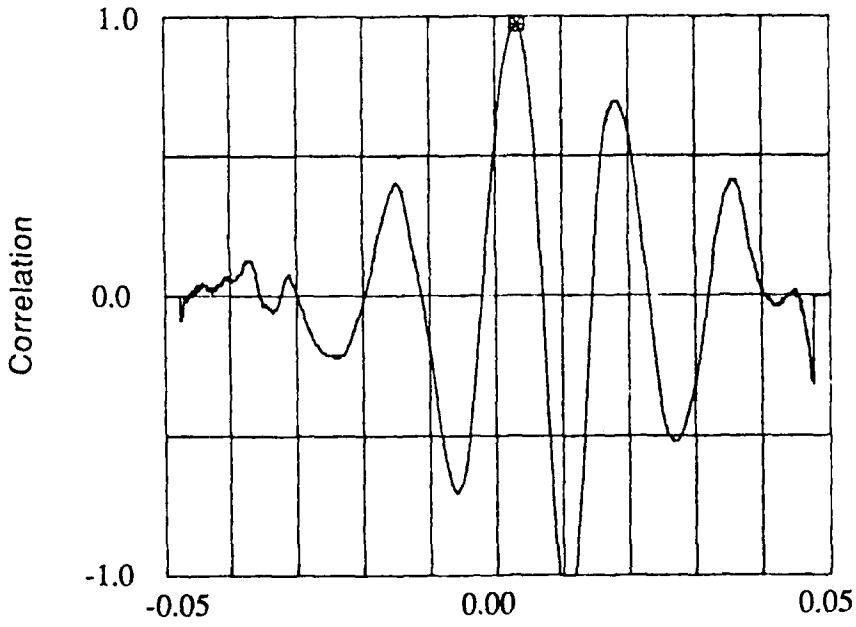

Time Shift, Sec
Cylinder Model, 40° Cable Angle, 18 FPS
Spanwise Distance Between Probes = 1.52 in.

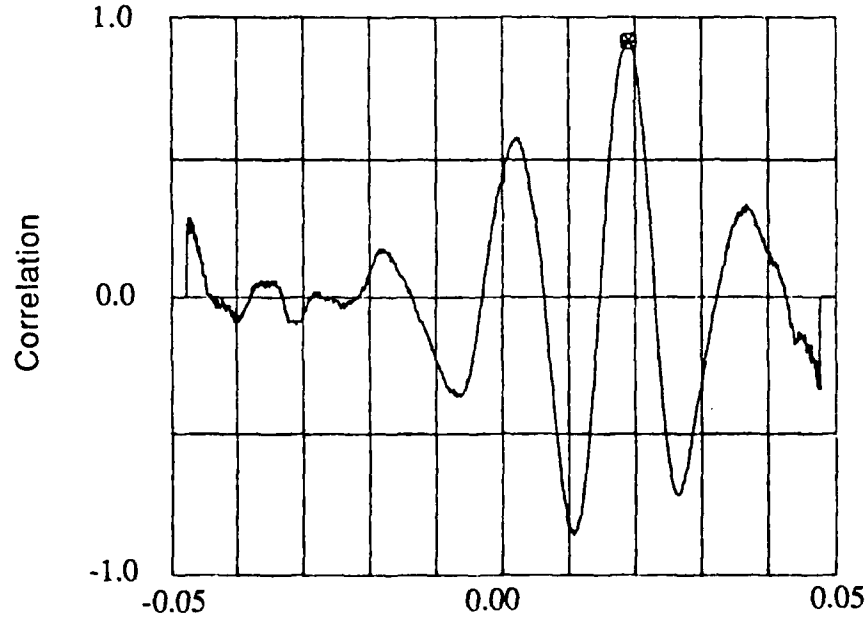

Time Shift, Sec
Cylinder Model, 40° Cable Angle, 18 FPS
Spanwise Distance Between Probes = 3.04 in.

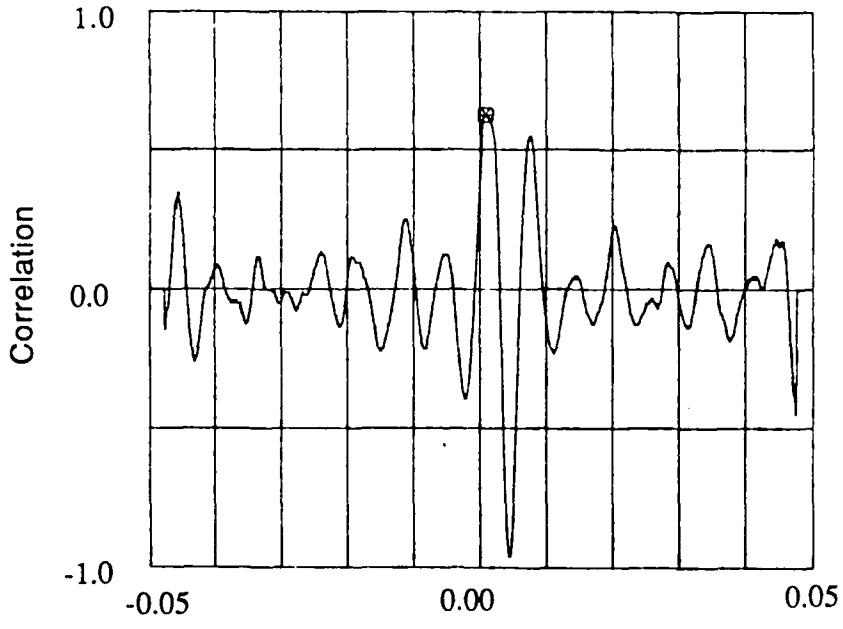

Time Shift, Sec
Cylinder Model, 40° Cable Angle, 45 FPS
Spanwise Distance Between Probes = 1.52 in.

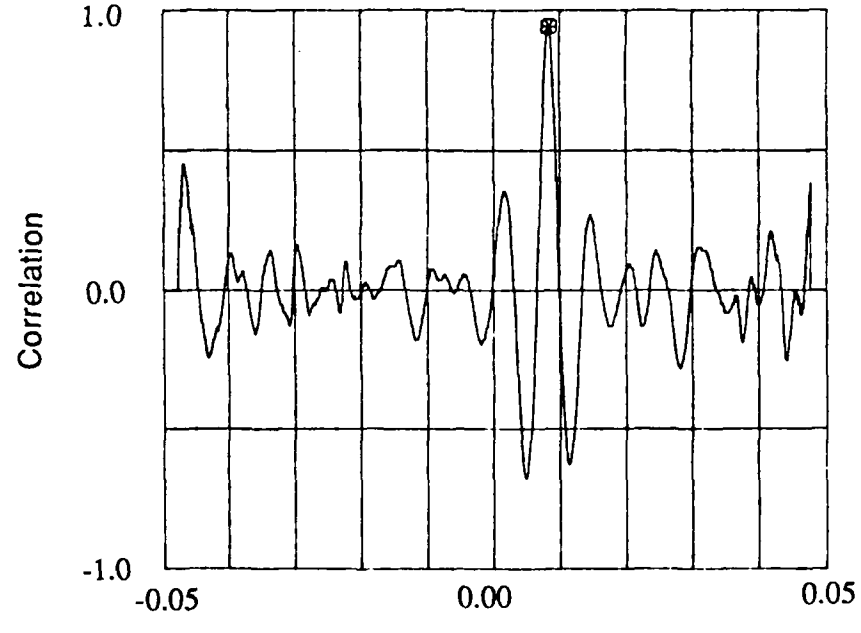

Time Shift, Sec
Cylinder Model, 40° Cable Angle, 45 FPS
Spanwise Distance Between Probes = 3.04 in.

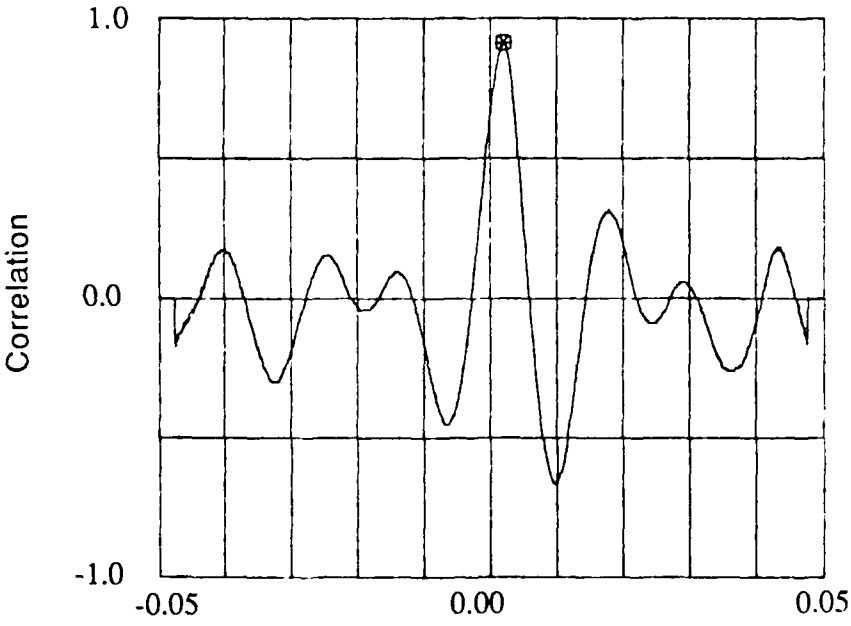

Time Shift, Sec
4 x 7, 40° Cable Angle, 18 FPS
Spanwise Distance Between Probes = 0.65 in.

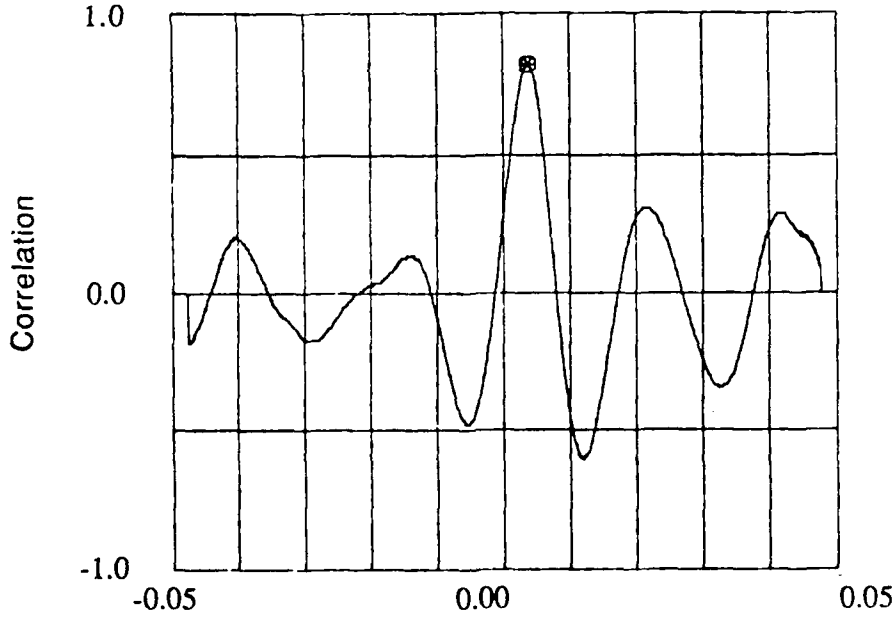

Time Shift, Sec
4 x 7, 40° Cable Angle, 18 FPS
Spanwise Distance Between Probes = 1.30 in.

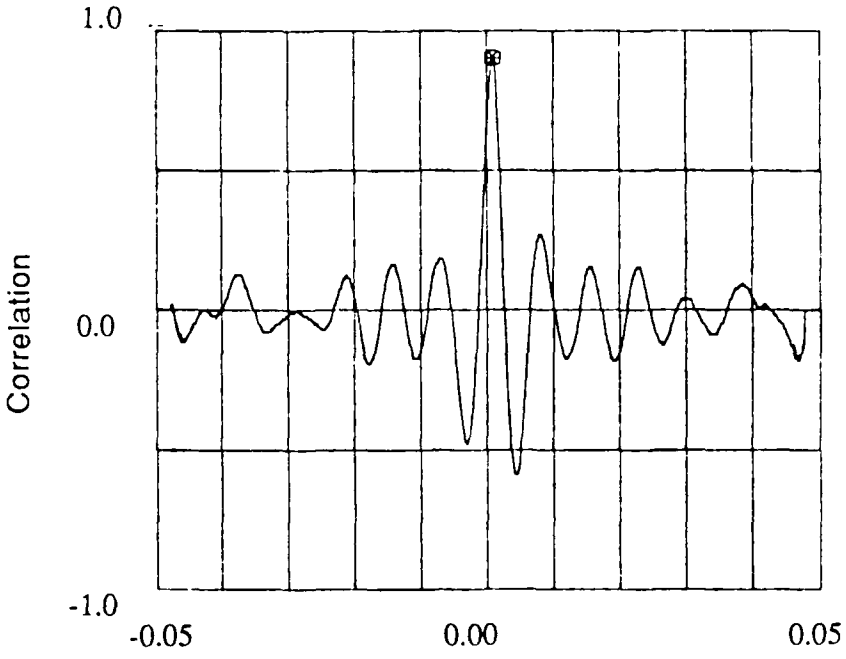

Time Shift, Sec
4 x 7, 40° Cable Angle, 45 FPS
Spanwise Distance Between Probes = 0.65 in.

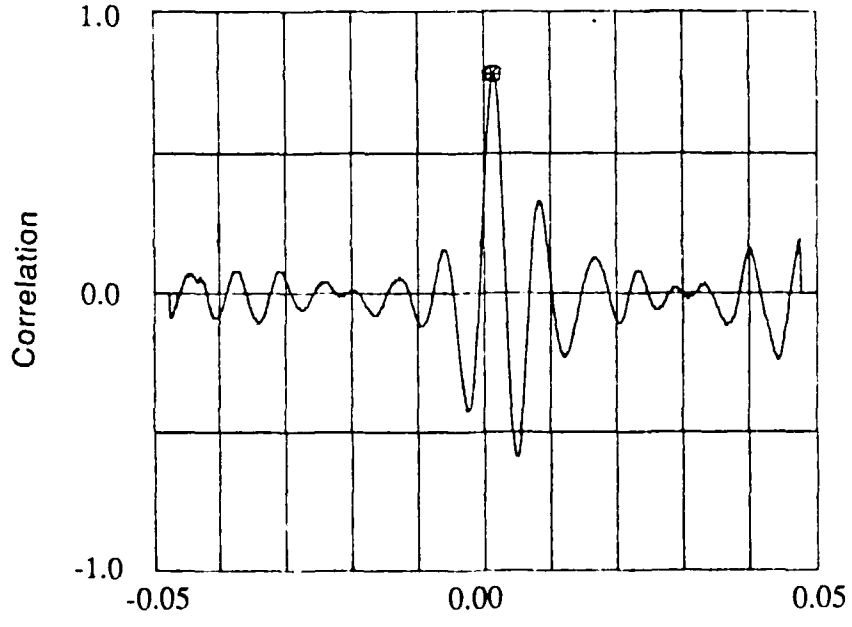

Time Shift, Sec
4 x 7, 40° Cable Angle, 45 FPS
Spanwise Distance Between Probes = 1.30 in.

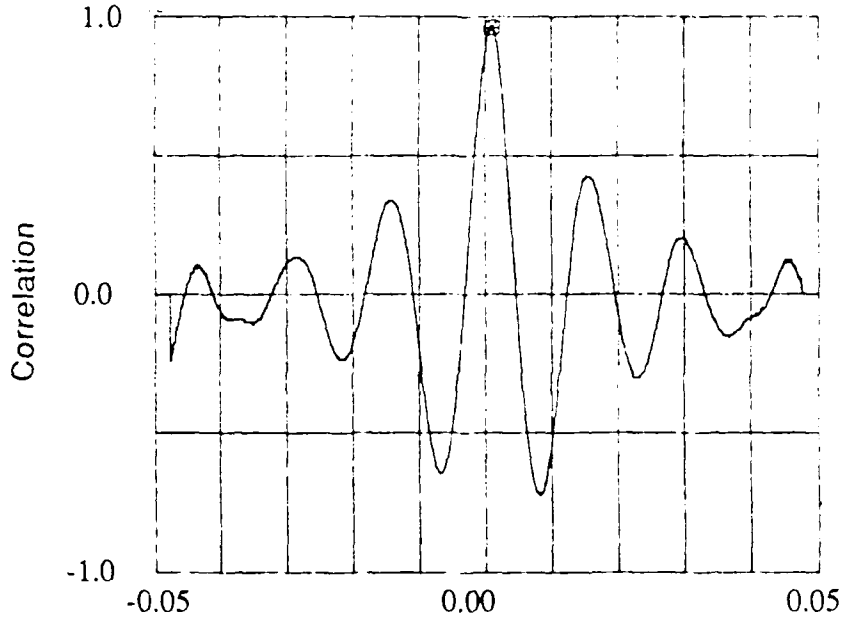

Time Shift, Sec
6 x 25, 40° Cable Angle, 18 FPS
Spanwise Distance Between Probes = 0.375 in.

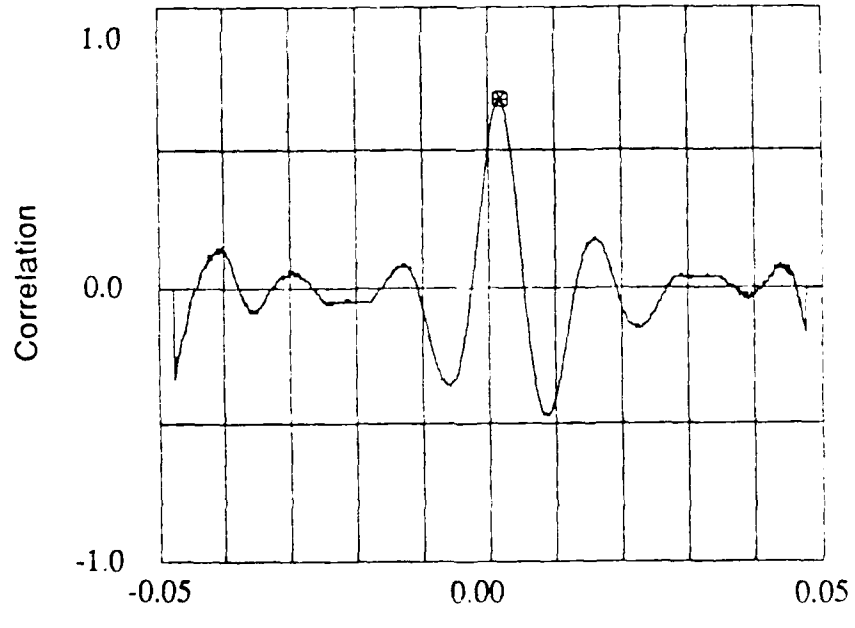

Time Shift, Sec
6 x 25, 40° Cable Angle, 18 FPS
Spanwise Distance Between Probes = 0.65 in.

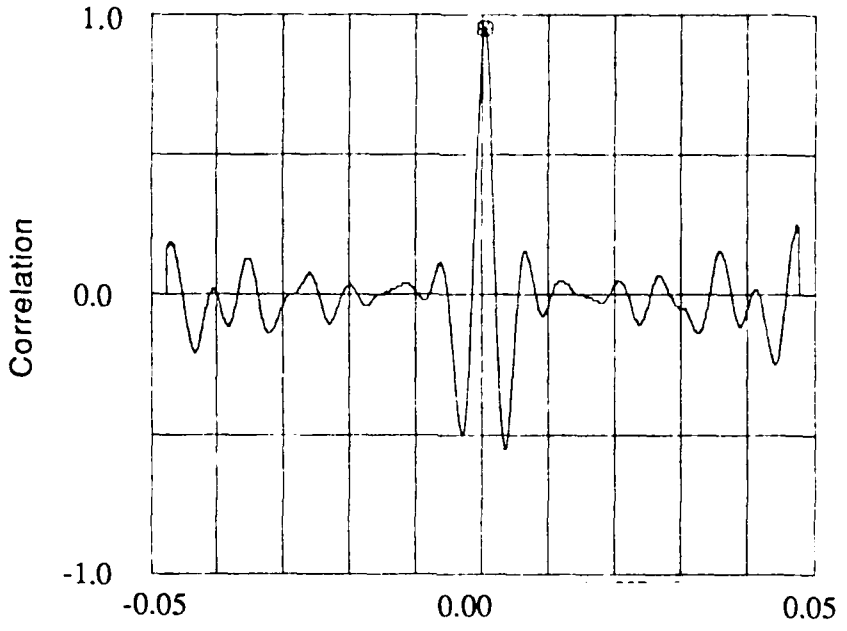

Time Shift, Sec
6 x 25, 40° Cable Angle, 45 FPS
Spanwise Distance Between Probes = 0.65 in.

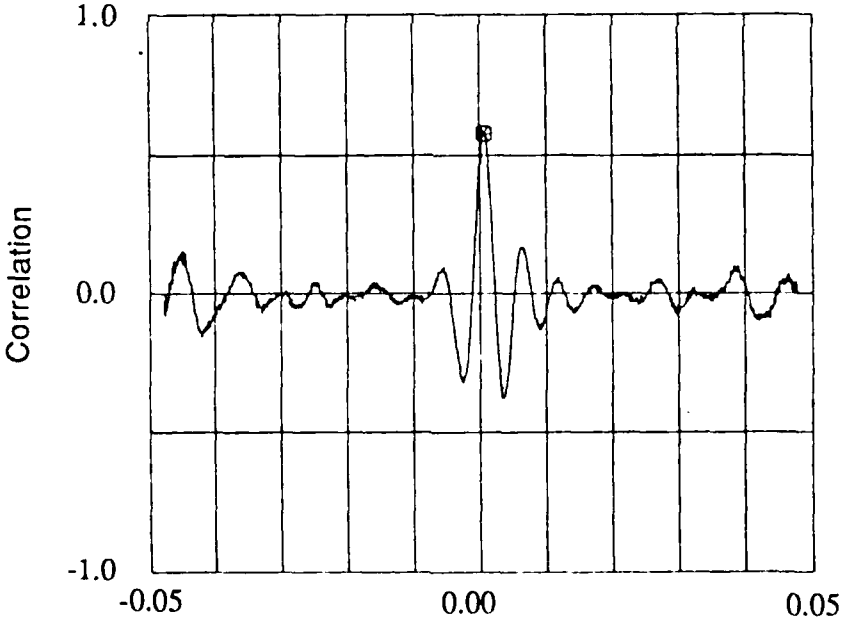

Time Shift, Sec
6 x 25, 40° Cable Angle, 45 FPS
Spanwise Distance Between Probes = 0.65 in.

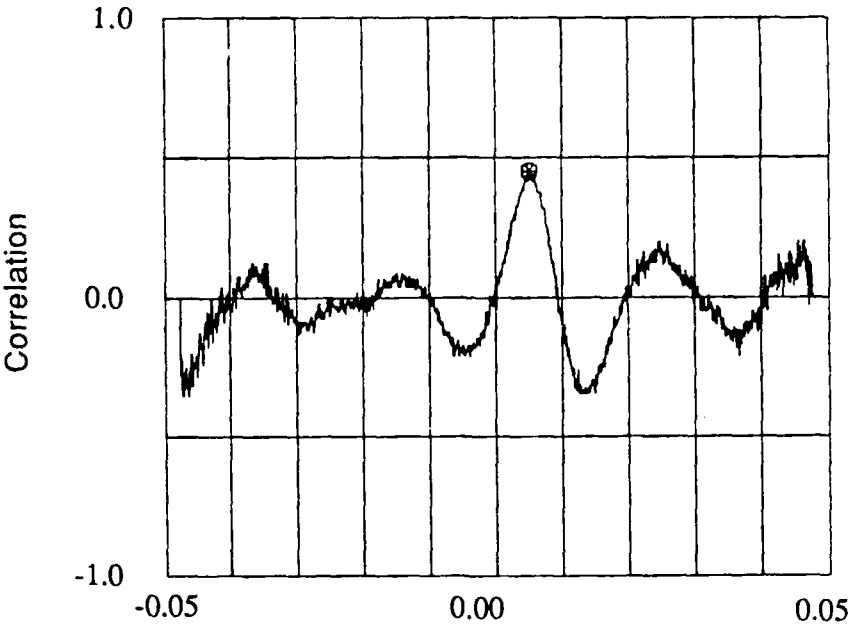

Time Shift, Sec
Cylinder Model, 20° Cable Angle, 18 FPS
Spanwise Distance Between Probes = 1.52 in.

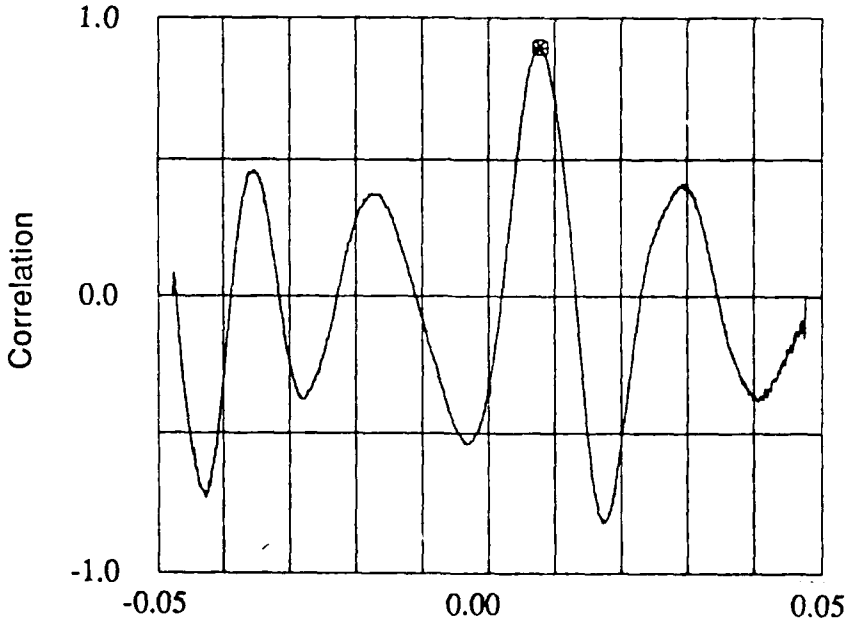

Time Shift, Sec
Cylinder Model, 20° Cable Angle, 18 FPS
Spanwise Distance Between Probes = 3.04 in.

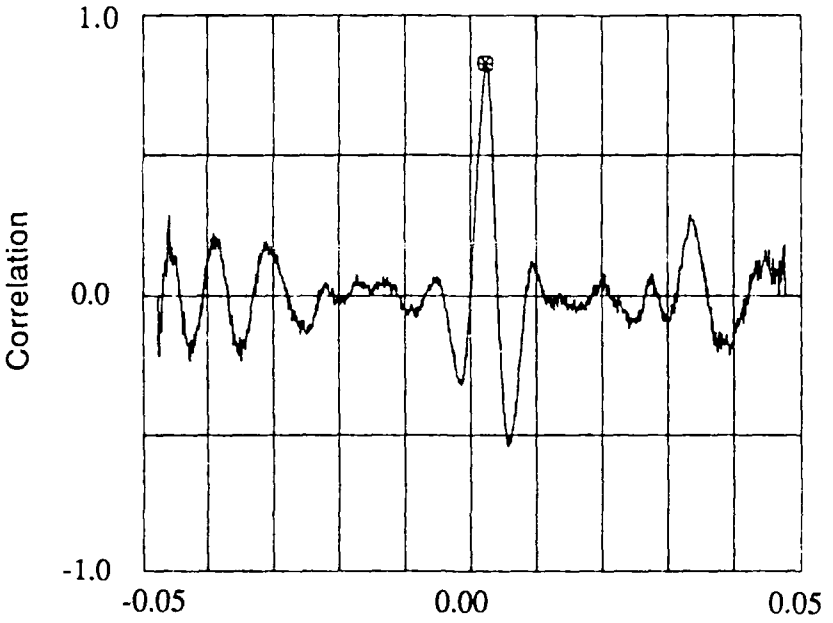

Time Shift, Sec
Cylinder Model, 20° Cable Angle, 45 FPS
Spanwise Distance Between Probes = 1.52 in.

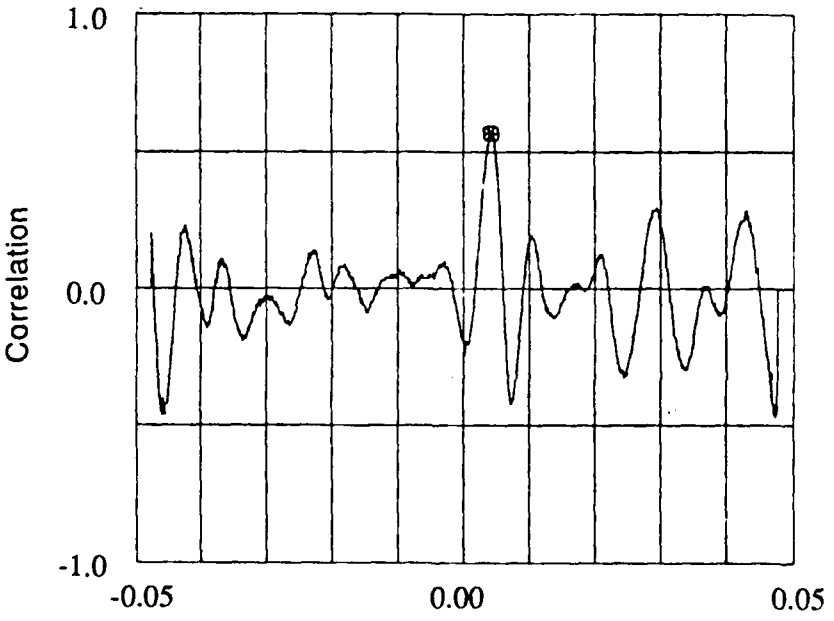

Time Shift, Sec
Cylinder Model, 20° Cable Angle, 45 FPS
Spanwise Distance Between Probes = 3.04 in.

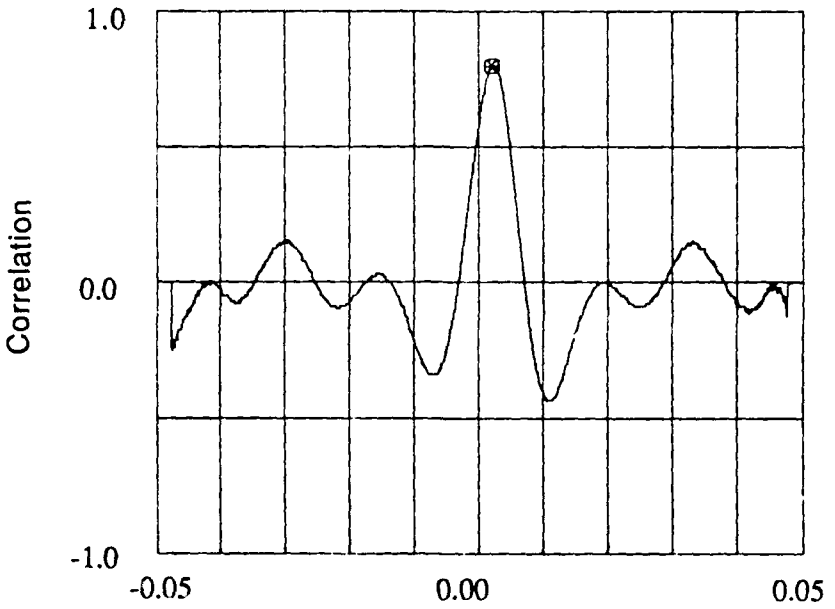

Time Shift, Sec
4 x 7, 20° Cable Angle, 18 FPS
Spanwise Distance Between Probes = 0.65 in.

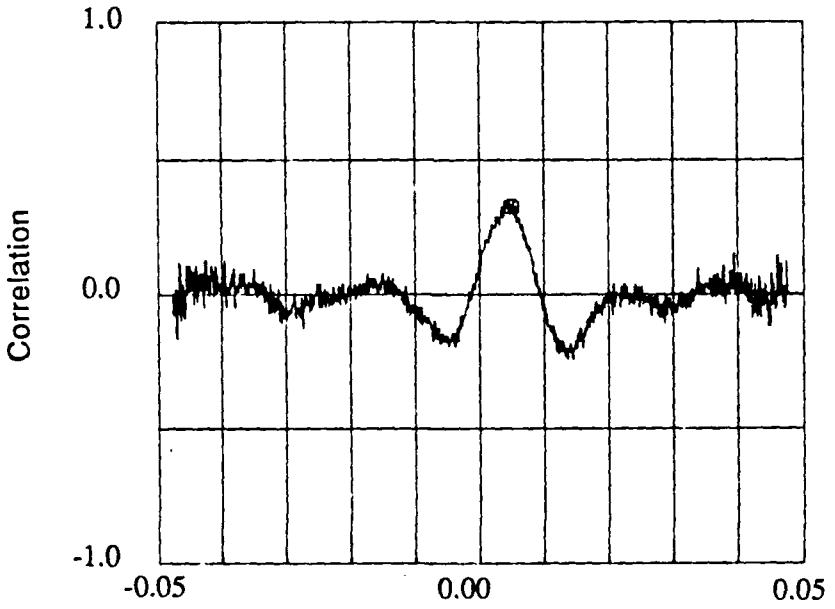

Time Shift, Sec
4 x 7, 20° Cable Angle, 18 FPS
Spanwise Distance Between Probes = 1.30 in.

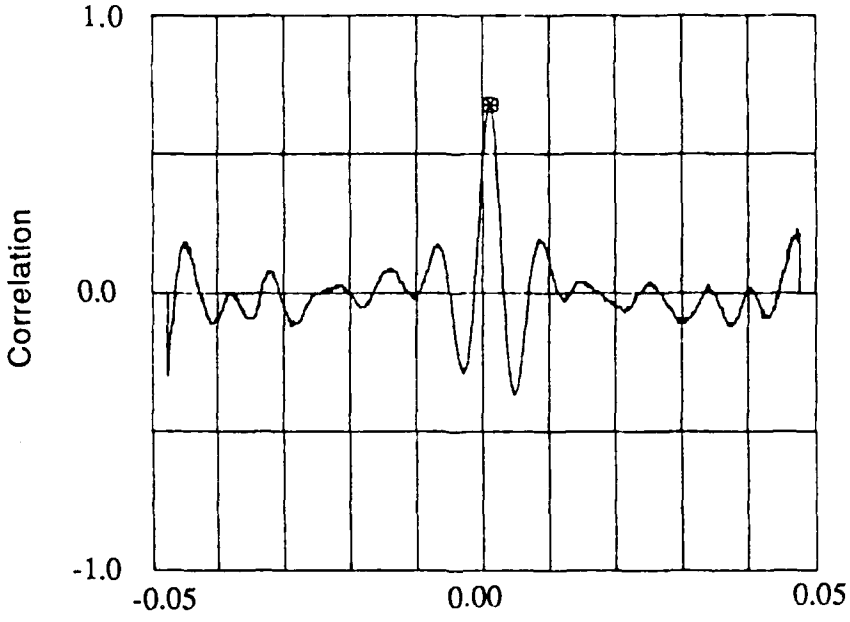

Time Shift, Sec
4 x 7, 20° Cable Angle, 45 FPS
Spanwise Distance Between Probes = 0.65 in.

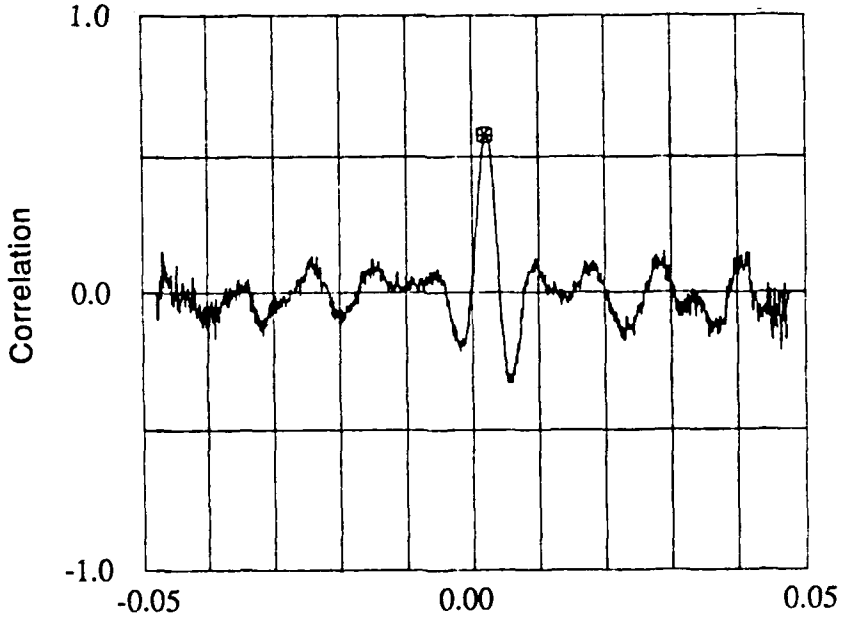

Time Shift, Sec
4 x 7, 20° Cable Angle, 45 FPS
Spanwise Distance Between Probes = 1.30 in.

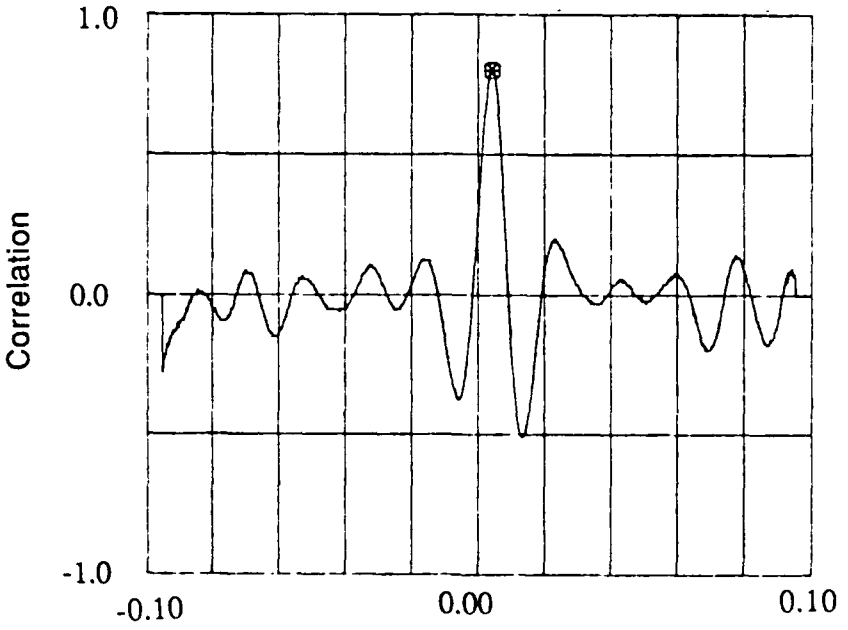

Time Shift, Sec
6 x 25, 20° Cable Angle, 18 FPS
Spanwise Distance Between Probes = 1.30 in.

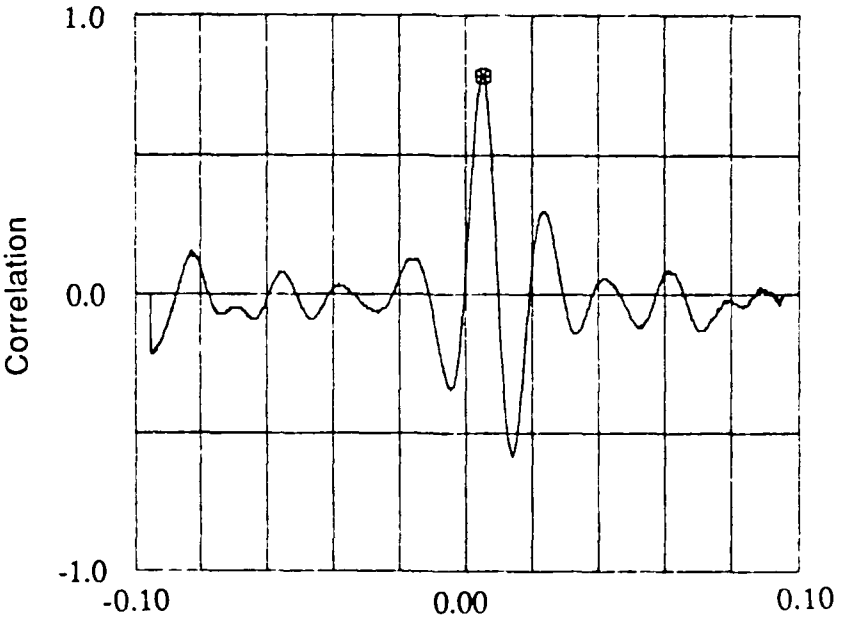

Time Shift, Sec
6 x 25, 20° Cable Angle, 18 FPS
Spanwise Distance Between Probes = 1.625 in.

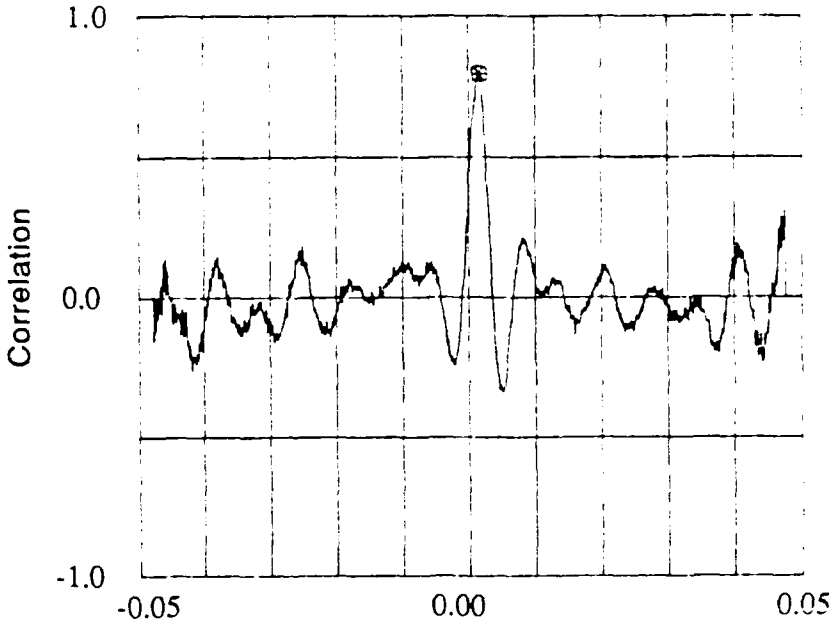

Time Shift, Sec
6 x 25, 20° Cable Angle, 45 FPS
Spanwise Distance Between Probes = 1.300 in.

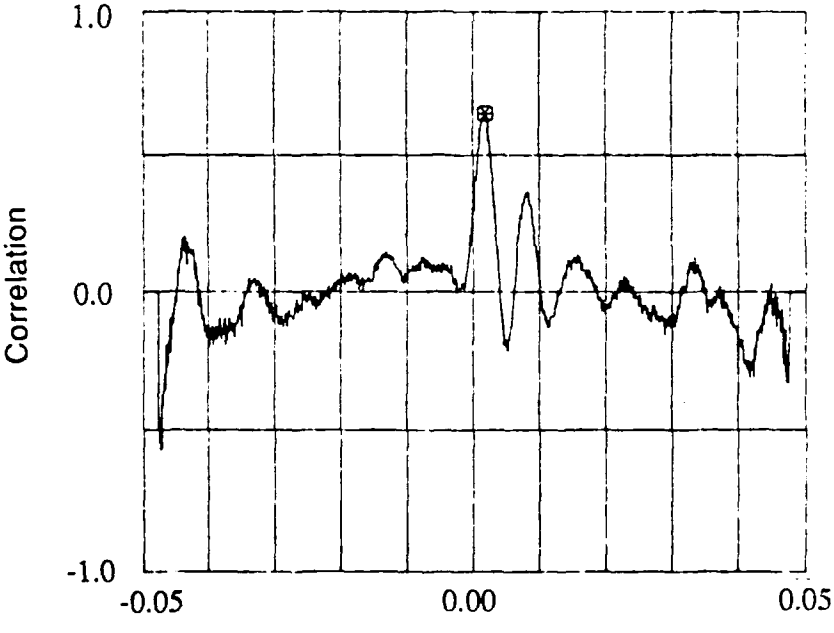

Time Shift, Sec
6 x 25, 20° Cable Angle, 45 FPS
Spanwise Distance Between Probes = 1.625 in.

DISTRIBUTION LIST

		Copy No.
---	Chief of Naval Research (Office of Naval Technology) 800 North Quincy Street, Arlington, VA 22217-5000	
	(Library)	1
	(Code 23, Dr. A. J. Faulstich)	2
	(Code 235, W. Ching)	3
	(Code 1121 OT, Dr. S. Ramberg)	4
	(Code 1132 F, Dr. S. Lekoudis)	5
162	Commander, Naval Air Systems Command	
	(Library)	6
	(PMA-210, B. Emshwiller)	7
	(PMA-210, K. Haas)	8
---	Commander, Naval Civil Engineering Laboratory	
	(Library)	9
	(Code L43, D. Meggit)	10
	(Code L03C, J. Dummer)	11
	(Code L44, Dr. W. Nordell)	12
223	Commander, Naval Research Laboratory	
	(Library)	13
	(Code 5841, Dr. R. Peltzer)	14
	(Code 5841, Dr. O. M. Griffin)	15
427	Commander, Naval Sea Systems Command	
	(Library)	16
	(PMS 407D, J. Grembi)	17
236	Commander, David Taylor Research Center	
	(Library)	18
	(Code 1541, D. Pickett)	19
	(Code 1541, R. Rispin)	20
266	Commander, Naval Underwater Systems Center, Newport	
	(Library)	21
	(Code 8333, S. Hassan)	22
146	Commander, Mine Warfare Command	
	(Library)	23
	(Code N4A, G. Pollitt)	24
075	Director, Defense Technical Information Center	25,26